Reflection and Transmission Characteristics of Porous Rubble-Mound Breakwaters

by

Ole Secher Madsen and Stanley M. White

MISCELLANEOUS REPORT NO. 76-5
MARCH 1976

Prepared for
U.S. ARMY, CORPS OF ENGINEERS
COASTAL ENGINEERING RESEARCH CENTER
Kingman Building
Fort Belvoir, Va. 22060

Limited free distribution within the United States of single copies of this publication has been made by this Center. Additional copies are available from:

National Technical Information Service
ATTN: Operations Division
5285 Port Royal Road
Springfield, Virginia 22151

Contents of this report are not to be used for advertising, publication, or promotional purposes. Citation of trade names does not constitute an official endorsement or approval of the use of such commercial products.

The findings in this report are not to be construed as an official Department of the Army position unless so designated by other authorized documents.

REPORT DOCUMENTATION PAGE

READ INSTRUCTIONS BEFORE COMPLETING FORM

1. REPORT NUMBER
MR 76-5

2. GOVT ACCESSION NO.

3. RECIPIENT'S CATALOG NUMBER

4. TITLE (and Subtitle)
REFLECTION AND TRANSMISSION CHARACTERISTICS OF POROUS RUBBLE-MOUND BREAKWATERS

5. TYPE OF REPORT & PERIOD COVERED
Miscellaneous Report

6. PERFORMING ORG. REPORT NUMBER

7. AUTHOR(s)
Ole Secher Madsen
Stanley M. White

8. CONTRACT OR GRANT NUMBER(s)
DACW72-74-C-0001

9. PERFORMING ORGANIZATION NAME AND ADDRESS
Department of Civil Engineering
Massachusetts Institute of Technology
Cambridge, Massachusetts 02139

10. PROGRAM ELEMENT, PROJECT, TASK AREA & WORK UNIT NUMBERS
E31230

11. CONTROLLING OFFICE NAME AND ADDRESS
Department of the Army
Coastal Engineering Research Center (CERRE-SP)
Kingman Building, Fort Belvoir, VA 22060

12. REPORT DATE
March 1976

13. NUMBER OF PAGES
~~138~~ 137 p

14. MONITORING AGENCY NAME & ADDRESS (if different from Controlling Office)

15. SECURITY CLASS. (of this report)
UNCLASSIFIED

15a. DECLASSIFICATION/DOWNGRADING SCHEDULE

16. DISTRIBUTION STATEMENT (of this Report)
Approved for public release; distribution limited.

17. DISTRIBUTION STATEMENT (of the abstract entered in Block 20, if different from Report)

18. SUPPLEMENTARY NOTES

19. KEY WORDS (Continue on reverse side if necessary and identify by block number)

Breakwaters	Friction factor	Reflection coefficient
Energy dissipation	Hydraulics	Rubble-mound breakwater
Empirical relationships	Porous material	Transmission coefficient
Wave reflection	Wave transmission	

20. ABSTRACT (Continue on reverse side if necessary and identify by block number)

This report presents the results of a study of the reflection and transmission characteristics of porous rubble-mound breakwaters. An attempt was made at making the procedures entirely self-contained by introducing empirical relationships for the hydraulic characteristics of the porous material and by establishing experimentally an empirical relationship for the friction factor that expresses energy dissipation on the seaward slope of a breakwater.

PREFACE

This report is published to provide coastal engineers with the resu of research on the reflection and transmission characteristics of porous rubble-mound breakwaters. The work was carried out under the coastal processes program of the U.S. Army Coastal Engineering Research Center (CERC).

The report was prepared by Ole Secher Madsen, Associate Professor of Civil Engineering, and Stanley M. White, Graduate Research Assistant, Ralph M. Parsons Laboratory, Department of Engineering, Massachusetts Institute of Technology, under CERC Contract No. DACW72-74-C-0001. The research was conducted at the Ralph M. Parsons Laboratory from 1 December 1973 through 30 November 1975. The authors acknowledge the assistance of Mr. James W. Eckert, who participated in the development of the accurate method for determining experimental reflection coefficients. The advice and encouragement of Dr. Robert M. Sorensen, Chief, Special Projects Branch, CERC, are greatly appreciated.

Dr. R.M. Sorensen was the CERC contract monitor for the report, under the general supervision of Mr. R.P. Savage, Chief, Research Division.

Comments on this publication are invited.

Approved for publication in accordance with Public Law 166, 79th Congress, approved 31 July 1945, as supplemented by Public Law 172, 88th Congress, approved 7 November 1963.

JAMES L. TRAYERS
Colonel, Corps of Engineers
Commander and Director

CONTENTS

TABLES

CONTENTS

TABLES--Continued

FIGURES

CONTENTS

FIGURES--Continued

SYMBOLS AND DEFINITIONS

a_i = incident wave amplitude

a_{max} = maximum wave amplitude

a_{min} = minimum wave amplitude

a_r = reflected wave amplitude (complex)

a_t = transmitted wave amplitude (complex)

a_+ = complex wave amplitude

a_- = complex wave amplitude

a_I = wave amplitude of equivalent incident wave

A = complex vertical amplitude of wave motion on slope at stillwater level

A_b = wave excursion amplitude

C^*_f = friction factor

d = average stone diameter

d_r = reference stone diameter

d_{II} = stone size as defined in Section III

e = 2.71

$\overline{\overline{E}}_D$ = average rate of energy dissipation

E_F = energy flux

f = nondimensional friction factor

f_b = linearized bottom friction factor

f_w = wave friction factor

F_d = volume force

F_p = pressure force

F_I = inertia force

F_s = slope friction constant

g = acceleration due to gravity

h = water depth along sloping breakwater face

h_o = constant water depth seaward of breakwater

H_i = incident wave height

H_{max} = maximum wave height

H_{min} = minimum wave height

Δh_j = horizontal slice thickness

ΔH_e = head difference for equivalent breakwater

ΔH_n = head loss in material n

ΔH_T = head difference for trapezoidal breakwater

i = $\sqrt{-1}$

k = wave number

k_o = wave number corresponding to constant depth region

k_i = imaginary part of wave number

k_r = real part of wave number

K_m = momentum coefficient

ℓ = length of crib-style breakwater

ℓ_e = equivalent length of crib-style breakwater

ℓ_n = length of porous material n

ℓ_s = submerged horizontal length of impermeable slope

L = wavelength

L_H = distance parameter used in permeameter tests

M_F = momentum flux

n = porosity

N = number of experiments performed

p = pressure

p_η = pressure of water surface

Q = discharge per unit length

ΔQ_j = discharge associated with slice j

R = reflection coefficient

R_c = critical Reynolds number

R_d = particle Reynolds number

R_{dm} = particle Reynolds number of model

R_m = measured reflection coefficient

R_p = predicted reflection coefficient

R_{ps} = predicted reflection coefficient (simplified formula)

R_u = ratio of runup to incident wave height

R_I = reflection coefficient determined in Section II

R_{II} = reflection coefficient determined in Section III

S = parameter defined by equation (5)

S_* = parameter defined by equation (28)

t = time

T = transmission coefficient

T = wave period

T_I = transmission coefficient calculated in Section II

u = complex horizontal velocity component

U = horizontal velocity component

U_b = horizontal velocity component at the bottom

U_j = horizontal discharge velocity component through a slice

U_s = horizontal seepage velocity

$\overline{U}$ = average horizontal velocity component

U_η = horizontal velocity component at the free surface

w = complex vertical velocity component

W = vertical velocity component

W_b = vertical velocity component at the bottom

W_s = vertical seepage velocity

W_η = vertical velocity component at the free surface

x = horizontal coordinate

y = parameter defined by equation (103)

z = vertical coordinate

α = laminar resistance coefficient

α_o = constant associated with empirical formula for α

β = turbulent resistance coefficient

β_o = constant associated with empirical formula for β

β_r = hydrodynamic characteristic of reference material

β_s = angle of impermeable slope

δ = arbitrary phase angle

ε = parameter as defined by equation (18)

ζ = complex free surface elevation

$|\zeta_o|$ = maximum free surface elevation in front of breakwater

$|\zeta_\ell|$ = maximum free surface elevation behind breakwater

η = time-dependent free surface elevation

κ = added mass coefficient

λ = parameter as defined by equation (34)

ν = kinematic viscosity

ρ = density

ω = radian frequency, $\frac{2\pi}{T}$

ϕ = friction angle

ϕ_b = bottom friction angle

τ = shear stress

τ_b = bottom shear stress

Ψ = parameter as defined by equation (28)

Δ = measurement error

$\forall$ = volume

$\forall_m$ = volume of solids

REFLECTION AND TRANSMISSION CHARACTERISTICS OF POROUS RUBBLE-MOUND BREAKWATERS

by

Ole Secher Madsen and Stanley M. White

I. INTRODUCTION

Porous structures consisting of quarry stones of various sizes often offer an excellent solution to the problem of protecting a harbor against the action of incident waves. When used for this purpose it is important that the coastal engineer is able to assess the effectiveness of a given breakwater design by predicting the amount of wave energy that will transmit through the breakwater.

Both the transmission and the reflection characteristics of a porous structure are important. Thus, the severity of the wave motion resulting from the partially standing wave system on the seaward side of a breakwater will determine the accessibility of the harbor during storm conditions. This wave motion outside the harbor will determine the sediment transport patterns near the structure, and will also affect the wave motion within the breakwater enclosure by governing the wave motion at the harbor entrance. Therefore, the ability to predict the reflection and transmission characteristics of a porous structure is of utmost importance to an overall sound engineering design.

The interaction of incident waves with a porous sturcture is a rather complex problem, one which probably will defy an accurate analytical solution for the foreseeable future. With incident waves of various frequencies and the possible occurrence of wave breaking on the seaward slope of the structure, the problem is amenable to an analytical solution only by the adoption of a set of simplifying assumptions. With the addition of the energy dissipation associated with frictional effects on the seaward slope as well as with the flow within the porous structure, it appears the only possible solution is to perform scale-model tests.

Performing a scale-model test for the interaction of waves with a porous structure is, however, not a simple matter, and it presents a separate set of problems even when tests are limited to normally incident waves. It has recently been possible to perform tests for incident waves composed of several frequencies by using programmable wave generators. However, some difficulties are associated with this type of testing procedure. Thus, it is possible to perform tests corresponding to a given incident wave spectrum only by trial and error. Even limiting testing conditions to periodic incident waves leaves some unresolved questions regarding the influence of scale effects. Thus, the Reynolds number is modeled by the length scale $^{(3/2)}$ in a Froude model; this lack of Reynolds similarity may affect the energy dissipation on the seaward slope of the structure as well as the dissipation within the structure. These problems associated with scale-model tests should not be interpreted to mean that model tests are of no value. They are mentioned here merely to point out that even accurately conducted model tests have their sources of errors which should be considered in the interpretation of the test results.

Although scale-model tests have weaknesses, model tests are believed to present the best solution to the problem of wave interaction with porous structures. However, a simple analytical model, although approximate, does offer possibilities for performing a reasonably sound preliminary design which may then be subjected to a model study to add the final touch to the design. This procedure will reduce the significant cost associated with the performance of model tests. For this reason this investigation approaches the problem of wave transmission through and reflection from a porous structure on an analytical basis. An analytical treatment of this complex problem must be based on several simplifying assumptions. The basic assumptions are:

(a) Incident waves are periodic, relatively long, and normally incident.

(b) Fluid motion is adequately described by the linearized governing equations.

(c) Waves do not break on the seaward slope of the structure.

Since the design wave conditions for most breakwaters correspond to relatively long waves, i.e., waves of a length exceeding say ten times the depth of water, the first assumption is physically reasonable with the assumption of normal incidence being made for simplicity. From the assumption of linearized governing equations, it is, in principle, possible to generalize the solution to cover the conditions corresponding to incident waves prescribed by their amplitude spectrum. With the present lack of knowledge about the mechanics of wave breaking the third assumption is dictated by necessity. This third assumption may seem unrealistic. However, most porous structures have steep seaward slopes on which relatively long incident waves may remain stable.

With these assumptions, an analytical solution to the problem of wave transmission through and reflection from a porous structure is sought. The solution technique is based on the fundamental argument that the problem of reflection from and transmission through a structure may be regarded as one of determining the partition of incident wave energy among reflected, transmitted, and dissipated energy. The problem is in accounting for this partition and, in particular, in evaluating the energy dissipation associated with the wave structure interaction.

This energy dissipation consists of two separate components; one is associated with the flow within the porous structure (the internal energy dissipation), and the other is associated with the energy dissipation on the seaward slope (the external energy dissipation).

Section II of this report discusses, in an idealized manner, the internal energy dissipation by considering the problem of the interaction of waves and a homogeneous porous structure of rectangular cross section. This problem was treated by Sollitt and Cross (1972) who presented a review of previously published analytical studies of the problem. The present approach, which was published by Madsen (1974), follows the approach of Sollitt and Cross (1972) but arrives at an explicit analytical solution for the linearized flow resistance of the porous medium, thus circumventing Sollitt's and Cross' tedious iterative procedure which involved the use of high speed computers. Furthermore, empirical relationships relating the flow resistance of a porous medium to stone size and porosity are suggested and the final result is an explicit analytical solution for the reflection and transmission coefficients of rectangular breakwaters. This solution is tested against the experimental observations of Wilson (1971) and Keulegan (1973), and found to yield quite accurate results. The explicit solution may also be used to assess the severity of scale effects in model tests with porous structures.

Section III of this report discusses the problem of the energy dissipation on the seaward slope of a porous breakwater by considering the associated problem of energy dissipation on a rough impermeable slope. Since the stone size below the cover layer of a trapezoidal, multilayered breakwater is generally quite small, the seaward slope will essentially act as an impermeable rough slope. With the assumption of nonbreaking waves the energy dissipation on the rough slope is expressed by accounting for the bottom frictional effects. An analytical solution for the reflection coefficient is obtained and the bottom friction, which is linearized, is related to a wave friction factor by invoking Lorentz' principle of equivalent work. To evaluate this solution it is necessary to have an empirical relationship for this wave friction factor. Such an empirical relationship is established experimentally for rough slopes whose roughness is adequately modeled by gravel, i.e., natural stones. The experiments reveal the need for an accurate method for the determination of reflection coefficients from experimental data. Such a method is developed and the semiempirical procedure for estimating the reflection coefficient of rough impermeable slopes is tested against a separate set of experiments. The procedure yields accurate results and is believed to present a physically more realistic approach to this problem than the semiempirical method presented by Miche (1951).

Section IV of the report synthesizes the results obtained in Sections II and III into a rational procedure for the estimate of reflection and transmission coefficients of trapezoidal, multilayered breakwaters. The procedure accounts for the external energy dissipation by considering the seaward slope to be essentially impermeable. Subtracting the externally dissipated energy the partition of the remaining energy among reflected, transmitted, and internally dissipated energy is determined by considering the interaction of an equivalent incident wave (representing the remaining wave energy), with a homogeneous rectangular breakwater which is hydraulically equivalent to the trapezoidal, multi-layered breakwater. This procedure which attempts to account for the energy dissipation where it takes place, in contrast to the procedure developed by Sollitt and Cross (1972), yields excellent predictions of the reflection and transmission coefficients obtained experimentally by Sollitt and Cross.

II. TRANSMISSION AND REFLECTION CHARACTERISTICS OF RECTANGULAR CRIB-STYLE BREAKWATERS

1. Preliminary Remarks.

This section presents a theoretical treatment of the problem of wave transmission through and reflection from a porous structure of rectangular cross section. The basic assumptions are:

(a) Relatively long normally incident waves which are considered to be adequately described by linear long wave theory.

(b) The porous structure is homogeneous and of rectangular cross section.

(c) The flow resistance within the porous structure is linear in the velocity, i.e., of the Darcy-type.

The essential features of the derivation and mathematical manipulation of the governing equations are presented in Appendix A to enable the treatment to be relatively brief and to the point. The theoretical solution for the transmission and reflection coefficient is obtained based on the above assumptions and results in a solution which depends on the friction factor arising from the linearization of the resistance law, which for prototype conditions may be expected to be quadratic rather than linear in the velocity.

A flow resistance of the Dupuit-Forchheimer type (Bear, et al., 1968) is assumed, and an empirical relationship relating flow resistance to stone size, porosity, and fluid viscosity gives a fair representation of experimentally observed hydraulic properties of porous media. Adopting this empirical formulation of the flow resistance for a porous medium in conjunction with Lorentz' principle of equivalent work leads to a determination of the linearized flow resistance factor in terms of the characteristics of the porous material and the incident wave characteristics. In this manner an explicit solution for the reflection and transmission coefficients for a crib-style breakwater is obtained.

Knowledge of the incident wave characteristics, the breakwater geometry, and the characteristics (stone size and porosity) of the porous material is sufficient for the prediction of reflection and transmission coefficients. The procedure was tested against experimentally observed reflection and transmission coefficients (Keulegan, 1973; Wilson, 1971) and yielded accurate predictions of transmission coefficients; the reflection coefficients are less accurately predicted. The discrepancy between predicted and observed reflection coefficients may be partly attributed to experimental errors in the determination of reflection coefficients.

The flow resistance within the porous structure accounts for a laminar and a turbulent contribution. Therefore, the theoretical development may be used to shed some light on the important problem of scale effects in hydraulic model tests with porous structures.

2. Analytical Solution for Transmission and Reflection Coefficients of Crib-Style Breakwaters.

With the assumption of normally incident waves the problem to be considered is illustrated in Figure 1.

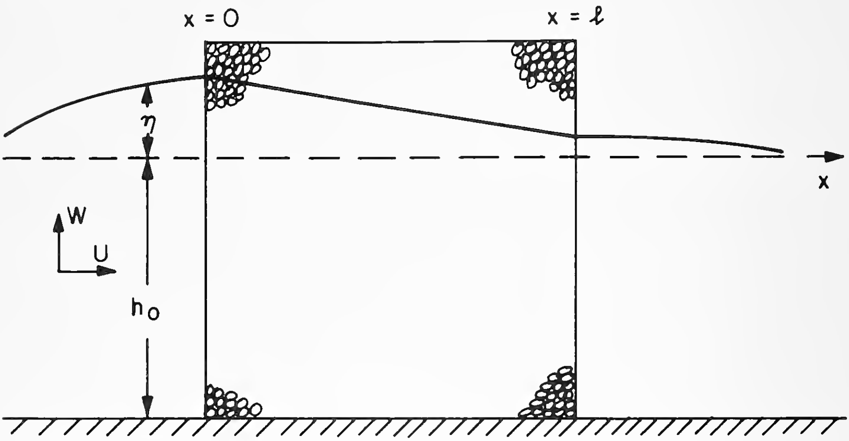

Figure 1. Definition sketch.

The rectangular porous structure is located between x=0 and x=ℓ, i.e., the width of the breakwater is ℓ. With the assumption of relatively long incident waves described by linear long wave theory, the equations governing the motion outside the structure are:

$$\frac{\partial \eta}{\partial t} + h_o \frac{\partial U}{\partial x} = 0 \qquad \text{(continuity)} \tag{1}$$

and

$$\frac{\partial U}{\partial t} + g \frac{\partial \eta}{\partial x} = 0 \qquad \text{(conservation of momentum)}, \tag{2}$$

in which η is the free surface elevation relative to the stillwater level, h_o is the constant depth outside the structure, U is the horizontal water particle velocity, g is the acceleration due to gravity, and the bottom shear stress term introduced in the derivation of equations (A-24) and (A-25) in Appendix A has been omitted.

For the flow within the porous structure, the linearized governing equations are derived in Appendix A, equations (A-74) and (A-75), and may in the present context be written as:

$$n \frac{\partial \eta}{\partial t} + h_o \frac{\partial U}{\partial x} = 0 \qquad \text{(continuity)} \tag{3}$$

and

$$\frac{S}{\eta} \frac{\partial U}{\partial t} + g \frac{\partial \eta}{\partial x} + f \frac{\omega}{n} U = 0 \quad \text{(conservation of momentum)}, \tag{4}$$

in which ω is the radian frequency, $2\pi/T$, of the periodic wave motion, n is the porosity of the porous medium, U is the horizontal discharge velocity, i.e., equivalent to the velocity variable used in equations (1) and (2), S is a factor expressing formally the effect of unsteady motion (see App. A)

$$S = 1 + \kappa(1 - n), \tag{5}$$

where κ is an added mass coefficient. With κ expected to be of the order $0 \leq \kappa \leq 0.5$, equation (5) shows that $1 \leq S \leq 1.5$. The nondimensional friction factor, f, arising from the linearization of the flow resistance is related to the flow resistance, which more realistically is given by a Dupuit-Forchheimer relationship through

$$f \frac{\omega}{n} = \alpha + \beta|U| \tag{6}$$

in which the hydraulic properties of the porous medium are expressed by the coefficients α and β. The coefficient α expresses the laminar flow resistance, which is linear in the velocity. The turbulent flow resistance which is quadratic in the velocity, is expressed by the coefficient β. The friction factor is regarded as constant, i.e., independent of x and t, in the following.

With the equations being linear, complex variables may be used. Thus, looking for a periodic solution of radian frequency, ω, we may take

$$\eta = \text{Real}\ \{\zeta(x)e^{i\omega t}\} \tag{7}$$

and

$$U = \text{Real}\ \{u(x)e^{i\omega t}\} \tag{8}$$

in which $i = \sqrt{-1}$ and the amplitude functions ζ and u are functions of x only. These amplitude functions will generally be complex, i.e., consist of a real and an imaginary part. The magnitude of the amplitude function, $|\zeta|$ or $|u|$, expresses the maximum value, i.e., the amplitude, of this variable. Only the real part of the complex solutions for η and U constitutes the physical solutions.

Introducing equations (7) and (8) in equations (1) and (2) the general solution for the motion outside the porous structure may be obtained as discussed in Appendix A

$$\left.\begin{aligned} \zeta &= a_i e^{-ik_o x} + a_r e^{ik_o x} \\ u &= \sqrt{\frac{g}{h_o}}\,(a_i e^{-ik_o x} - a_r e^{ik_o x}) \end{aligned}\right\} \quad x \leq 0 \tag{9}$$

$$\left.\begin{aligned} \zeta &= a_t e^{-ik_o(x-\ell)} \\ u &= \sqrt{\frac{g}{h_o}}\; a_t e^{-ik_o(x-\ell)} \end{aligned}\right\} \quad x \geq \ell \tag{10}$$

in which a_i is the amplitude of the incident wave, which without loss in generality may be taken as real. The reflected and transmitted complex wave amplitudes are a_r and a_t, respectively. The magnitudes of a_r and a_t, i.e., $|a_r|$ and $|a_t|$, express the values of the physical wave amplitudes. The wave number, $k_o=2\pi/L$, is given by the familiar long wave expression

$$k_o = \frac{\omega}{\sqrt{gh_o}} \; . \tag{11}$$

The preceding expressions show that we expect an incident wave, a_i, propagating in the positive x-direction to coexist with a reflected wave, a_r, propagating in the negative x-direction in front of the structure, $x \leq 0$. Behind the structure, $x \geq \ell$, only a transmitted wave, a_t, is expected to propagate in the positive x-direction.

The general solution for the flow within the structure is found (App. A), by introducing equations (7) and (8) in equations (3) and (4). The solution, which consists of a wave propagating in the positive x-direction, of complex amplitude a_+, and a wave propagating in the negative x-direction, of complex amplitude a_-, is given by

$$\left.\begin{aligned} \zeta &= a_+ e^{-ikx} + a_- e^{ik(x-\ell)} \\ u &= \sqrt{\frac{g}{h_o}}\ \frac{n}{\sqrt{S-if}}\ (a_+ e^{-ikx} - a_- e^{ik(x-\ell)}) \end{aligned}\right\}\quad 0 \leq x \leq \ell \tag{12}$$

with the complex wave number, k, given by

$$k = \frac{\omega}{\sqrt{gh_o}}\ \sqrt{S-if} = k_o\ \sqrt{S-if}\ . \tag{13}$$

Equation (13) shows the wave number to be complex, i.e., to have a real as well as an imaginary part. The solution of equation (13) should be chosen such that the imaginary part is negative since this will lead to a wave motion exhibiting an exponentially decreasing amplitude in the direction of propagation as discussed in Appendix A.

The general solutions for the motions in the three regions given by equations (9), (10), and (12) show the problem to involve four unknown quantities. These unknowns are the complex wave amplitudes a_r, a_t, a_+, and a_- and they may be determined by matching surface elevations and velocities at the common boundaries of the various solutions. Thus, we obtain at x=0 from equations (9) and (12):

$$a_i + a_r = a_+ + a_- e^{-ik\ell} \tag{14}$$

and

$$a_i - a_r = \frac{n}{\sqrt{S-if}}\ (a_+ - a_- e^{-ik\ell}) \tag{15}$$

and at $x=\ell$ from equations (10) and (12)

$$a_t = a_+ e^{-ik\ell} + a_- \tag{16}$$

and

$$a_t = \frac{n}{\sqrt{S-if}} (a_+ e^{-ik\ell} - a_-) \tag{17}$$

To solve this set of equations we introduce the shorthand notation

$$\varepsilon = \frac{n}{\sqrt{S-if}} \quad . \tag{18}$$

Multiplying equation (16) by ε and adding and subtracting equation (17) result in

$$a_+ = \frac{1+\varepsilon}{2\varepsilon} e^{ik\ell} a_t \tag{19}$$

and

$$a_- = - \frac{1-\varepsilon}{2\varepsilon} a_t , \tag{20}$$

which may be introduced in equation (12) to yield the velocity within the structure

$$u = \sqrt{\frac{g}{h_o}} \; a_t \left\{\frac{1+\varepsilon}{2} e^{-ik(x-\ell)} + \frac{1-\varepsilon}{2} e^{ik(x-\ell)}\right\} \quad . \tag{21}$$

Adding equations (14) and (15) and introducing a_+ and a_- from equations (19) and (20) yield, after some simple algebraic manipulations, an expression for the complex amplitude of the transmitted wave

$$\frac{a_t}{a_i} = \frac{4\varepsilon}{(1+\varepsilon)^2 e^{ik\ell} - (1-\varepsilon)^2 e^{-ik\ell}} \quad . \tag{22}$$

Similarly an expression for the complex amplitude of the reflected wave is obtained by subtracting equation (15) from equation (16) and introducing equations (19) and (20)

$$\frac{a_r}{a_i} = \frac{(1-\varepsilon^2)(e^{ik\ell} - e^{-ik\ell})}{(1+\varepsilon)^2 e^{ik\ell} - (1-\varepsilon)^2 e^{-ik\ell}} \quad . \tag{23}$$

These expressions may easily be shown to be identical to those given by Kondo (1975) when it is realized that the factor γ used by Kondo is related to ε through $\gamma = 1/\varepsilon$.

To investigate the general behavior of the solution for the transmission and the reflection coefficient as given by equations (22) and (23) it is seen from equation (18) that

$$\varepsilon = \frac{n}{\sqrt{S-if}} = \frac{n/\sqrt{S}}{\sqrt{1-i(f/S)}} \quad , \tag{24}$$

and that the wave number, k, given by equation (13) may be expressed as

$$k = k_o \sqrt{S-if} = nk_o \frac{1}{\varepsilon} = nk_o \frac{\sqrt{1-i(f/S)}}{n/\sqrt{S}} \quad . \tag{25}$$

Thus, it is seen that the general solutions for the transmission coefficient

$$T = \frac{|a_t|}{a_i} \tag{26}$$

and the reflection coefficient

$$R = \frac{|a_r|}{a_i} \tag{27}$$

may be regarded as functions of the variables $n/\sqrt{S}$, f/S, and $nk_o\ell$, i.e., the general solution for R and T may be presented as a series of graphs, each graph corresponding to a particular value of $n/\sqrt{S}$ and giving R or T as functions of $nk_o\ell$ and f/S. An example of this solution is presented in Figures 2 and 3 which correspond to a value of $n/\sqrt{S}$ = 0.45.

As previously mentioned, a series of graphs is needed for different values of $n/\sqrt{S}$. In fact such a series of graphs was developed corresponding to values of $n/\sqrt{S}$ = 0.35, 0.40, 0.45, and 0.50. If it is assumed that the values of n, $nk_o\ell$, and f are known, the graph to be used would depend on the value chosen for the coefficient S given by equation (5). As discussed in conjunction with the introduction of the parameter S, its actual value is poorly understood except that it is expected to take on values in the interval $1 \leq S \leq 1.5$. Now, if taking

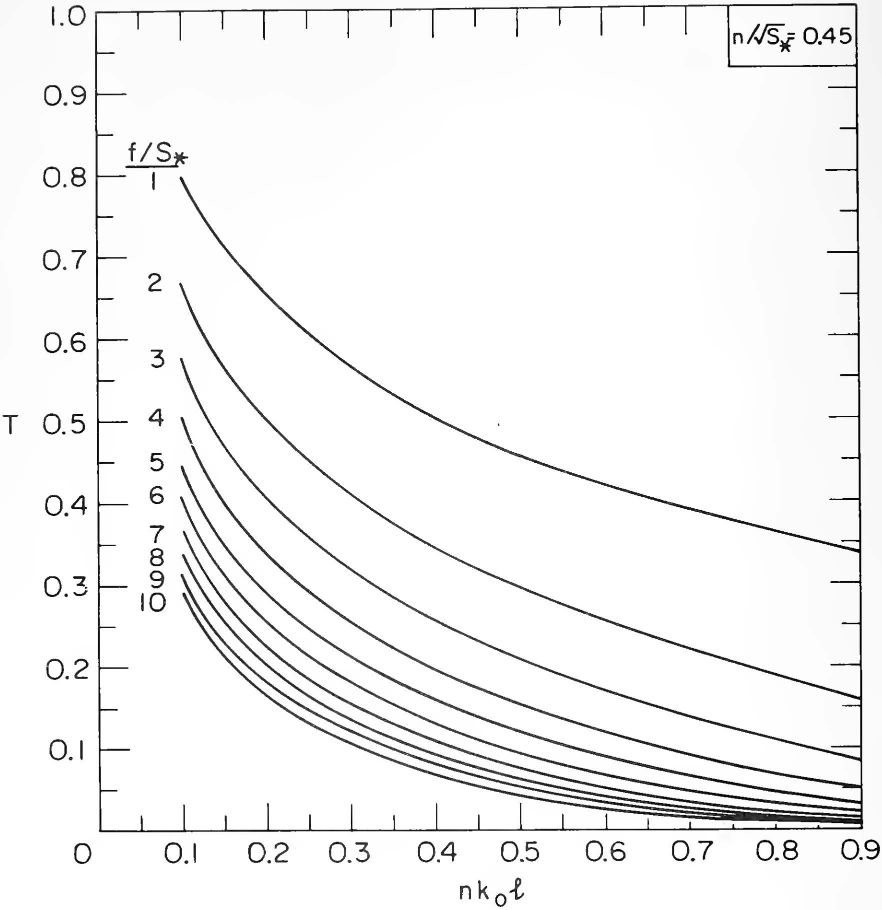

Figure 2. Transmission coefficient for crib-style breakwaters. S_* defined by equation (28). For $nk_o\ell < 0.1$ use equation (35).

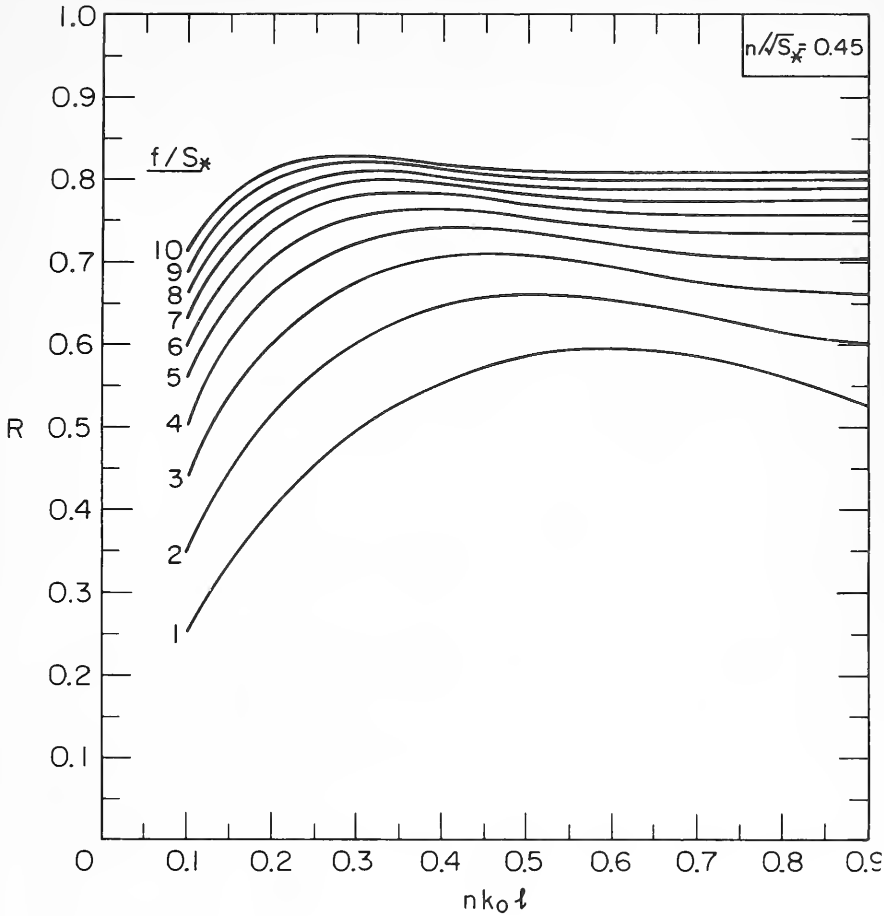

Figure 3. Reflection coefficient for crib-style breakwaters. S_* defined by equation (28). For $nk_o\ell < 0.1$ use equation (36).

$n = 0.45$, $nk_o\ell = 0.2, 0.4, 0.6$, and 0.8, and $f = 5$, one possible choice of S is to take it equal to unity, i.e., using the graphs corresponding to $n/\sqrt{S} = 0.45$ with $nk_o\ell$ and $f/S = f$ to obtain values of R and T. An extreme alternate choice would be to assume $S = 1.67$, i.e., using the graphs prepared for $n/\sqrt{S} = 0.45/\sqrt{1.67} = 0.35$ with the values of $nk_o\ell$ and $f/S = f/1.67 = 3.0$. It was found this way that the estimates of R and T varied at most by 0.01 with the above choices of S. This may be taken as an indication of the insignificant importance of the value assigned to the coefficient S.

Thus, it is concluded that the value assigned to the coefficient S is of little consequence and that we may safely take $S = 1.0$. However, this result may be utilized to simplify the presentation of results. Thus, rather than presenting a series of graphs for different values of $n/\sqrt{S}$, one set of graphs, for example corresponding to $n/\sqrt{S_*} = 0.45$, suffices. The factor S_* is without physical significance and is determined by requiring that the value of $n/\sqrt{S_*} = 0.45$ for a given structure for which n, the porosity, is known. Thus, if n is known the value of S_* is obtained from

$$S_* = \left(\frac{n}{0.45}\right)^2 , \tag{28}$$

and Figures 2 and 3 may be used with $nk_o\ell$ and f/S_* to obtain estimates of R and T.

a. Simplified Solution for Structures of Small Width. For many breakwaters the width, ℓ, is of the same order of magnitude as the depth of water, h_o. Thus, for relatively long incident waves, k_oh_o and consequently $k_o\ell$ may be assumed to be small. Thus, with the assumption of $k_o\ell << 1$, the general formulas for the reflection and transmission coefficients given in the previous section may be simplified considerably.

The nature of the simplification is expressed by expanding the exponentials in terms of their Taylor series, i.e.,

$$e^{\pm ik\ell} = 1 \pm ik\ell + O(k\ell)^2 \tag{29}$$

and adopting $O(k\ell)^2$ as the degree of accuracy of the simplified expressions.

Introducing the expansion given by equation (29) in equation (22) yields:

$$\frac{a_t}{a_i} = \frac{4\varepsilon}{(1+\varepsilon)^2(1+ik\ell) - (1-\varepsilon)^2(1-ik\ell)} + 0(k\ell)^2 = \frac{1}{1+ik\ell\,\dfrac{1+\varepsilon^2}{2\varepsilon}} =$$

$$\frac{1}{1+i\,\dfrac{k_o\ell}{2n}\,(S-if+n^2)} + 0(k\ell)^2 \tag{30}$$

in which equations (13) and (18) have been introduced.

Similarly, equation (23) may be simplified to read

$$\frac{a_r}{a_t} = \frac{i\dfrac{k_o\ell}{2n}(S-if-n^2)}{1+i\dfrac{k_o\ell}{2n}(S-if+n^2)} + 0(k\ell)^2 = \frac{S-if-n^2}{S-if+n^2-i\,\dfrac{2n}{k_o\ell}} + 0(k\ell)^2 \quad . \tag{31}$$

Finally, the simplified expression for the horizontal velocity amplitude within the structure is obtained from equation (21) as

$$\frac{u}{a_i\sqrt{\dfrac{g}{h_o}}} = \frac{1 + ink_o(\ell-x)}{1+i\,\dfrac{k_o\ell}{2n}\,(S-if+n^2)} + 0(k\ell)^2 \quad . \tag{32}$$

To obtain the simplified formulas for the transmission and reflection coefficients from equations (30) and (31) the absolute value is obtained under the assumption that $k\ell$ and $k_o\ell << 1$. From equation (30) it is seen that the transmission coefficient to the adopted degree of accuracy is given by

$$\left|\frac{a_t}{a_i}\right| = T = \frac{1}{1 + \dfrac{k_o\ell f}{2n}} + 0(k\ell)^2 \quad . \tag{33}$$

Introducing

$$\lambda = \frac{k_o\ell f}{2n} \tag{34}$$

the transmission coefficient is therefore given by

$$T = \frac{1}{1+\lambda} + O(k\ell)^2 \quad . \tag{35}$$

In obtaining the reflection coefficient from equation (31) it is seen that the real part of the denominator, $S+n^2$, may be neglected as being small relative to the imaginary part $-i\ (f + 2n/k_o\ell)$ since $k_o\ell << 1$. In the numerator, however, the term $S-n^2$ must be retained since it is of the same order as f unless it is assumed that $f >> 1$. Thus, the simplified solution for the reflection coefficient is obtained from equation (31) as

$$\frac{|a_r|}{a_i} = R = \sqrt{\frac{(S-n^2)^2}{f^2} + 1}\ \left(\frac{\lambda}{1+\lambda}\right) + O(k\ell)^2 \quad , \tag{36}$$

which shows that $R \cong \lambda/(1+\lambda)$ if $f > 1$. Thus, for $f > 1$, which is usually the case, the transmission and the reflection coefficient are independent of the value of the coefficient S. This supports the finding discussed in Section II.1 where it was concluded that the value assigned to S was of minor importance.

For later use, the simplified expression for the horizontal velocity within the structure is found from equation (32) to be

$$\frac{|u|}{a_i\sqrt{\frac{g}{h_o}}} = \frac{1}{1+\lambda} + O(k\ell)^2 \quad , \tag{37}$$

i.e, the velocity within the structure is identical to the velocity associated with the transmitted wave.

The simplified formulas derived here are limited to small values of $nk_o\ell$ by virtue of the nature of the approximation. The equations for T and R (eqs. 35 and 36) may be shown to be in good agreement with the general solutions presented in Figures 2 and 3 for values of $nk_o\ell < 0.2$.

The simplified formulas for the transmission and reflection coefficient may be derived from very simple considerations. Thus, if an incident long wave of amplitude, a_i, is considered normally incident on a structure the maximum free surface elevation in front of the structure may be taken as

$$|\zeta_o| = (1+R)\ a_i \tag{38}$$

with a velocity

$$|u_o| = (1-R)\ a_i \sqrt{\frac{g}{h_o}} \quad . \tag{39}$$

Behind the structure the maximum surface elevation is given by

$$|\zeta_\ell| = T\ a_i \tag{40}$$

with the horizontal velocity being

$$|u_\ell| = T\ a_i \sqrt{\frac{g}{h_o}} \tag{41}$$

The above formulas disregard any phase difference between the reflected, incident, and transmitted waves and are therefore limited to extremely narrow structures.

Disregarding storage within the structure the velocities, $|u_o|$ and $|u_\ell|$, must be equal which leads to

$$1 - R - T = 0 \quad . \tag{42}$$

To obtain an additional equation it is realized that the resistance to the flow through the structure is balancing the pressure force on the structure. This leads, with the linearized flow resistance introduced previously, to

$$f \frac{\omega}{n} \ell |u_\ell| = g(1 + R - T)\ a_i \quad , \tag{43}$$

which for long waves, $\omega = k_o \sqrt{gh}$ and u_ℓ given by equation (41) lead to

$$\frac{k_o \ell f}{2n} 2T = 2\lambda T = 1 + R - T \quad , \tag{44}$$

in which λ, as given by equation (34), has been introduced. Solving equations (42) and (44) for T and R gives

$$T = \frac{1}{1+\lambda} \tag{45}$$

and

$$R = \frac{\lambda}{1+\lambda} \tag{46}$$

thus showing that the preceding simple analysis has reproduced the essential features of the simplified solutions for the transmission and reflection coefficients.

b. Explicit Determination of the Linearized Friction Factor. The general graphical solution for R and T (Figs. 2 and 3) and the simplified solutions (eqs. 35 and 36) require knowledge of the linearized friction factor, f, to be of use. This friction factor which was formally introduced by equation (6) may be determined by invoking Lorentz' principle of equivalent work. This principle, whose use and application are discussed in detail in Appendix A, is particularly appropriate for use in the present context, since the flow resistance within the structure contributes to the problem as a dissipator of energy. Hence, invoking Lorentz' principle, which states that the average rate of energy dissipation should be identical whether evaluated using the true nonlinear resistance law or its linearized equivalent, yields:

$$\bar{\bar{E}}_D = \frac{1}{\forall} \int_{\forall} d\forall \left[\frac{1}{T} \int_0^T \rho f \frac{\omega}{n} U^2 \, dt\right] =$$

$$\frac{1}{\forall} \int_{\forall} d\forall \left[\frac{1}{T} \int_0^T \rho(\alpha U^2 + \beta |U| U^2) dt\right] \tag{47}$$

in which $\forall$ is the volume per unit length occupied by the porous structure, T is the wave period, and $\bar{\bar{E}}_D$ is the spatial and temporal average rate of energy dissipation per unit volume.

The value of U to be used in equation (47) should correspond to the general solution given by equation (21). However, keeping in mind the approximate nature of Lorentz' principle as well as the uncertainties involved in assessing the values of α and β, the simple solution, valid only for $nk_o\ell < 0.2$ (eq. 37) is used. Equation (37) shows $|u|$ and hence U, as given by equation (8) to be independent of location within the porous structure. Since U is necessarily periodic, with period T, the averaging process indicated by equation (47) is readily performed and leads to the following relationship:

$$f \frac{\omega}{n} = \alpha + \beta \frac{8}{3\pi} |u| \quad . \tag{48}$$

With $|u|$ given by equation (37) this is seen to be a quadratic equation in f

$$f \frac{\omega}{n} = \alpha + \beta \frac{8}{3\pi} a_i \sqrt{\frac{g}{h_o}} \frac{1}{1 + \frac{k_o \ell f}{2n}} \qquad (49)$$

which has the solution

$$f = \frac{n}{k_o \ell} [-(1- \frac{k_o \ell \alpha}{2\omega}) + \sqrt{(1 + \frac{k_o \ell \alpha}{2\omega})^2 + \frac{16\beta}{3\pi} a_i \frac{\ell}{h_o}}] . \qquad (50)$$

Thus, an explicit solution for the linearized friction factor in terms of the breakwater geometry, the incident wave characteristics and the hydraulic properties of the porous medium (α and β), has been obtained.

The problem of determining f and hence the reflection and transmission coefficients of a rectangular crib-style breakwater has therefore been reduced to the problem of determining the appropriate values of the constants α and β in the Dupuit-Forchheimer relationship for flow resistance in a porous medium. Engelund (1953) suggested the following empirical formulas based on a review of several investigations involving porous media characterized as sands.

$$\alpha = \alpha_o \frac{(1-n)^3}{n^2} \frac{\nu}{d^2} \qquad (51)$$

and

$$\beta = \beta_o \frac{1-n}{n^3} \frac{1}{d} , \qquad (52)$$

in which ν is the kinematic viscosity of the pore fluid and d is a characteristic diameter of the porous material. These relationships are essentially of the type also suggested by Bear, et al. (1968). Engelund (1953) proposed the values of the constants α_o and β_o to be

$$780 \leq \alpha_o \leq 1{,}500 \text{ or more}$$

$$1.8 \leq \beta_o \leq 3.6 \text{ or more} . \qquad (53)$$

The constant α which is associated with a flow resistance linear with velocity expresses a Darcy-type resistance, i.e., laminar,whereas β is associated with a turbulent resistance. Introducing equations (51) and (52) in equation (48), this may be written:

$$f \frac{\omega}{n} = \beta \frac{8}{3\pi} |u| (1 + \frac{3\pi}{8} \frac{\alpha}{\beta |u|}) = \beta \frac{8}{3\pi} |u| (1 + \frac{R_c}{R_d}) \quad , \tag{54}$$

in which the "particle Reynolds number" R_d is given by

$$R_d = \frac{|u| d}{\nu} \quad , \tag{55}$$

and the "critical Reynolds number" R_c is given by

$$R_c = \frac{3\pi}{8} (1-n)^2 n \frac{\alpha_o}{\beta_o} \simeq 0.17 \frac{\alpha_o}{\beta_o} \quad , \tag{56}$$

as discussed in Appendix A. With α_o and β_o chosen to correspond to the mean values of the ranges indicated in equation (53), the value of the critical Reynolds number is expected to be of the order 70. Thus, for small values of R_d, i.e., $R_d \leq 10$, the flow and the resistance are purely laminar;for large values of R_d, as will be the case for most prototype conditions, i.e., $R_d \geq 1{,}000$, the flow will be turbulent in nature.

Rather than using equation (50) directly with the empirical formulas suggested by equations (51) and (52) it is illustrative to take the relationship for f as given by equation (54) and treating R_d, depending upon the solution through its dependence on $|u|$, as a known quantity. Introducing $|u|$ from equation (37) leads to an implicit expression for f.

$$f = \frac{n}{k_o \ell} [\sqrt{1 + (1 + \frac{R_c}{R_d}) \frac{16\beta}{3\pi} a_i \frac{\ell}{h_o}} - 1] \tag{57}$$

which may also be interpreted as an implicit formula for the factor $\lambda = k_o \ell f/(2n)$. This formula clearly reveals the possible scale effects associated with hydraulic modeling of porous structures to be an increase in the value of f, since R_d would be lower in the model than in the prototype if a Froude model criterion is used.

With the empirical formulas for the hydraulic properties of a porous medium given, a completely explicit procedure for determining the transmission and reflection characteristics of a rectangular crib-style breakwater has been developed.

3. Comparison with Experimental Results.

a. Empirical Formulas for Flow Resistance of a Porous Medium. The procedure developed in Section II.2 for the prediction of transmission and reflection coefficients of porous breakwaters involves the use of empirical relationships for the hydraulic properties of a porous medium. Thus, only if these empirical relationships may be applied with confidence can the procedure itself be regarded as accurate.

For steady flow the Dupuit-Forchheimer resistance law reads

$$-\frac{\partial H}{\partial x} = \frac{1}{g}(\alpha + \beta U)U \quad , \tag{58}$$

in which H is the piezometric head.

In permeameter tests it is customary to measure the head loss, ΔH, over a distance, L_H, for various values of the discharge velocity U. Rearranging equation (58) in a manner similar to that introduced in Section II.2 this may be written

$$g\frac{\Delta H}{L_H} = \beta U^2\left(1 + \frac{\alpha}{\beta U}\right) = \beta_o \frac{(1-n)^2}{n^3}\frac{U^2}{d}\left(1 + \frac{8}{3\pi}\frac{R_c}{R_d}\right) \quad , \tag{59}$$

in which R_d and R_c are given by equations (55) and (56), respectively and β has been introduced according to equation (52). Realizing that the porosity, n, of the porous material tested may vary it is convenient to introduce a reference porosity, n_r, and to write equation (58) in the form

$$C_f^* = \frac{gd}{U^2}\frac{\Delta H}{L_H}\left(\frac{1-n_r}{1-n}\right)\left(\frac{n}{n_r}\right)^3 = \beta_o \frac{1-n_r}{n_r^3}\left(1 + \frac{8}{3\pi}\frac{R_c}{R_d}\right) \tag{60}$$

From experiments the value of C_f^* may be evaluated and plotted against $R_d = Ud/\nu$. The results obtained by Sollitt and Cross (1972, Tables F-1 through F-6) are presented in this manner in Figure 4 with the grain diameter, d, being chosen as the median diameter of the gravel tested and taking $n_r = 0.46$ as the reference porosity. The data exhibit a remarkably low degree of scatter and are well represented by the relationship suggested by equation (59) with $\beta_o = 2.7$ and $R_c = 170$. For comparison, the curve corresponding to $\beta_o = 2.7$ and $R_c = 70$, which correspond to the mean values of the ranges suggested by Engelund's (1953) analysis, equation (53) is shown. Although inferior to the curve corresponding to $R_c = 170$, this curve provides a fair representation of the data.

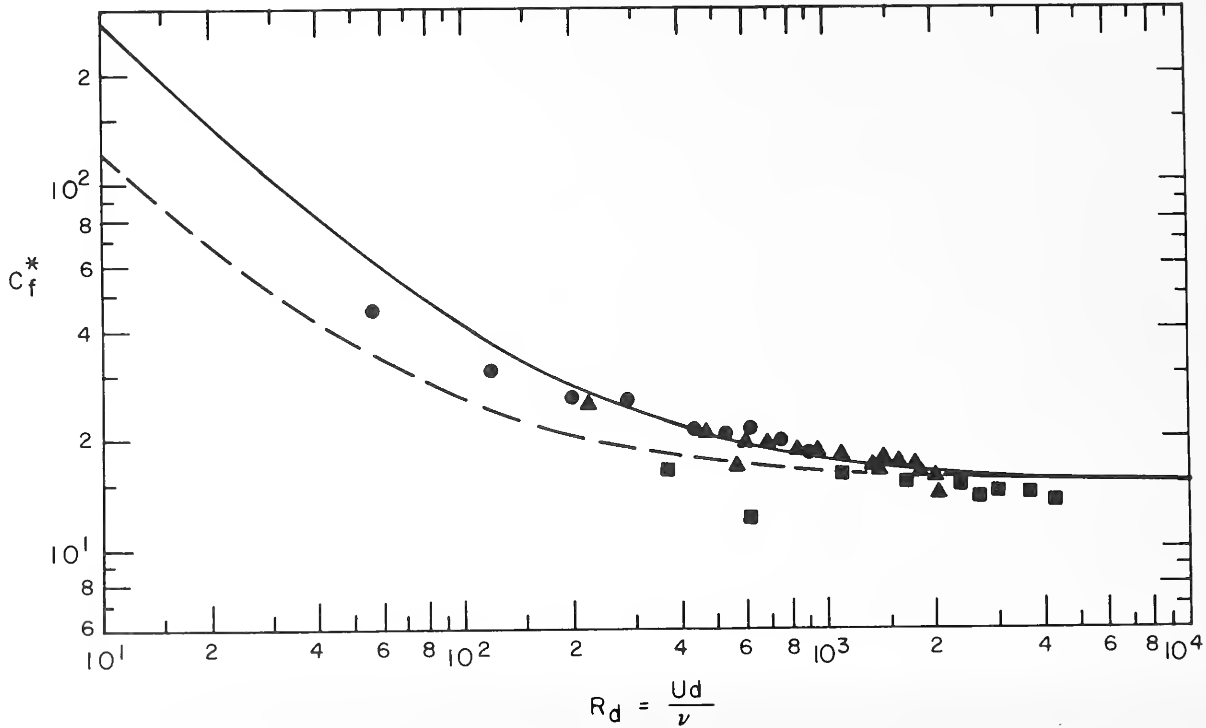

Figure 4. Empirical formula for flow resistance in a porous medium. Experimental data by Sollitt and Cross (1972, Tables F1 through F6); ● : d = 0.031 ft; ▲ : d = 0.0625 ft; ■ : d = 0.125 ft. Empirical relationship, equation (60) with reference porosity n_r = 0.46; ——— : β_o = 2.7, R_c = 170; — — : β_o = 2.7, R_c = 70.

An additional set of data is provided by Keulegan (1973, Table 20). Again the reference porosity is taken as $n_r = 0.46$ and the diameter, d, as the median diameter of the gravel tested. These data are plotted in Figure 5 and exhibit considerably more scatter than that of Sollitt and Cross (1972). The data are fairly well represented by the curve given by equation (59) corresponding to $\beta_o = 2.2$ and $R_c = 70$ whereas the curve corresponding to $\beta_o = 2.7$ gives values of C_f^* slightly on the high side. It should be noted that the data used in Figure 5 are the uncorrected data as obtained by Keulegan (1973). The scatter exhibited in Figure 5 may therefore partly be attributed to the effect of shape of the granular material.

All in all the comparison of the empirical formulas with the experimental data is quite good when considering that the formulas originally were derived from experiments with sand whereas here they are compared with experiments performed with gravel, i.e., of diameters an order of magnitude larger. Whether or not the same formulas may be extended further to prototype scales (rubble) with complete confidence is a question which remains to be answered. However, at present it does seem that a value of $\beta_o \simeq 2.7$ may be used as a reasonable first approximation.

b. Comparison between Predicted and Observed Reflection and Transmission Coefficients of Rectangular Breakwaters. The empirical formulas for the hydraulic properties of a porous medium were shown to be reasonably satisfactory in reproducing observed characteristics of porous media in steady flow. The ultimate test of these formulas is, however, their use as part of the entire procedure developed in Section II.2 for the prediction of transmission and reflection coefficients of crib-style breakwaters. Two sets of experimental data on reflection and transmission characteristics of porous rectangular breakwaters are available for this purpose (Wilson, 1971; Keulegan, 1973).

The experiments by Wilson (1971, Tables 5,6, and 7) were performed on three different scales, and for the present purpose only, the experimental data corresponding to relatively long waves, $k_o h_o \simeq 0.5$, are utilized. Wilson's experimental data for R and T are plotted in Figures 6,7, and 8 as functions of the incident wave steepness, H_i/L. The predicted variation of R and T with H_i/L following the procedure developed in Section II.2 is shown based on the assumption of $\beta_o = 2.7$, $R_c = 170$, and $R_c = 70$. In view of the results presented in Figure 4 it is hardly surprising that the experimental data are represented better by the curves corresponding to $R_c = 170$ than by the choice $R_c = 70$. The predicted values of the transmission coefficient, T, are seen to be in excellent agreement with experimental values whereas the agreement between reflection coefficients leaves something to be desired.

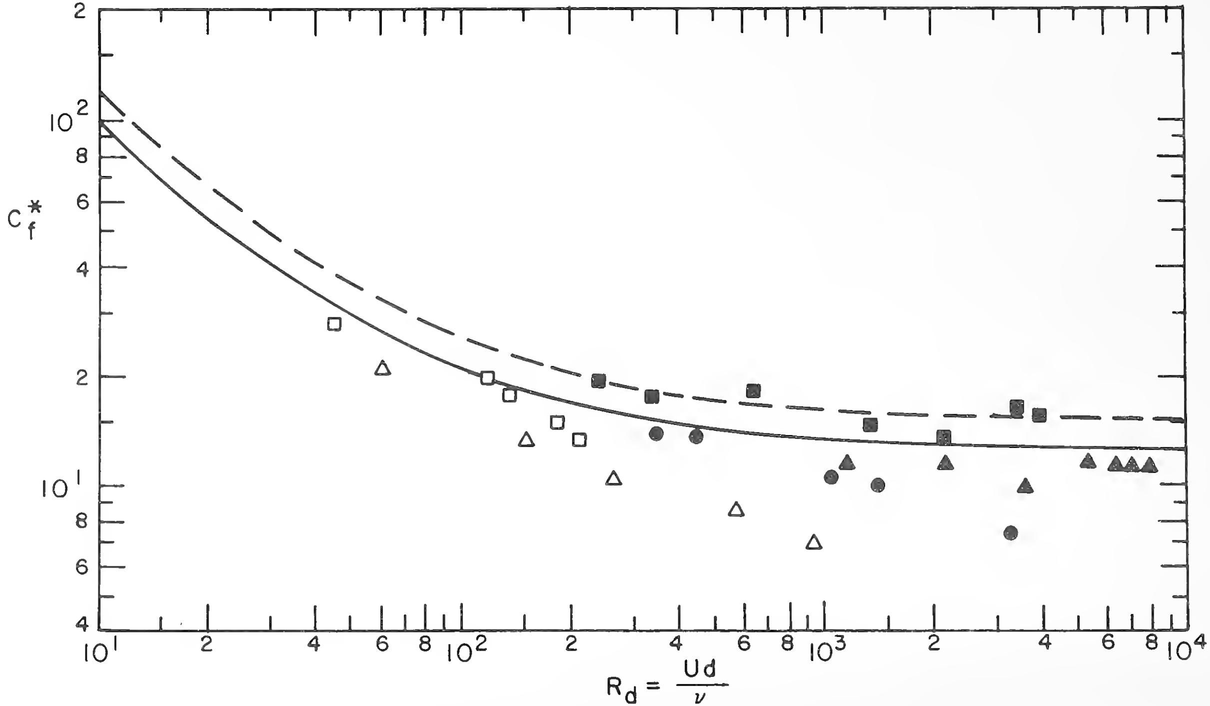

Figure 5. Empirical formula for flow resistance in a porous medium. Experimental data by Keulegan (1973, Table 20); □ : d = 0.036 ft; △ : d = 0.052 ft; ● : d = 0.078 ft; ■ : d = 0.115 ft; ▲ : d = 0.188 ft. Empirical relationship, equation (60), with reference porosity n_r = 0.46; ——— : β_o = 2.2, R_c = 70; — — — : β_o = 2.7, R_c = 70.

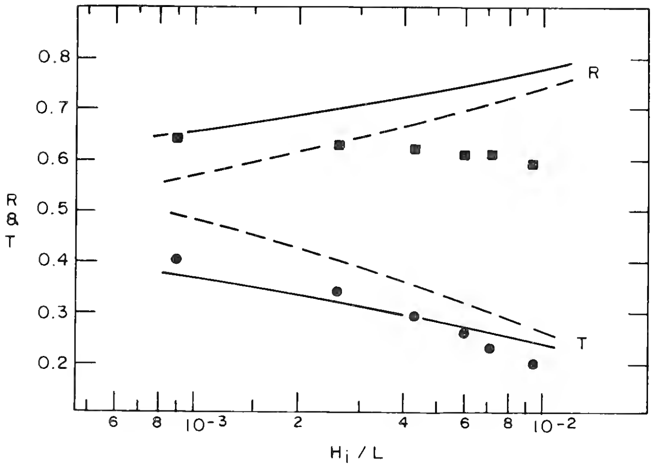

Figure 6: Comparison between Predicted and Experimental Transmission, T, and Reflection Coefficients, R. Wilson's (1973, Table 5) data with $k_o h_o$ = 0.482, d = 0.031 ft, ℓ = h_o = 0.432 ft; ■ : Reflection Coefficient; ● : Transmission Coefficient. Predicted values; —— : β_o = 2.7, R_c = 170; — —: β_o = 2.7, R_c = 70.

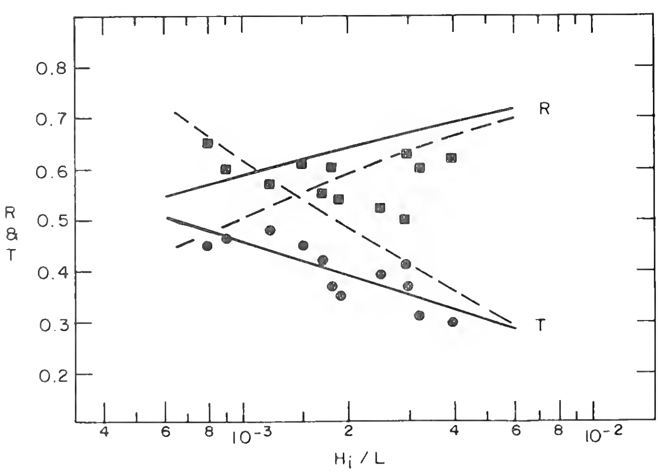

Figure 7: Comparison between Predicted and Experimental Transmission, T, and Reflection Coefficients, R. Wilson's (1973, Table 6) data with 0.45 · $k_o h_o$ 0.51, d = 0.0625 ft, ℓ = h_o = 1.0 ft; ■ : Reflection Coefficient; ● : Transmission Coefficient. Predicted values; —— : β_o = 2.7, R_c = 170; — —: β_o = 2.7, R_c = 70.

The experimental values of the reflection coefficient were obtained from Healy's formula (Eagleson and Dean, 1966)

$$R = \frac{H_{max} - H_{min}}{H_{max} + H_{min}} \quad , \tag{61}$$

where H_{max} is the maximum wave height (measured at the antinode) and H_{min} is the minimum wave height (measured at the node) of the wave envelope in the reflected wave region. Equation (61) shows that H_{min} is considerably smaller than H_{max} when the reflection coefficient approaches unity. If it is assumed that H_{max} is correctly determined but the value obtained for the minimum wave height incorporates an error, Δ, equation (61) may be written

$$R = \frac{H_{max} - H_{min}}{H_{max} + H_{min}} \; \frac{1 - \dfrac{\Delta}{H_{max} - H_{min}}}{1 + \dfrac{\Delta}{H_{max} + H_{min}}} \quad , \tag{62}$$

in which H_{max} and H_{min} are assumed to be the true values. The error, Δ, in the experimental determination of H_{min} will generally be positive due to nonlinear effects. Equation (62) therefore shows that the experimentally determined reflection coefficient will be lower than the true reflection coefficient due to the measurement error, Δ. This problem is addressed in detail in Section III.3; here it is just pointed out to illustrate that one must pay special attention to minimizing the experimental error in the determination of H_{min}. No particular attention was paid to this problem by Wilson (1971) who applied equation (61) directly. It is clear from equation (62) that with the error Δ increasing with increasing nonlinearity of the incident waves, i.e., with increasing H_i/L, a trend of determining an experimental reflection coefficient which decreases with incident wave height results. This may partly explain the behavior of the experimentally determined reflection coefficients in Figures 6,7, and 8 as being nearly constant with H_i/L whereas the predicted reflection coefficients show R to increase with increasing values of H_i/L.

Since Wilson's (1971) experiments essentially correspond to scale models of the same structure, performed for different length scales, these experiments give an excellent exposition of the scale effects associated with hydraulic-model tests of porous structures. It is seen from the generally good agreement between predicted and observed transmission coefficients that the present analytical procedure may be used with confidence in assessing the influence of scale effects on experiments of this type. The Froude model criterion applies only so long as the flow resistance is predominantly turbulent, i.e., f is given by equation (57) with $R_c/R_d << 1$. The scale effect is accounted for in the present analysis by the inclusion of the effect of the ratio R_c/R_d which in a Froude model will be greater in the model than in the prototype.

An additional set of experiments is reported by Keulegan (1973). These experiments were performed for rectangular breakwaters of different materials and widths ℓ = 0.25, 0.5, and 1 foot. As an example the experimental data corresponding to relatively long waves, $h_o/L = 0.1$, as reported by Keulegan (1973, Table 12) are plotted in Figures 9, 10, and 11 versus H_i/L. For comparison the predictions afforded by the procedure developed in Section II.2 are also shown. The choice of parameters $\beta_o = 2.2$, $R_c = 70$ yields a slightly better representation of the experimental data as could be expected from the comparison made in Figure 5. However, the predictions obtained from $\beta_o = 2.7$, $R_c = 70$ are fairly good. The discrepancy between observed and predicted reflection coefficients is of the type noted in conjunction with the comparison with Wilson's (1971) data and may again partially be attributed to experimental errors in the determination of R. Keulegan's (1973) and Wilson's data on the reflection coefficient show the tendency of decreasing slightly with increasing height of the incident waves. However, it is noted that the experimental reflection coefficient (Fig. 9) increases slightly with H_i/L. Since the reflection coefficient for this set of experiments is relatively small, $R \simeq 0.3$, the error in the experimental determination of H_{min} may be expected to be rather small, thus essentially substantiating the previous hypothesis for the nature of the discrepancy.

As a final comparison between the experimental data presented by Keulegan (1973) and the analytical procedure developed in this study, Figures 12 and 13 show a comparison between observed and predicted transmission and reflection coefficients for all the experiments reported by Keulegan corresponding to $h_o/L \simeq 0.1$ and $H_i/h_o = 0.1$. With the generally good agreement between the experimental and predicted transmission coefficients exhibited in Figures 9,10, and 11, the comparison given in Figure 12 shows the general applicability of the present procedure to predict transmission coefficients. The comparison of reflection coefficients given in Figure 13 is quite encouraging. However, it should be recalled that the predicted trend of increasing R with H_i/L was not observed in the experimental data.

4. Discussion and Application of Results.

A theoretical solution for the transmission and reflection characteristics of a homogeneous breakwater of rectangular cross section was obtained. The main assumptions were that the incident waves should be normal to the breakwater and that the motion should be adequately described by linear long wave theory. The general solution for the transmission coefficient, T, and the reflection coefficient, R, is presented in graphical form in Figures 2 and 3. For small values of

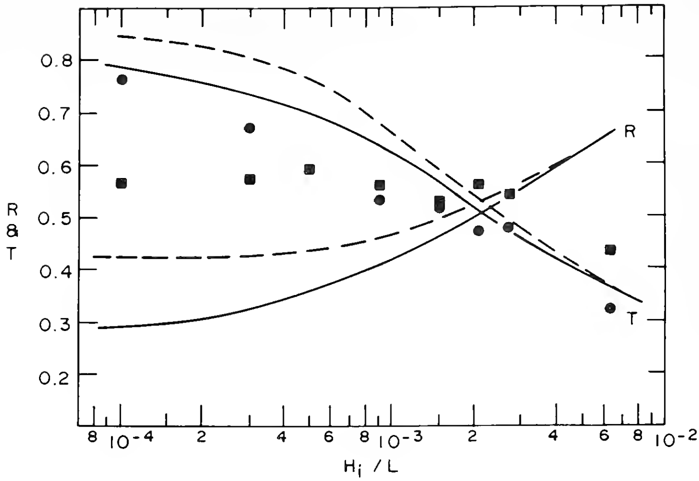

Figure 8: Comparison between Predicted and Experimental Transmission, T, and Reflection Coefficients, R. Wilson's (1973, Table 7) data with $k_o h_o$ = 0.503, d = 0.125 ft, ℓ = h_o = 1.81 ft; ■ : Reflection Coefficient; ● : Transmission Coefficient. Predicted values; ——— : β_o = 2.7, R_c = 170; — —: β_o = 2.7, R_c = 70.

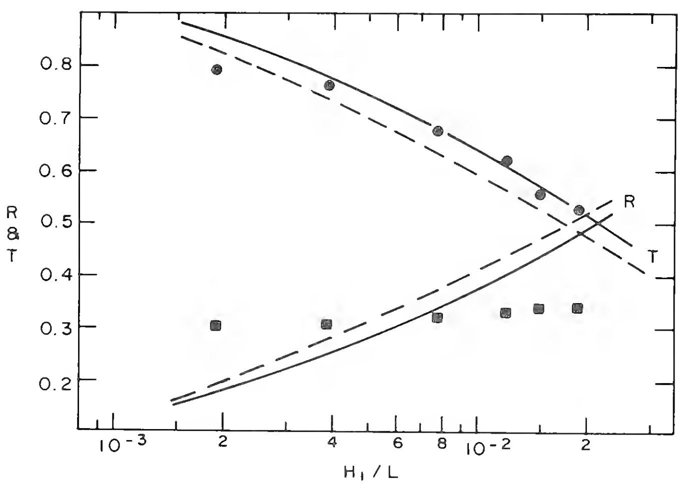

Figure 9: Comparison between Predicted and Experimental Transmission, T, and Reflection Coefficients, R. Keulegan's (1973, Table 12) data for h_o/L = 0.1, d = 0.078 ft, h_o = 1 ft, ℓ = 0.25 ft; ■ : Reflection Coefficient; ● : Transmission Coefficient. Predicted values; ——— : β_o = 2.2, R_c = 70; —— ——: β_o = 2.7, R_c = 70.

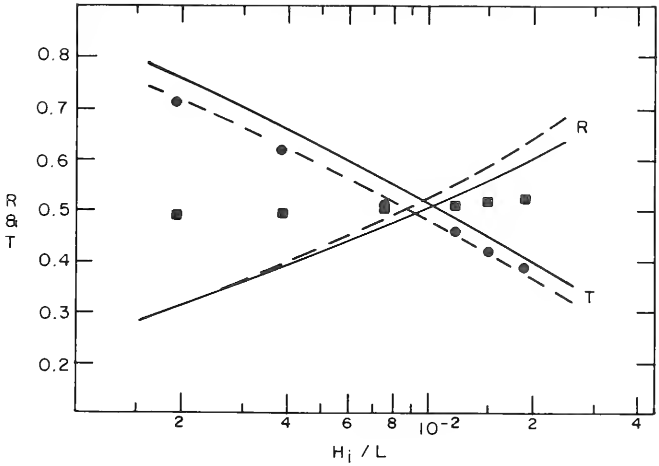

Figure 10: Comparison between Predicted and Experimental Transmission, T, and Reflection Coefficients, R. Keulegan's (1973, Table 12) data with h_o/L = 0.1, d = 0.078 ft., h_o = 1 ft, ℓ = 0.5 ft; ■ : Reflection Coefficient; ● : Transmission Coefficient. Predicted values; ——: β_o = 2.2, R_c = 70; — —: β_o = 2.7, R_c = 70.

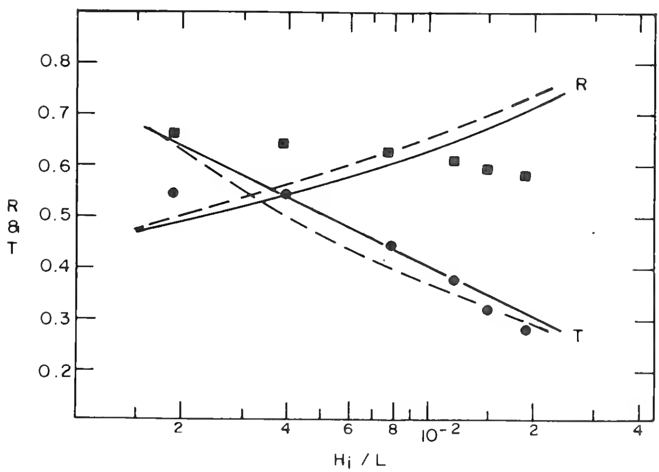

Figure 11: Comparison between Predicted and Experimental Transmission, T, and Reflection Coefficients, R. Keulegan's (1973, Table 12) data with h_o/L = 0.1, d = 0.078 ft, h_o = 1 ft, ℓ = 1.0 ft; ■ : Reflection Coefficient; ● : Transmission Coefficient. Predicted values; ——: β_o = 2.2, R_c = 70; — —: β_o = 2.7, R_c = 70.

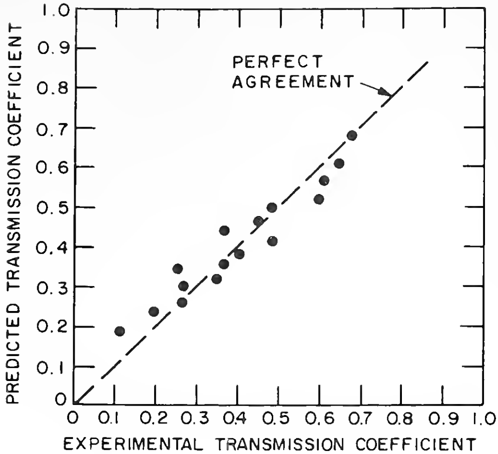

Figure 12: Comparison between Predicted and Experimental Transmission Coefficients. Experiments for $H_i/h_o = 0.1$ by Keulegan (1973, Tables 4, 8, 12 and 16). Predictions based on $\beta_o = 2.7$ and $R_c = 70$.

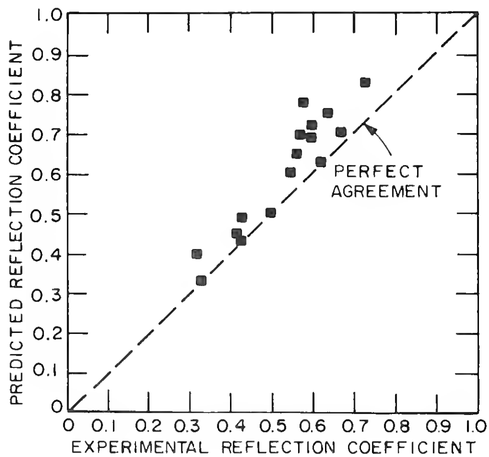

Figure 13: Comparison between Predicted and Experimental Reflection Coefficients. Experiments for $H_i/h_o = 0.1$ by Keulegan (1973, Tables 4, 8, 12 and 16). Predictions based on $\beta_o = 2.7$ and $R_c = 70$.

the width of the breakwater, ℓ, relative to the incident wavelength, L, a set of simple formulas was derived for T and R, equations (35) and (36).

From equations (35) and (36) as well as from Figures 2 and 3 it is seen that the transmission coefficient increases and the reflection coefficient decreases with decreasing values of $nk_o\ell$. This is in agreement with expectations since low values of $k_o\ell$ indicate a long wave relative to the width of the structure thus essentially making the structure transparent to the incident waves. An increase in frictional effects, which are accounted for by the linearized friction factor, f, is seen to cause an increase in the reflection coefficient and a decrease in the transmission coefficient. In this respect it is seen from equation (57), which is the explicit solution for the linearized friction factor, f, that the frictional effects increase with increasing amplitude of the incident waves, thus reflecting the nonlinear nature of the flow resistance of the porous structure.

The procedure developed is, through the adoption of empirical relationships for the hydraulic properties of the porous medium, entirely explicit. The required information is the incident wave characteristics (a_i and L), the breakwater geometry (ℓ and h_o), and the characteristics of the porous material (stone size, d, and porosity, n). The ability of the procedure to predict experimentally observed transmission and reflection characteristics of crib-style breakwaters was demonstrated. It was found that the procedure yields excellent predictions of the transmission coefficient whereas some discrepancy between observed and predicted reflection coefficients was noted. This discrepancy may be partly attributed to experimental error in the determination of the reflection coefficient.

Numerical Example. The following numerical example is included to illustrate the application of the procedure developed for the prediction of transmission and reflection coefficients of a porous rectangular breakwater. The information which is assumed available is listed in Table 1. To illustrate the assessment of scale effects the problem is considered both for a prototype and for a Froude model with length scale 1 to 25.

As discussed in Section I the procedure developed in this Section of the report accounts for the partition of incident wave energy among reflected, transmitted, and internally dissipated energy. Thus, the present Section forms part of the ultimate procedure for the prediction of reflection and transmission characteristics of trapezoidal, multi-layered breakwaters. The energy dissipation taking place on the seaward slope of a trapezoidal breakwater is discussed in Section III which also includes a numerical example. The incident wave characteristics listed in Table 1 correspond to the incident wave assumed in the numerical example presented in Section III, Table 4, after subtracting the amount of energy dissipated on the seaward slope of a trapezoidal

Table 1. Information used in numerical sample calculations.

	Prototype	Froude Model length scale 1:25
Incident Wave Amplitude a_I in feet	1.45	0.058
Wave Period T in seconds	12.5	2.5
Water Depth h_o in feet	29.2	1.167
Incident Wavelength[1] L in feet	366.0	14.56
Breakwater Width ℓ in feet	63.0	2.52
Stone Diameter $d = 1/2(d_{max} + d_{min})$ in feet	1.56	0.0625
Porosity[2] n	0.435	0.435

[1] L may be obtained from linear wave theory using h_o and T.

[2] The porosity is assumed. Sensitivity of results to this assumption should be investigated.

breakwater. The present numerical example together with the numerical example presented in Section III therefore illustrate the detailed calculations involved in the procedure for the prediction of reflection and transmission coefficients of trapezoidal, multilayered breakwaters which is developed in Section IV. The model breakwater characteristics listed in Table 1 correspond to the characteristics of the crib-style breakwater which is hydraulically equivalent to the breakwater configuration tested by Sollitt and Cross (1972). The determination of the hydraulically equivalent breakwater is discussed in detail in Section IV.3.

To use the general solution presented graphically in Figures 2 and 3 the value of S_* is obtained from equation (28)

$$S_* = \left(\frac{n}{0.45}\right)^2 = \left(\frac{0.435}{0.45}\right)^2 = 0.935 \quad . \tag{63}$$

The value of the parameter $nk_o\ell$ may also be determined directly from the information contained in Table 1

$$nk_o\ell = (0.435)(2\pi)\,\frac{\ell}{L} = (0.435)(2\pi)\,\frac{63}{366} = 0.47 \quad , \tag{64}$$

which is valid for the prototype as well as for the Froude model. It is noticed that the value of $nk_o\ell$ is sufficiently large for Figures 2 and 3 to be used. If $nk_o\ell$ had been below 0.1 the simplified formulas, equations (35) and (36), should be used with $S = 1.0$.

The remaining task is the determination of the friction factor, f, from equation (57). For the prototype conditions it is expected that turbulent flow resistance dominates so that the factor R_c/R_d may be neglected in equation (57). Therefore the remaining expression becomes:

$$f = \frac{n}{k_o\ell}\left[\sqrt{1 + \frac{16\beta}{3\pi}\, a_I\, \frac{\ell}{h_o}} - 1\right] \quad . \tag{65}$$

In this expression the value of β is taken according to equation (52) with $\beta_o = 2.7$, a reasonable estimate as discussed in Section II.3. Thus,

$$f = \frac{n}{k_o\ell}\left[\sqrt{1 + \frac{16\beta_o}{3\pi}\,\frac{1-n}{n^3}\,\frac{a_I}{d}\,\frac{\ell}{h_o}} - 1\right] =$$

$$\frac{0.435}{2\pi\; 63/366}\left[\sqrt{1 + \frac{16}{3\pi}\,2.7\,\frac{0.565}{(0.435)^3}\,\frac{1.45}{1.56}\,\frac{63}{29.2}} - 1\right] =$$

$$0.4\,\left[\sqrt{1 + 63} - 1\right] = 2.8 \quad . \tag{66}$$

This value of f is obtained for the prototype conditions assuming $R_d >> R_c$ where R_d is the particle Reynolds number defined by equation (55) with $|u|$ given by equation (37). To check this assumption the value of λ is obtained from equations (34) and (66) as

$$\lambda = \frac{k_o \ell f}{2n} = \frac{(2\pi\ 63/366)2.8}{0.87} = 3.5 \quad , \tag{67}$$

and therefore from equation (37)

$$|u| = a_I \sqrt{\frac{g}{h_o}} \left(\frac{1}{1+\lambda}\right) = 1.45 \sqrt{\frac{32.2}{29.2}} \left(\frac{1}{1+3.5}\right) = 0.34 \text{ ft/sec} . \tag{68}$$

This gives a value of the particle Reynolds number

$$R_d = \frac{|u|d}{\nu} = \frac{0.34\ (1.56)}{10^{-5}} = 5.3 \text{ X } 10^4 \tag{69}$$

where the kinematic viscosity has been assumed given by $\nu = 10^{-5} \text{ft}^2/\text{sec}$. This value is clearly much greater than the value of the critical Reynolds number, R_c, which is of the order 100. Thus, the value of f determined by equation (66) holds for the prototype condition and the necessary parameters for use in conjunction with Figures 2 and 3 may be determined for the prototype

$$\left.\begin{aligned} nk_o\ell &= 0.47 \\ S_* &= 0.935 \\ f/S_* &= 2.8/0.935 = 3.0 \end{aligned}\right\} \text{Prototype} \quad , \tag{70}$$

and Figures 2 and 3 yield for the prototype:

Transmission coefficient = T = 0.22

Reflection coefficient = R = 0.71 . (71)

For the Froude model one may as a first approximation adopt the assumption that $R_d >> R_c$, in which case the estimate of f obtained for the prototype still holds, i.e., f = 2.8 is a first estimate. To evaluate the value of the particle Reynolds number, R_d, the procedure is as previously outlined and from the well-known scaling of Reynolds numbers in a Froude model,

$$(\text{Reynolds number scale}) = (\text{length scale})^{3/2} \quad , \tag{72}$$

it follows from the length scale of 1:25 and from equation (69) that

$$R_{dm} = 5.3\ (10^4)\ (\frac{1}{25})^{3/2} = 425\ . \tag{73}$$

This is not a value much greater than R_c and it is therefore necessary to incorporate the Reynolds number effect in equation (57) when evaluating f. For this purpose it is assumed that a simple test has shown that

$$R_c = 170 \quad ; \ \beta_o = 2.7 \quad , \tag{74}$$

for the material used in the model.

Taking R_d as given by equation (73) the expression for f (eq. 57) reads:

$$f = \frac{n}{k_o \ell}\ [\sqrt{1 + \frac{16\beta}{3\pi}\ (1 + \frac{R_c}{R_d})\ a_I\ \frac{\ell}{h_o}} - 1] =$$

$$0.4\ [\ \sqrt{1 + (1 + \frac{170}{425})63} -1] = 3.4 \quad , \tag{75}$$

in which the analogy with the manipulations performed in equation (66) has been utilized. From this result an updated value of λ is obtained since $\lambda = f/0.8 = 4.25$. This value of λ is different from the value. $\lambda = 3.5$, used in determining the particle Reynolds number R_d used in the evaluation of equation (75). With this new value of λ, equations (37) and (55) may be used to obtain a new value of R_d. This in turn may be introduced in equation (75) to get a new value of f and the procedure may be continued until convergence is achieved. It may be shown that

$$R_{d,2} = R_{d,1}\ \frac{1+\lambda_1}{1+\lambda_2} \quad , \tag{76}$$

in which $R_{d,2}$ is the new estimate of R_d, whereas $R_{d,1}$ is the previous estimate and λ_1 and λ_2 are the old and new estimates of λ, respectively.

This procedure is generally rapidly converging. Thus, the next iteration outlined above yields f = 3.46 which is reasonably close to the initial estimate obtained in equation (75).

For the Froude scale model the parameters therefore become

$$\left.\begin{aligned} nk_o\ell &= 0.47 \\ S_* &= 0.935 \\ f/S_* &= 3.46/0.935 = 3.7 \end{aligned}\right\} \text{Model} \tag{77}$$

and Figures 2 and 3 yield:

$$\begin{aligned} &\text{Transmission coefficient} = T = 0.19 \\ &\text{Reflection coefficient} = R = 0.73 \quad . \end{aligned} \tag{78}$$

By comparing the predicted results for the model (eq. 78), and for the prototype (eq. 71), it is seen that the scale effect has increased the reflection coefficient, whereas the transmission coefficient is decreased. For the present example the scale effects are not pronounced, but in other situations it may be a very important factor to consider (Figs. 6, 7, and 8)

III. REFLECTION COEFFICIENTS OF ROUGH IMPERMEABLE SLOPES

1. Preliminary Remarks.

In the previous section of this report an analytical solution for the idealized problem of wave transmission through and reflection from rectangular breakwaters was obtained. Since most breakwaters are of trapezoidal, rather than rectangular cross section, a considerable amount of energy may be dissipated on the seaward slope of the breakwater. This external dissipation of energy is not accounted for in the analysis of porous crib-style breakwaters. To account for the external dissipation of energy on the seaward slope of a trapezoidal breakwater the associated problem of energy dissipation on a rough impermeable slope is considered both theoretically and experimentally.

A theoretical analysis of this problem is based on the following assumptions:

(a) Relatively long normally incident waves which may be considered to be adequately described by linear long wave theory.

(b) Energy dissipation on the rough impermeable slope may be represented as the energy dissipation due to bottom frictional effects.

The first assumption is identical to the assumption made in Section II of this report. The second assumption presumes that the effect of energy dissipation due to wave breaking is minor. This may seem to be a restrictive assumption. When realizing that the seaward slopes of breakwaters are generally steep, this assumption is quite reasonable. At any rate, the main purpose of the theoretical analysis is to produce a rational framework within which the experimental results for reflection coefficients of rough impermeable slopes may be analyzed.

The essential features of the mathematical manipulations and the derivation of the governing equations are presented in Appendix A to enable the treatment to be relatively brief and to the point. The frictional effects on the rough slope are accounted for by introducing a term relating the bottom shear stress to the square of the horizontal orbital velocity through the use of a wave friction factor, f_w, analogous to that introduced by Jonsson (1966). The bottom shear stress is linearized and a theoretical solution for the reflection coefficient of rough impermeable slopes is obtained in terms of a linearized slope friction factor. By using Lorentz' principle of equivalent work an implicit solution for the reflection coefficient of rough impermeable slopes is obtained in terms of incident wave characteristics, slope geometry, and the wave friction factor, f_w, which expresses the effect of slope roughness.

An extensive experimental investigation is performed to establish an empirical relationship for the wave friction factor. The experimental investigation utilizes measured reflection coefficients of rough impermeable slopes in conjunction with the theoretical results to obtain values of the wave friction factor. The experimental investigation shows the need for a method for obtaining accurate estimates of reflection coefficients from experimental data. Such a method is developed and the end product of the experimental investigation is empirical relationships for the wave friction factor. The experiments are performed with slope roughnesses modeled by gravel and are therefore applicable only when the slope roughness elements consist of natural stones. Separate experimental investigations should be carried out to establish empirical relationships for f_w, corresponding to other surface roughness elements, e.g., concrete armor units.

The result of the combined use of the empirical relationship for f_w and the theoretical developments is a "semiempirical" procedure for estimating the reflection coefficient and hence the energy dissipation of rough slopes. The procedure requires knowledge of the incident wave characteristics (amplitude and wavelength) and the slope characteristics (slope angle and stone size). The procedure was tested against a separate set of experiments and yielded quite accurate results.

2. Theoretical Solution for the Reflection Coefficient of Rough Impermeable Slopes.

The problem to be considered is illustrated in Figure 14.

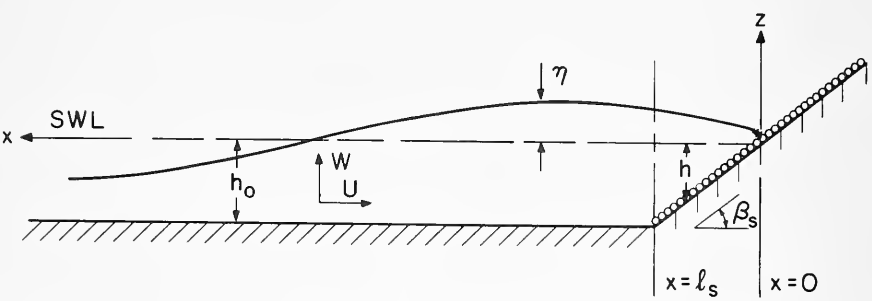

Figure 14. Definition sketch.

With the assumption of relatively long incident waves the governing equations for arbitrary bottom topography are derived in Appendix A, equations (A-20) and (A-21). The linearized forms of these equations are given by equations (A-24) and (A-25)

$$\frac{\partial \eta}{\partial t} + \frac{\partial}{\partial x}(hU) = 0 \tag{79}$$

and

$$\frac{\partial U}{\partial t} + g\frac{\partial \eta}{\partial x} + f_b \omega U = 0 \quad , \tag{80}$$

in which η is the surface elevation relative to the stillwater level, U is the horizontal velocity component, h is the local depth, g is the acceleration due to gravity, ω is the radian frequency, $\omega = 2\pi/T$, of the incident waves and f_b is a linearized friction factor defined by equation (A-23)

$$f_b \omega = \frac{\frac{1}{2} f_w |U|}{h} \tag{81}$$

in which f_w is a wave friction factor relating bottom shear stress, τ_b, fluid density ρ, and the velocity, i.e.,

$$\tau_b = \frac{1}{2} \rho f_w |U| U \quad . \tag{82}$$

The linearized equations (eqs. 79 and 80), are solved by assuming a periodic solution of radian frequency, ω, and introducing complex variables defined by

$$\eta = \text{Real}\{\zeta(x) e^{i\omega t}\} \tag{83}$$

and

$$U = \text{Real}\{u(x) e^{i\omega t}\} \quad , \tag{84}$$

in which the amplitude functions ζ and u are functions of x only, $i = \sqrt{-1}$, and only the real part of the complex solution constitutes the physical solution.

In the constant depth region, $h = h_o$, in front of the slope, bottom friction is neglected (i.e., $f_w = f_b = 0$ for $x > \ell_s$) and the general solution reduces to the solution given in Section II.2 for $x < 0$. With the change of the orientation of the x-axis (positive away from the slope as seen from Figure 14) the general solution for $x > \ell_s$ is

$$\left.\begin{aligned} \zeta &= a_i e^{ik_o x} + a_r e^{-ik_o x} \\ u &= -\sqrt{\frac{g}{h_o}}\,(a_i e^{ik_o x} - a_r e^{-ik_o x}) \end{aligned}\right\}\ x \geq \ell_s \ , \tag{85}$$

where a_i is the amplitude of the incident wave, which without loss of generality may be taken to be real, and a_r is the complex amplitude of the reflected wave. The wave number, $k_o = 2\pi/L$, where L is the wave-length of the incident wave, is given by

$$k_o = \frac{\omega}{\sqrt{gh_o}} \ . \tag{86}$$

On the rough impermeable slope, $0 \leq x \leq \ell_s$, the effect of bottom friction is retained and equation (80) may be written

$$u = -\frac{g}{i\omega(1-if_b)}\frac{\partial\zeta}{\partial x} \quad ; \quad 0 \leq x \leq \ell \ , \tag{87}$$

when equations (83) and (84) are introduced.

Multiplying equation (87) by h to obtain an expression for $\partial(uh)/\partial x$ and introducing this in equation (79) yield the governing equation

$$\frac{\partial}{\partial x}\left(h\frac{\partial\zeta}{\partial x}\right) + \frac{\omega^2(1-if_b)}{g}\,\zeta = 0 \quad ; \quad 0 \leq x \leq \ell_s \ . \tag{88}$$

With the depth varying linearly on the slope, i.e.,

$$h = x\tan\beta_s \quad ; \quad 0 \leq x \leq \ell_s \ , \tag{89}$$

equation (88) is seen to be a special form of the Bessel Equation (Hildebrand, 1965) with the solution

$$\zeta = A\,J_o\left(2\sqrt{\frac{\omega^2(1-if_b)x}{g\tan\beta_s}}\right) \quad ; \quad 0 \leq x \leq \ell_s \ , \tag{90}$$

in which J_o is the Bessel function of the first kind of order zero. The general solution includes also the Bessel function of the second kind, Y_o. However, this solution blows up at the origin, $x = 0$, and for the solution to remain finite at $x = 0$ this part of the general solution is omitted. For $x \to 0$, J_o approaches unity so that the arbitrary constant A in equation (90) is the complex vertical amplitude of the wave motion at the intersection of the stillwater level and the slope, i.e., $|A|$ may be interpreted as a measure of the runup on the slope. It should be realized that the linearized solution, as discussed in Appendix A, is based on the assumption that $|\eta| << h$. Thus, since $h = 0$ at $x = 0$ the solution given by equation (90) cannot be considered valid near $x = 0$. However, Meyer and Taylor (1972) have shown that a linear solution gives essentially the same value of the runup as does the more realistic solution based on the nonlinear shallow-water wave equations. Thus, some physical significance may be attached to the magnitude of A, $|A|$, as being an approximate value of the runup on the slope.

With ζ given by equation (90) the horizontal velocity is evaluated from equation (87)

$$u = -iA \sqrt{\frac{g}{(1-if_b)x \tan\beta_s}} \; J_1\left(2 \sqrt{\frac{\omega^2(1-if_b)x}{g \tan\beta_s}}\right); \quad 0 \leq x \leq \ell_s , \qquad (91)$$

in which J_1 is the Bessel function of the first kind of order one.

With the general solution given by equations (85), (90), and (91) the complex amplitude of the reflected wave, a_r, and the complex runup amplitude, A, are determined by matching the solutions for ζ and u at their common boundary, $x = \ell_s$. Thus, at $x = \ell_s$

$$a_i e^{ik_o\ell_s} + a_r e^{-ik_o\ell_s} = A \, J_o(2k_o\ell_s \sqrt{1-if_b}) \qquad (92)$$

and

$$a_i^{\,ik_o\ell_s} - a_r e^{ik_o\ell_s} = A \, \frac{i}{\sqrt{1-if_b}} \, J_1 \, (2k_o\ell_s \sqrt{1-if_b}) \qquad (93)$$

in which $h_o = \ell_s \tan\beta_s$ and equation (86) have been introduced.

These equations are readily solved to give the complex amplitude of the reflected wave.

$$\frac{a_r}{a_i} = \frac{J_o(2k_o\ell_s\sqrt{1-if_b}) - \dfrac{i}{\sqrt{1-if_b}} J_1(2k_o\ell_s\sqrt{1-if_b})}{J_o(2k_o\ell_s\sqrt{1-if_b}) + \dfrac{i}{\sqrt{1-if_b}} J_1(2k_o\ell_s\sqrt{1-if_b})} e^{i2k_o\ell_s} \qquad (94)$$

and the complex runup amplitude

$$\frac{A}{2a_i} = \frac{e^{ik_o\ell_s}}{J_o(2k_o\ell_s\sqrt{1-if_b}) + \dfrac{i}{\sqrt{1-if_b}} J_1(2k_o\ell_s\sqrt{1-if_b})} \; . \qquad (95)$$

It can be seen from equation (94) that $|a_r|$, which is the physical amplitude of the reflected wave, is equal to a_i for $f_b = 0$. Since $f_b = 0$ expresses the condition that the energy dissipation on the slope is zero, this is to be expected.

Equations (94) and (95) show that the important parameters in determining the reflected wave amplitude and the runup amplitude are the length of the slope relative to the length of the incident waves in front of the slope, ℓ_s/L, and the friction factor, f_b, arising from the linearization of the bottom friction term. Since the linearized friction factor appears in the form $\sqrt{1-if_b}$ it is expedient to introduce the friction angle ϕ defined by

$$\tan 2\phi = f_b \quad ; \quad 0 \leq 2\phi \leq \frac{\pi}{2} \; , \qquad (96)$$

since

$$\sqrt{1-if_b} = (1 + \tan^2 2\phi)^{1/4} \; e^{-i\phi} \; . \qquad (97)$$

In terms of the relative slope length, ℓ_s/L, and the friction angle, ϕ, the reflection coefficient, $R = |a_r|/a_i$, may be determined from equation (94). This solution is presented in graphical form in Figure 15.

Similarly the nondimensional runup amplitude,

$$R_u = \frac{|A|}{2a_i} \; , \qquad (98)$$

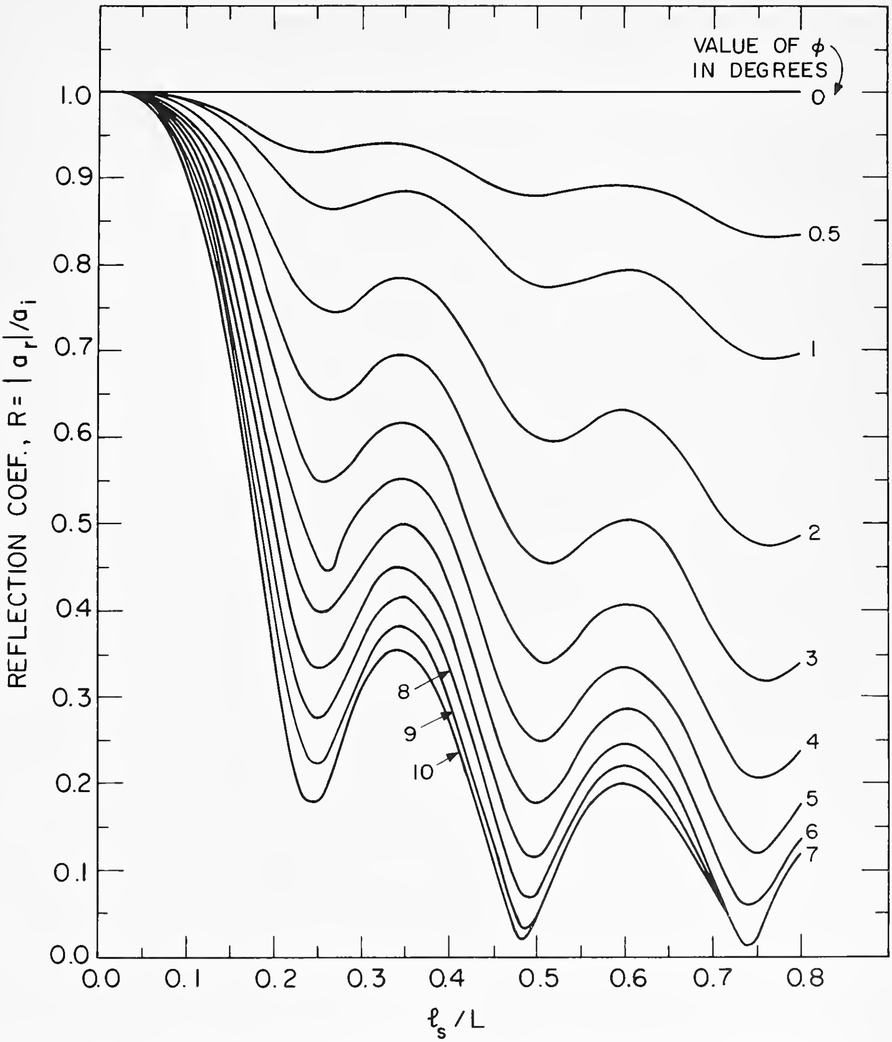

Figure 15. Reflection coefficient, R, of rough impermeable slopes as a function of ϕ and ℓ_s/L.

is obtained from equation (95) and is presented in graphical form in Figure 16.

The solutions for R and R_u were obtained through the use of complex computer programs for Bessel functions with complex arguments which are part of the Massachusetts Institute of Technology (MIT) Information Processing Center's IBM System 370 computer library routines.

With the solution for R as presented graphically in Figure 15 it is seen that knowledge of ℓ_s/L and ϕ enables one to determine the value of R or conversely, if R and ℓ_s/L were known Figure 15 may be used to obtain the corresponding value of ϕ.

a. Determination of the Friction Angle, ϕ. The value of the linearized friction factor, f_b, or the friction angle, ϕ, was considered constant (i.e., independent of x and t) in the analysis presented in the preceding section. This friction factor was introduced through equation (81) and corresponds to a linearized bottom shear stress as given by equation (82)

$$\tau_b = \rho f_b \omega h U = \rho\omega h U \tan 2\phi \quad . \tag{99}$$

With the rate of energy dissipation per unit area of the slope given by $E_D = \tau_b U$, as discussed in Appendix A, the average rate of energy dissipation per unit area of the slope is given by

$$\overline{\overline{E}}_D = \rho\omega\tan 2\phi \; \frac{\cos\beta_s}{\ell_s} \int_0^{\ell_s} h \frac{dx}{\cos\beta_s} \; \{\frac{1}{T}\int_0^T U^2 \, dt\} \; , \tag{100}$$

in which U is the real part of the solution given by equation (84) with u given by equation (91). Since U is necessarily periodic the time averaging in equation (100) is readily performed so that

$$\overline{\overline{E}}_D = \frac{1}{2} \; \rho\omega \; \tan 2\phi \; \frac{\tan\beta_s}{\ell_s} \int_0^{\ell_s} x \; |u|^2 \, dx \quad . \tag{101}$$

From equation (91) it is seen that

$$u = -iA \frac{J_1(2k_o\ell_x \sqrt{1-i\tan 2\phi}\; y^{1/2})}{\sqrt{1-i\tan 2\phi}\sqrt{\frac{h_o}{g}} \; y^{1/2}} \quad , \tag{102}$$

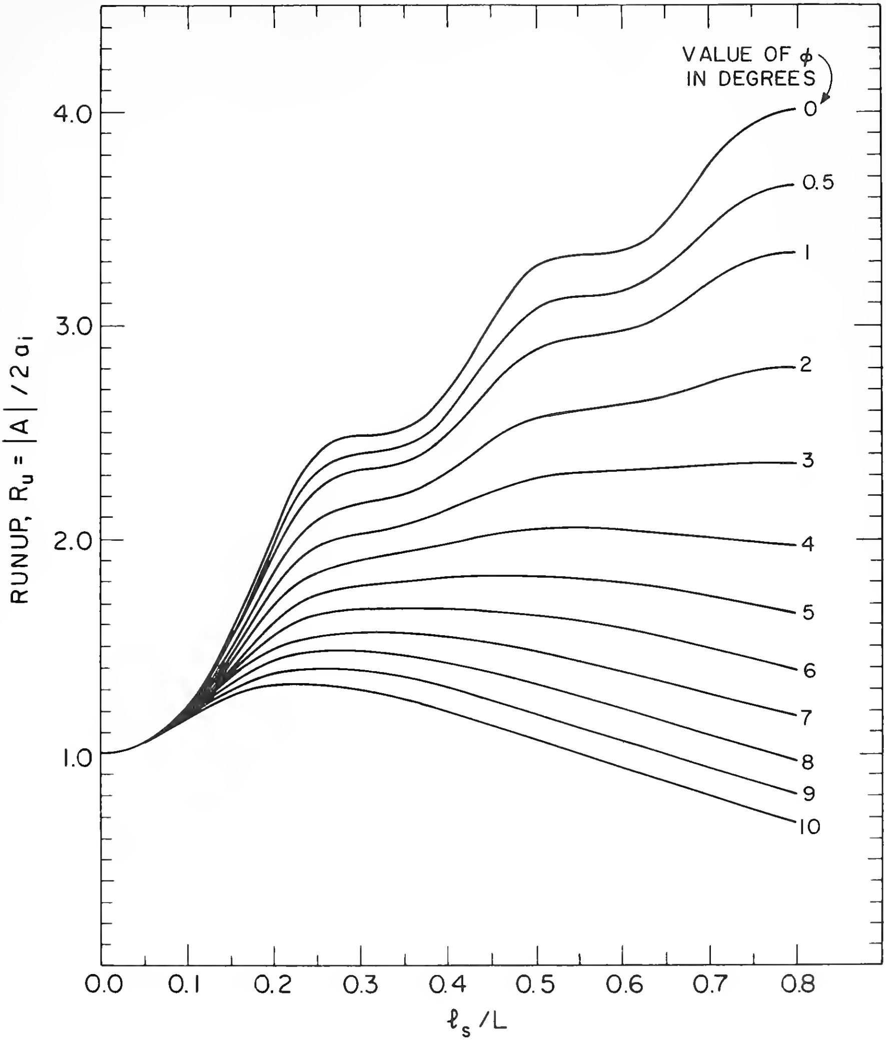

Figure 16. Runup, R_u, on rough impermeable slopes as a function of ϕ and ℓ_s/L.

in which

$$y = \frac{x}{\ell_s} \quad . \tag{103}$$

Introducing equation (86) this may be written

$$|u| = |A| \; \omega\ell_s \frac{1}{h_o} \left| \frac{J_1(2\Psi y^{1/2})}{\Psi\, y^{1/2}} \right| \quad , \tag{104}$$

in which

$$\Psi = k_o\ell_s \sqrt{1-i\ \tan 2\phi} \quad . \tag{105}$$

Inserting equation (104) in equation (101) the average rate of energy dissipation per unit surface area of the rough slope may be written:

$$\overline{\overline{E}}_D = \{\frac{1}{2}\,\rho \frac{|A|^2}{h_o^{\,2}} \omega^3 \ell_s^{\,3} \tan\beta_s \int_0^1 y \left| \frac{J_1(2\Psi y^{1/2})}{\Psi y^{1/2}} \right|^2 dy\} \tan 2\phi \quad . \tag{106}$$

If the average rate of energy dissipation is evaluated using the nonlinear expression for the bottom shear stress (eq. 82) one obtains

$$\overline{\overline{E}}_D = \frac{1}{2}\,\rho f_w \frac{\cos\beta_s}{\ell_s} \int_0^{\ell_s} \frac{dx}{\cos_s} \{\frac{1}{T}\int_0^T |U|U^2\, dt\} \quad , \tag{107}$$

where U again is periodic and given by equation (84) with u given by equation (91). Performing the time averaging and introducing $|u|$ as given by equation (104) the average rate of energy dissipation per unit area of the slope becomes

$$\overline{\overline{E}}_D = \frac{2}{3\pi}\ \rho f_w \frac{|A|^3}{h_o^{\,3}} \omega^3 \ell_s^{\,3} \int_0^1 \left| \frac{J_1(2\Psi y^{1/2})}{\Psi y^{1/2}} \right|^3 dy \quad . \tag{108}$$

Using Lorentz' principle of equivalent work by equating equations (106) and (108) results in the following expression for the friction angle ϕ:

$$\tan 2\phi = f_w \frac{|A|}{h_o} \frac{1}{\tan\beta_s} F_s , \tag{109}$$

in which F_s is a slope friction constant given by

$$F_s = \frac{4}{3\pi} \frac{\int_0^1 \left| \frac{J_1(2\Psi y^{1/2})}{\Psi y^{1/2}} \right|^3 dy}{\int_0^1 y \left| \frac{J_1(2\Psi y^{1/2})}{\Psi y^{1/2}} \right|^2 dy} . \tag{110}$$

With Ψ given by equation (105) it is seen that the slope friction constant, as given by equation (110) is a function of the relative slope length, ℓ_s/L, and of the friction angle, ϕ. The evaluation of the integrals and hence $F_s = F_s(\ell_s/L, \phi)$ is performed numerically using the IBM System 370 computer library routines previously mentioned and F_s is presented in graphical form in Figure 17.

b. Methodology for the Determination of the Reflection Coefficient of Rough Slopes. It is clear from Figures 16 and 17 that equation (109) is an implicit relationship for the friction angle, ϕ, since $|A|$ as well as F_s are functions of ϕ. If it is assumed that the wave friction factor, f_w, in equation (109) is known for given incident wave (a_i, L, h_o) and slope (ℓ_s) characteristics, equation (109) may be solved in an iterative manner. For an assumed value of ϕ and knowing ℓ_s/L, Figures 16 and 17 may be used to obtain values of $|A| = R_u 2a_i$ and F_s. With these values introduced in equation (109) a new value of ϕ is obtained and the procedure is continued until convergence is achieved. Once the value of the friction angle is determined, the reflection coefficient, R, is readily obtained from Figure 15.

The preceding methodology for obtaining the reflection coefficient of rough slopes is straightforward. However, it does rest on one very important assumption--that the value of the wave friction factor, f_w, is known. Although similar to Jonsson's (1966) wave friction factor his expressions for f_w are not expected to hold in the present context which justifies asking: What has been gained by the theoretical development presented in the previous sections?

To answer this question imagine that the problem had been approached on a purely empirical basis. Then, the effects of slope geometry and incident wave characterisitcs in addition to the slope roughness would have had to have been considered. The present theoretical development has circumvented such an extensive experimental investigation by establishing an analytical model, which essentially accounts for the

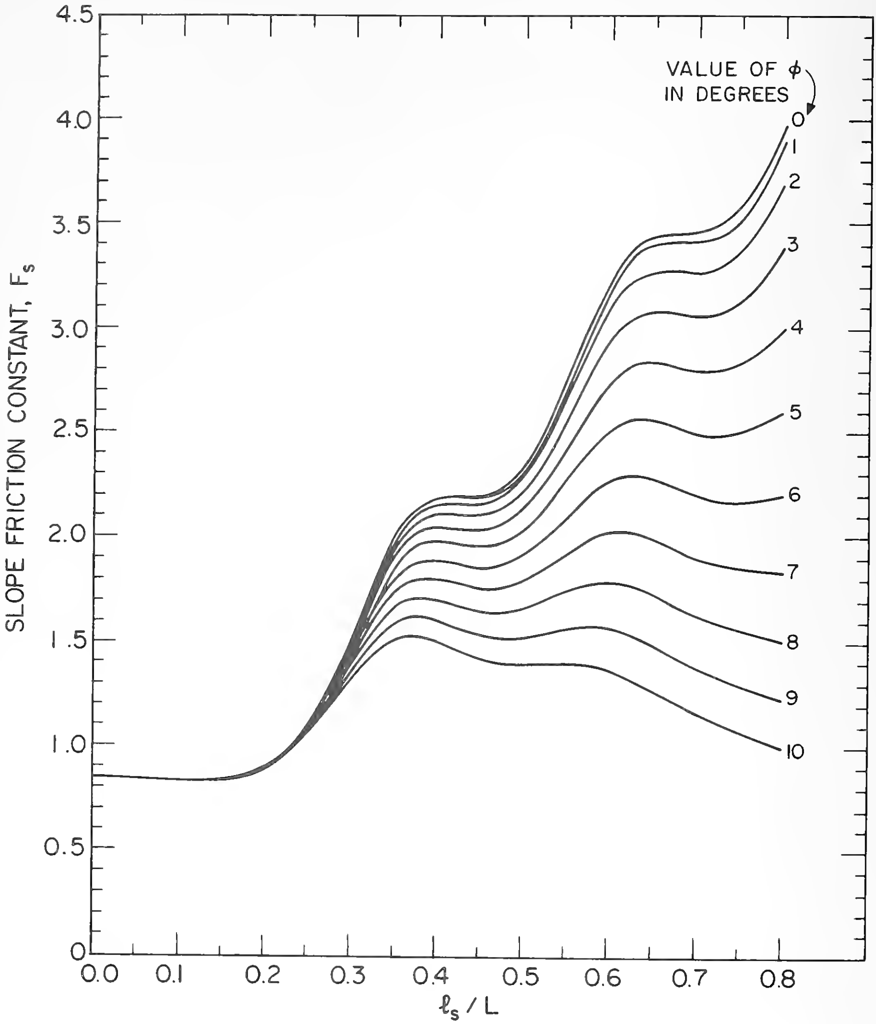

Figure 17. Slope friction constant, F_s, in equation (109) as a function of ϕ and ℓ_s/L.

effects of slope geometry and incident wave characteristics leaving the burden of expressing the influence of slope roughness on the wave friction factor, f_w. This considerable reduction in experimental effort is the reason for the theoretical development. Thus, the theoretical analysis has identified the fundamental unknown parameter as the wave friction factor, f_w. For the method to be applicable an empirical relationship for f_w must be established and here the physical interpretation of f_w as a wave friction factor may be used as a guide.

For fully rough turbulent flow conditions, Jonsson (1966) found for waves over a rough boundary that his wave friction factor is a function of the boundary roughness, d, relative to the excursion amplitude, A_b, of the orbital particle motions above the bed, i.e.,

$$f_w = f_w\left(\frac{d}{A_b}\right) \quad . \tag{111}$$

For fully developed steady flow over a rough boundary, the characteristic length scale is the water depth and the friction factor corresponding to fully rough turbulent flow conditions is a function of the boundary roughness, d, relative to the depth of flow,

$$f_w = f_w\left(\frac{d}{h}\right) \quad . \tag{112}$$

In the present context it is expected that the flow is a mixture of a boundary layer-type flow (eq. 111) and a fully developed flow (eq. 112),and it may therefore be expected that the empirical formula for the wave friction factor, f_w, in equation (110) is of the form:

$$f_w = f_w\left(\frac{d}{A_b} , \frac{d}{h}\right) \quad . \tag{113}$$

As a representative value of the excursion amplitude, A_b, the value obtained from the theoretical solution (eq. 91) evaluated at $x = 0$ is taken, i.e.,

$$A_b = |u|/\omega = \frac{|A|}{\tan\beta_s} \quad , \tag{114}$$

and $h = h_o$ is taken as a representative value of the depth. Thus, it is anticipated that an empirical relationship

$$f_w = f_w\left(\frac{d \tan\beta_s}{|A|} , \frac{d}{h_o}\right) \quad , \tag{115}$$

for the wave friction factor exists. To determine this empirical relationship is the purpose of the experimental investigation described in Section III.3.

3. Experimental Investigation.

The theoretical analysis of the reflection coefficient of rough impermeable slopes described in Section III.2 suggests a rather simple experimental procedure for the determination of the value of f_w. Imagine that an experiment is performed in which the reflection coefficient, R, is determined for given slope (d and ℓ_s) and incident wave characteristics (a_i and L). With ℓ_s/L and R known, Figure 15 may be used to obtain the corresponding value of ϕ. $|A| = R_u\ 2a_i$ and F_s may then be obtained from Figures 16 and 17 and equation (109) written in the form:

$$f_w = \tan\beta_s \frac{h_o}{|A|} \frac{1}{F_s} \tan 2\phi \quad , \tag{116}$$

may be used to obtain the value of f_w.

Performing a series of experiments for various slope and incident wave characteristics and analyzing the results as outlined above will produce a number of values of f_w from which an empirical relationship of the type suggested by equation (115) may be established.

It should be pointed out that this procedure for the analysis of experimental data relies heavily on the theoretical development presented in Section III.2. The resulting empirical relationship for f_w therefore incorporates not only the true physical dependency of f_w on the relative roughness, but reflects also inadequacies of the theoretical development. This is important to keep in mind, since it means that the resulting relationship for f_w becomes an integral part of the entire procedure for the determination of reflection coefficients of rough impermeable slopes.

From the preceding the aim of the experimental investigation is to determine accurately the reflection coefficient of rough impermeable slopes for a variety of slope and incident wave characteristics.

a. Experimental Setup and Procedures. The experiments were performed in a wave flume at the Ralph M. Parsons Laboratory at MIT. This flume is glass walled and is 80 feet (24.4 meters) long, 15 inches (0.38 meter) wide, and the constant water depth in front of the slope was for the major part of the experiments kept at h_o = 1 foot (0.305 meter). A piston-type wavemaker capable of producing periodic waves of periods within the range of 0.6 second < T < 2.2 seconds is located at one end of the flume. Experiments were performed for three wave periods T = 2.0, 1.8, and 1.6 seconds which with h_o = 1 foot correspond to depth to length ratios of the incident waves h_o/L=0.092, 0.105, and 0.12, respectively.

A variable slope of rigid construction was installed approximately 60 feet (18 meters) from the generator. Care was taken to completely seal the gaps between the variable slope, the glass-side walls, and bottom for each slope angle tested to eliminate the effect of leakage around the slope and ensure that the slope was truly impermeable. To develop various slope roughnesses plywood boards with glued-on roughness elements, gravel of diameter d = 0.5, 1, 1.5, and 2 inches (1.25, 2.5, 3.8, and 5 centimeters) were attached to the slope. In this manner experiments for various slope roughnesses were readily performed for a given value of the slope angle, $\tan\beta_s$. Photos of the various roughness boards are shown in Figure 18.

Each experiment for a given value of T, d, and $\tan\beta_s$ was performed by running the wavemaker continuously. After approximately 2 minutes, a quasi-steady condition was established in which the wave motion at any point along the flume was periodic with period T equal to that of the wavemaker. When this quasi-steady state was established the free surface variation with time was recorded at 4-inch (10 centimeters) intervals along the flume over a distance of approximately 10 feet (3 meters) of the constant depth region of the flume. The free surface variation was measured by a parallel wire-resistance wave gage and was recorded on a two-channel recorder (Sanborn). The slope and the instrumentation are shown in Figure 19. From the measurements the incident wave height and the reflection coefficient are determined as discussed in Section 3.b. This procedure was repeated for four values of the incident wave height by changing the wavemaker stroke with everything else being unchanged.

It was found that a quasi-steady state could be achieved only for wavemaker strokes below a certain value. Therefore, experiments are limited to values of the incident wave heights below approximately 2 inches (5 centimeters). This, in turn, means that the incident waves do not break on the slopes tested, thus corresponding to the assumption of nonbreaking waves made in the theoretical analysis.

From the preceding discussion of the experimental setup and testing procedures it is seen that a total of 48 experimental runs were performed for each value of the slope angle,(four different wave heights times three different wave periods times four different slope roughnesses). An additional 12 experiments were performed for a smooth slope for each value of the slope angle. For a smooth slope, which corresponds to $d \simeq 0$, the relationship suggested by equation (115) is unrealistic. For a smooth slope a dependency of the wave friction factor on a Reynolds number can be expected. The experimental results for smooth slopes were analyzed without resulting in a useable relationship for f_w. All the data, including the data obtained for smooth slopes, collected in the experimental investigation are presented in Appendix B.

b. Accurate Determination of Experimental Reflection Coefficients. Since the reflection coefficient obtained from each experimental run is used directly in conjunction with Figure 15 to obtain a corresponding

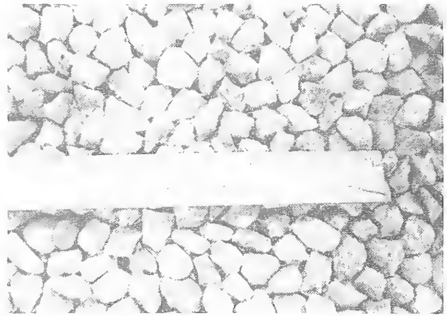

(a) d = 0.5 inch (1.25 cm)

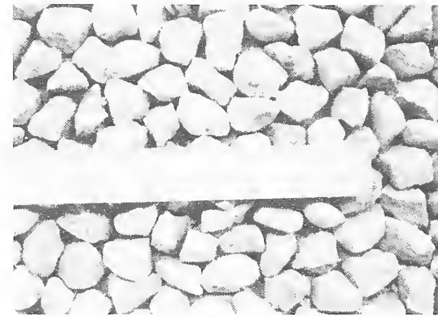

(b) d = 1 inch (2.5 cm)

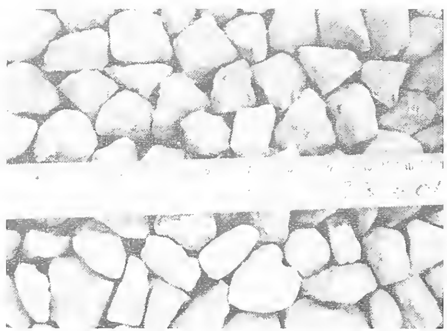

(c) d = 1.5 inches (3.8 cm)

(d) d = 2 inches (5 cm)

Figure 18. Slope roughness boards used in the experimental investigation.

(a) Rough slope in place

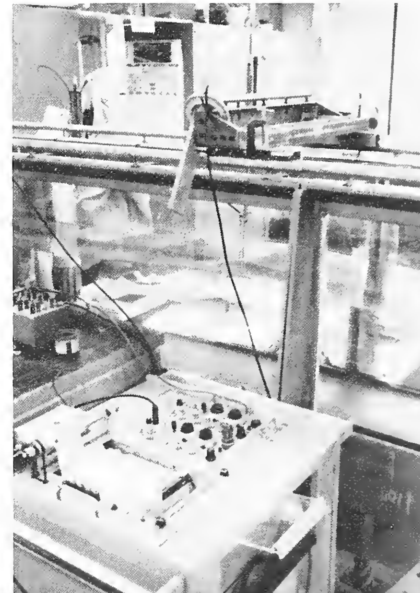

(b) Wave gage and Sanborn recorder

Figure 19. Experimental setup.

value of the friction angle, ϕ, it is of extreme importance that the reflection coefficient be accurately determined from the experimental data.

According to linear wave theory the wave motion in the constant depth region in front of the slope is given by equation (85). Introducing the expression:

$$a_r = |a_r| \, e^{i\delta} \tag{117}$$

for the reflected wave amplitude in equation (85), where δ is an arbitrary phase angle, the resulting wave amplitude, $|\zeta|$, may be expressed as

$$a(x) = |\zeta| = (a_i^2 + |a_r|^2 + 2a_i|a_r| \cos(2k_o x + \delta))^{1/2} \; , \tag{118}$$

which shows the wave amplitude to vary with distance along the constant depth part of the flume in a periodic manner. For values of $2k_o x + \delta = 0, \pm\, 2\pi$, etc. (i.e., at the antinodes) the resulting amplitude is a maximum,

$$a_{max} = a_i + |a_r| = a_i(1 + R) \; , \tag{119}$$

and for values of $2k_o x + \delta = \pm\, \pi$, etc. (i.e., at the nodes) the resulting amplitude is a minimum,

$$a_{min} = a_i - |a_r| = a_i(1 - R) \; . \tag{120}$$

Since the wave height, H, according to linear wave theory is twice the amplitude the preceding formulas show it, in principle, to be possible to determine the reflection coefficient, R, and the incident wave height, $H_i = 2a_i$, by merely seeking out a node and an antinode along the flume. Thus,

$$R = \frac{a_{max} - a_{min}}{a_{max} + a_{min}} = \frac{H_{max} - H_{min}}{H_{max} + H_{min}} \tag{121}$$

and

$$H_i = 2a_i = \frac{1}{2}(H_{max} + H_{min}) \; . \tag{122}$$

As discussed by Ursell, et al., (1960) the above formulas are valid also when the wave motion is weakly nonlinear, i.e., consists of a small second harmonic motion in addition to the primary first harmonic motion of period equal to that of the wavemaker.

The simple method for obtaining the reflection coefficient from an experiment, i.e., simply seeking out a node and an antinode, and using equations (121) and (122) appears to be the method used by Wilson (1971) and Keulegan (1973) as discussed in Section II.3.b. However, this may be a dangerous procedure to use when the reflection coefficient is large and nonlinear effects are pronounced as is often the case in experiments involving relatively long waves.

To illustrate this, the theoretical variation of the wave amplitude relative to the maximum wave amplitude is found from equation (118) to be

$$\frac{a(x)}{a_{max}} = \frac{H(x)}{H_{max}} = \left(1 + \frac{2R}{(1+R)^2}\left(\cos(2k_o x + \delta) - 1\right)\right)^{1/2} \quad . \qquad (123)$$

When the raw data for the wave height variation along the flume is plotted in this fashion versus x/L, the experimentally observed variation (open circles) in Figure 20 is seen to be somewhat erratic and not resembling the variation predicted by an equation such as equation (123). If one, in spite of this discrepancy between theory and observations, evaluates the reflection coefficient directly from the raw data shown in Figure 20 one finds $0.59 < R < 0.65$ with the estimate depending on which node and antinode are chosen. This may not seem to be an alarming variation, but a critical inspection of the surface profile recorded near a node (Fig. 21), reveals that the wave height observed at a node is practically entirely due to a second harmonic motion whose presence manifests itself clearly because of the near vanishing to the first harmonic motion at the nodes.

Since the theoretically predicted wave amplitude variation along the flume is based on linear theory, it applies only to the fundamental motion which has a period equal to that of the wavemaker. At each station along the flume where the free surface variation with time was recorded, the amplitude of the motion with a period equal to that of the wavemaker was extracted from the wave record by means of a Fourier series analysis. The Fourier series analysis is performed on the Ralph M. Parsons Laboratory Hewlett-Packard computer; the program is presented in Appendix C.

When plotting the variation of the amplitude of the first harmonic motion with distance along the constant depth part of the flume (full circles in Figure 20), apparent disorder becomes extremely organized and the observed variation of the amplitude of the first harmonic motion is in excellent agreement with the theoretical prediction afforded by equation (123) with $R = 0.88$.

The surprising thing to note from the data presented in Figure 20 is the drastically different reflection coefficient obtained from the

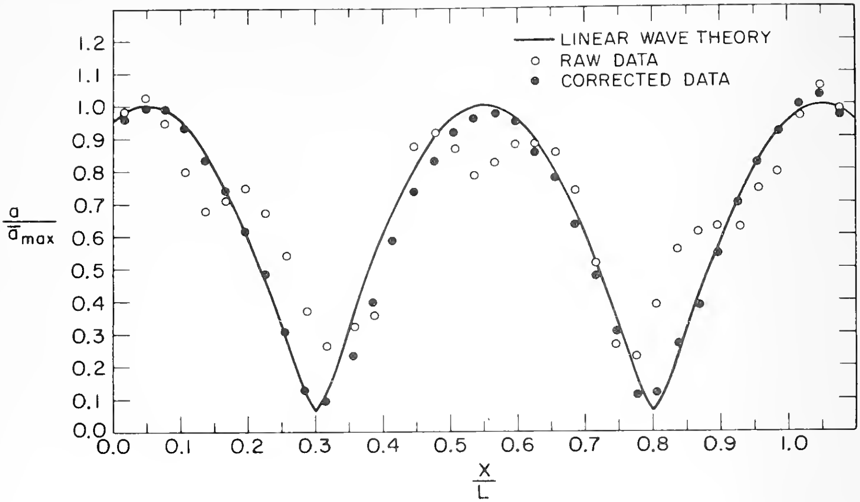

Figure 20. Wave amplitude variation along constant depth part of the flume. T = 2.0 sec., Tan β_S = 1/1.5. Curve corresponds to theoretical variation, equation (123), with R = 0.88.

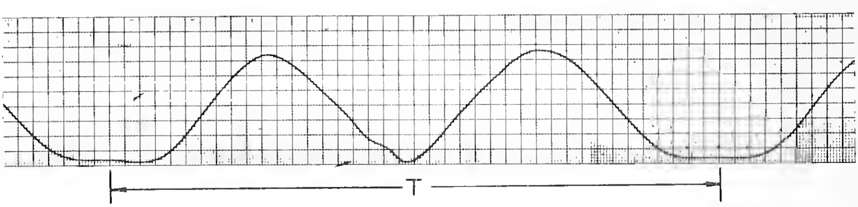

Figure 21. Wave record showing pronounced second harmonics at a node for experiments presented in Figure 20.

raw data ($R \sim 0.62$) and from the corrected data ($R = 0.88$). By using this procedure it was found that reflection coefficients determined from the variation of the amplitude of the first harmonic motion generally were within a range of $\pm$ 0.02 whereas a variation as large as $0.45 < R < 0.75$ was found for a single experimental run when the raw data were used directly. With the intended use of the data in mind, it is quite obvious that the accurate, although tedious, procedure of subjecting the wave records to a Fourier analysis had to be used throughout this study.

The pronounced effect of second or higher harmonic motions on the accurate determination of the reflection coefficients from experimental data is closely related to high values of the reflection coefficient since this entails the near vanishing of the first harmonic motion near the nodes. However, it should be noted that the decision of whether or not to use the time-consuming Fourier series procedure cannot be based solely on the magnitude of the reflection coefficient. Test number 33 (App. B) showed pronounced higher harmonic effects with a reflection coefficient of $R = 0.60$ whereas test number 62 exhibited only insignificant higher harmonics although the reflection coefficient for this test was 0.80. A visual inspection of the recorded wave profile at each station generally led to an accurate assessment of whether or not the Fourier series analysis was called for.

c. Empirical Relationship for the Wave Friction Factor, f_w. To establish a sufficient data base from which an empirical relationship for the wave friction factor, f_w, may be obtained, two series of experiments were performed for values of the slope $(\tan\beta_s) = 1/2.0$ and 1/3.0, respectively. For each slope a total of 48 experiments were performed as discussed in Section III.3.a. The data were analyzed in the manner described in Section III.3.b to yield values of the reflection coefficient, R. With the value of R determined for each experimental run and the value of ℓ_s/L known, Figure 15 was used to obtain ϕ and the corresponding value of f_w was obtained from equation (116).

Anticipating an empirical relationship for f_w of the type suggested by equation (115) the semiempirical values of f_w are plotted against the the value of $|A|/(d \tan\beta_s)$ in Figure 22. Although exhibiting a considerable amount of scatter the data do form four reasonably well-defined bands depending on the relative roughness, d/h_o, in conformance with the anticipated behavior. The experimental data and the details of the analysis leading to Figure 22 are presented in Appendix B.

Two families of straight-line approximations of the data are shown in Figure 22. One, the dashlines, has a 1 on 1 slope and leads to an extremely convenient empirical relationship for the wave friction factor

$$f_w = 0.25 \left(\frac{d}{h_o}\right)^{-0.74} \frac{d \tan\beta_s}{|A|} . \tag{124}$$

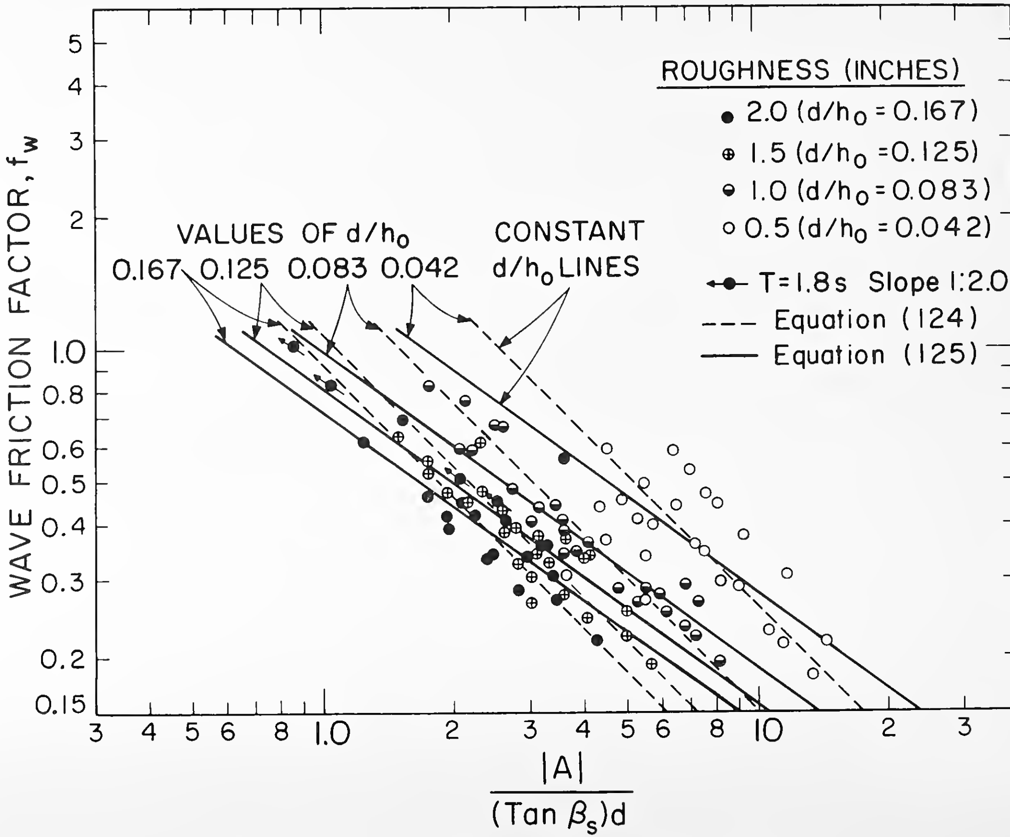

Figure 22. Empirical relationship for the wave friction factor, f_w.

The other, the full lines, has a 1 on 0.7 slope, (Fig. 22) and corresponds to an empirical relationship for the wave friction factor,

$$f_w = 0.29 \left(\frac{d}{h_o}\right)^{-0.5} \left(\frac{d \tan\beta_s}{|A|}\right)^{0.7} \quad . \tag{125}$$

The second relationship, equation (125), is superior to equation (124) in representing the data from single subsets of the experiments in which only the amplitude of the incident waves varied. One such typical subset of data points, corresponding to d = 2 inches (5 centimeters), T = 1.8 seconds and $\tan \beta_s = 1/2.0$, is indicated by full circles with arrows in Figure 22. The slope of a line connecting these data points is approximately 1 on 0.7; this slope reflects the experimental observation that the reflection coefficient generally decreased with increasing height of the incident waves. This is a consequence of the nonlinear nature of the energy dissipation on the rough slope and equation (125) is therefore to be considered superior to equation (124) which is included primarily because it possesses some convenient features.

4. Comparison of Predicted and Observed Reflection Coefficients of Rough Impermeable Slopes.

With the empirical relationships for f_w, (eqs. 124 or 125), the semiempirical procedure discussed in Section III.2.b for the prediction of the reflection coefficient of rough impermeable slopes is now complete. Whereas the theoretical analysis identified the wave friction factor as the physically fundamental parameter, the friction angle, ϕ, is the important parameter for the use of Figure 15. However, by merely introducing the empirical relationship for f_w in equation (109) an implicit equation for ϕ may be obtained.

By introducing equation (124) in equation (109) the following equation for ϕ is obtained:

$$\tan 2\phi = 0.25\left(\frac{d}{h_o}\right)^{0.26} F_s \ . \tag{126}$$

This equation is in principle implicit, since the slope friction constant F_s, as seen from Figure 17 is a function of ϕ. However, for small values of ℓ_s/L ($\ell_s/L < 0.3$), F_s is only a weak function of ϕ and equation (126) may therefore be regarded as an explicit equation for ϕ requiring knowledge of only the relative slope roughness, d/h_o. This may be a somewhat surprising result since it means that the value of the slope friction angle, ϕ, and hence the reflection coefficient obtained from Figure 15 is independent of the amplitude of the incident waves. As mentioned previously the main part of the experiments presented in

Figure 22 exhibited a slightly decreasing reflection coefficient with increasing incident wave amplitude which is not reproduced by this simple relationship for the slope friction angle. However, the feature of ϕ being independent of a_i, when equation (126) is adopted, is extremely convenient for use in problems where the incident wave is given in terms of its amplitude spectrum rather than as a monochromatic wave. This is the reason for including equation (126) in the present report and it leads to reasonably accurate results.

Upon substituting the relationship for f_w, given by equation (125) in equation (109) a less convenient but more accurate implicit equation for ϕ is obtained.

$$\tan 2\phi = 0.29\left(\frac{d}{h_o}\right)^{0.2}\left(\frac{|A|}{h_o \tan\beta_s}\right)^{0.3} F_s \quad . \tag{127}$$

This equation may be solved iteratively by assuming a value of ϕ and evaluating $|A| = R_u\, 2a_i$ and F_s from Figures 16 and 17, respectively. With these values a new value of ϕ may be obtained from equation (127) and the iteration may be continued until convergence is achieved. Since $|A|$ is a function of a_i, the incident wave amplitude, ϕ, is a function of a_i; the use of equation (127) will therefore reflect the observed decrease in reflection coefficient with increasing incident wave amplitude. Although seemingly more cumbersome, it should be mentioned that equation (127) is solved after a limited number of iterations (two iterations generally suffice).

For given incident wave and slope characteristics, a_i, L, h_o, ℓ_s, and d, either of the relationships for ϕ may be solved; the reflection coefficient is then obtained from Figure 15. To use this procedure to "predict" the reflection coefficients observed for the slope angles $\tan\beta_s$ = 1/2.0 and 1/3.0 does not constitute a test of the procedure since these data were used in establishing the empirical relationships for f_w and hence the procedure. However, with the degree of scatter exhibited in Figure 22 this may be a meaningful comparison in that it will indicate the ability of the procedure to reproduce the experimentally observed reflection coefficients.

To perform a more meaningful test of the procedure two separate sets of experiments were performed as previously described in Section III.3.b but for values of the slope angle $\tan\beta_s$ = 1/1.5 and 1/2.5; each of these tests consisted of 48 individual experiments. From knowledge of the incident wave and slope characteristics the procedure was used to predict the reflection coefficient of the slope. For each experiment two predicted values of the reflection coefficient, R_{ps} and R_p, were obtained depending on whether the slope friction angle ϕ was obtained from equation (126) (R_{ps}) or from equation (127) (R_p). The predicted reflection coefficients were compared with the measured reflection coefficient, R_m. The comparison was performed by evaluating the mean value of the quantity,

$$\left\langle \frac{R_m}{R_p} \right\rangle = \frac{\Sigma(R_m/R_p)}{N} , \tag{128}$$

and its standard deviation,

$$\sigma\left(\frac{R_m}{R_p}\right) = \left\{\frac{\Sigma(\langle R_m/R_p\rangle - R_m/R_p)^2}{N-1}\right\}^{1/2} , \tag{129}$$

in which N is the number of experiments performed for a given value of the slope.

The data used for this comparison are presented in Appendix B, and the results are presented in Table 2.

Table 2. Comparison of measured and predicted reflection coefficients of rough slopes.

Slope	ϕ from equation (126)		ϕ from equation (127)	
$\tan\beta_s$	$\langle R_m/R_{ps}\rangle$	$\sigma(R_m/R_{ps})$	$\langle R_m/R_p\rangle$	$\sigma(R_m/R_p)$
1 on 1.5	0.92	0.051	0.89	0.041
1 on 2.0	1.03	0.059	0.99	0.053
1 on 2.5	1.06	0.084	1.05	0.059
1 on 3.0	1.01	0.083	1.02	0.064

As is evident from the comparison in Table 2, the procedure is quite accurate in reproducing the reflection coefficients obtained for $\tan\beta_s = 1/2.0$ and $1/3.0$ in spite of the scatter exhibited in Figure 22. The procedure also predicts the reflection coefficients obtained for $\tan\beta_s = 1/2.5$ with a comparable degree of accuracy. Thus, for slopes $1/3.0 < \tan\beta_s < 1/2.0$ the procedure is quite accurate in predicting the reflection coefficient of rough slopes. The more elaborate empirical formula (eq. 127) for the slope friction angle, ϕ, is superior to the simpler formula (eq. 126) as could be expected. However, it is noted that even the simple formula leads to reasonably accurate estimates of R.

For the steepest slope tested, $\tan\beta_s = 1/1.5$, the procedure leads to consistent estimates of the reflection coefficient as evidenced by the low value of the standard deviation. However, the mean value of R_m/R_p, $\langle R_m/R_p \rangle$, is somewhat different from unity. Basically the measured reflection coefficients are on the average only about 90 percent of the values predicted by the semiempirical procedure developed here. The reason for this discrepancy may be sought in the steep slope angle which violates the basic assumption made in the theoretical analysis that the slope be relatively gentle. This assumption, which is discussed in Appendix A, means that the horizontal velocity is taken to be representative of the velocity parallel to the bottom. For smaller slopes this is a fairly good assumption, but as the slope becomes steeper the velocity parallel to the bottom may approach $U/\cos\beta_s$ where U is the horizontal velocity. This increase in near bottom velocity will increase the energy dissipation due to bottom friction and hence lead to smaller values of the reflection coefficient. Since the details of the wave motion on a steep slope are not known, the above discussion is only to be taken as a tentative explanation of the discrepancy between observed and predicted reflection coefficients for steep slopes.

For steep slopes the reflection coefficient is generally close to unity so this discrepancy may not be of a severe nature. It is recommended that the procedure developed here be used also for steep slopes with $1/2.0 < \tan\beta_s < 1/1.5$ with a correction factor being applied to the predicted reflection coefficient. For a slope of 1 on 1.5 this correction factor is taken as $\langle R_m/R_p \rangle$ (Table 2); for slopes between 1 on 1.5 and 1 on 2 an appropriate correction factor, smaller than unity, may be chosen corresponding to a linear interpolation between the values of $\langle R_m/R_p \rangle$.

All experiments discussed so far were performed for a water depth, h_o = 1 foot (0.305 meter), in the constant depth part of the flume. A separate short series of tests was performed with h_o = 16 inches (0.41 meter) for a value of $\tan\beta_s = 1/3.0$ and a surface roughness d = 2 inches (5 centimeters). The results of these tests are shown in Table 3.

The comparison between predicted and measured reflection coefficients presented in Table 3 shows an excellent agreement. It is of particular interest to note that a reflection coefficient as low as 0.42 was observed and predicted. Since the average rate of energy dissipation on the slope is obtained from

$$E_D = (1-R^2)\, E_F \quad , \tag{130}$$

in which E_F is the energy flux asscoiated with the incident waves, this means that 80 percent of the incident wave energy is dissipated on the

Table 3. Comparison of measured and predicted reflection coefficients (h_o = 16 inches (0.41 meter).

Wave Period (in seconds)	Incident Wave Height in centimeters	R Measured	R Predicted (eq. 127)	R Predicted (eq. 126)
2.0	1.86	0.49	0.50	
2.0	2.65	0.47	0.48	0.46
2.0	3.50	0.45	0.46	
2.0	4.05	0.43	0.45	
1.8	1.74	0.47	0.47	
1.8	2.47	0.45	0.46	0.43
1.8	3.10	0.43	0.44	
1.8	3.63	0.42	0.42	

slope. This is a surprisingly large energy dissipation, particularly when it is realized that the incident waves showed no sign of breaking on the slope. This considerable energy dissipation is therefore due mainly to bottom friction.

The procedure enables one to determine the wave runup in addition to the reflection coefficient. The determination of the wave runup, $|A|$, is an integral part of the procedure itself. Figure 16 is used both in establishing values of f_w from the experimental values of R, and in solving the empirical relationship (eq. 127) for the slope friction angle, ϕ. Thus, although not explicitly appearing in the final result, the procedure for the prediction of reflection coefficients of rough slopes relies implicitly on the runup prediction afforded by Figure 16. Therefore, it would be somewhat disturbing if the runup predicted by Figure 16 was drastically different from the runup occurring in the experiments. For this reason a simple observation was made of the runup in the experiments used in establishing the empirical relationships for f_w, and the observed runup was compared with the runup predicted from Figure 16. This comparison, involving the 96 experiments listed in Appendix B, shows a mean value of R_u (predicted)/R_u (observed) to be 1.15 with a standard deviation of 0.28. This agreement is not sufficient for the runup predictions afforded by Figure 16 to be used in actual design, but it does show that its use as part of the procedure for predicting the reflection coefficient of rough impermeable slopes is warranted. This comparison of predicted and observed runup, which is independent of the determination of the reflection coefficient, may also be taken as an independent check of the soundness of the procedure and the theoretical analysis developed here.

a. Limitations of the Procedure. The preceding comparison of measured and predicted values of the reflection coefficient of rough impermeable slopes has shown the semiempirical procedure to yield quite accurate results. However, it is important to realize that the significance of this favorable comparison is limited by the range of the independent variables tested here. Therefore, it should be used with caution whenever the values of $d \tan\beta_s/|A|$ and d/h_o are outside the range indicated by the experimental data in Figure 22.

Furthermore, the procedure relies on an experimentally established empirical relationship for the wave friction factor, f_w. In this investigation the empirical relationship was established from experiments in which the slope roughness elements were modeled by gravel. The procedure as it appears here is therefore applicable only for slopes whose roughness may be considered adequately modeled by gravel, i.e., natural stones, quarry stones, etc. To utilize the procedure for slopes protected by concrete armor units, an empirical relationship for f_w, representative of these armor units, should be established in a manner similar to that presented in Section III.3. It is beyond the scope of the present research to establish more general relationships for f_w.

Finally, the manner in which the theoretical results were used in the analysis of the experimental data to obtain values of f_w makes the resulting empirical relationships for f_w part of the procedure itself, i.e., the empirical relationships for f_w can be used with confidence only in conjunction with the present procedure for estimating the reflection coefficient of rough slopes.

As mentioned in Section III.3.b, experiments were performed also for smooth slopes. For smooth slopes the roughness is negligible and the empirical relationships for ϕ (eqs. 126 and 127) are invalid. The type of empirical formula anticipated for f_w was based on an assumption of fully rough turbulent flow conditions. To investigate if the experiments performed with rough slopes in this study do correspond to fully rough turbulent flow, the criterion established by Jonsson (1966) may be examined. For the present experiment the maximum value of $|A|/(d \tan\beta_s)$ is seen from Figure 22 to be of the order 20. Since this value corresponds to the parameter a_{1m}/k used by Jonsson (1966, Fig. 6) it is seen that fully rough turbulent flow should exist for values of the Reynolds number

$$Re = \frac{|A|^2 \omega}{\nu \tan^2\beta_s} > 10^4 \quad , \tag{131}$$

with $\nu = 10^{-5}$ ft^2/sec. It is readily shown that the major part of the experimental data presented in Appendix B satisfy this criterion. The experiments and the empirical formulas developed for the wave friction factor, f_w, therefore correspond to fully rough turbulent flow conditions.

When fully rough turbulent flow conditions exist in the model a Froude model will correctly reproduce the prototype conditions. A check of whether or not fully rough turbulent flow conditions may be expected in a particular model test may be performed in a manner similar to that described above, using Jonsson's (1966, Fig. 6) wave friction factor diagram.

5. Discussion and Application of Results.

A theoretical analysis of the reflection of water waves from rough impermeable slopes was performed based on the assumptions of relatively long, nonbreaking, and normally incident waves. The general solution for the reflection coefficient is presented in graphical form in Figure 15 which gives R as a function of the horizontal extent of the slope relative to the incident wavelength, ℓ_s/L, and a slope friction angle, ϕ.

The theoretical analysis accounts for the energy dissipation on the rough slope by including a term expressing the bottom shear stress. Therefore, the analysis introduces and identifies the physically fundamental parameter of the problem as a wave friction factor, f_w. This wave friction factor expresses the effect of slope roughness and is related to the slope friction angle, ϕ, through the use of Lorentz' principle of equivalent work. A series of experiments was performed in which an accurate determination of the reflection coefficient of rough impermeable slopes was used in conjunction with the theoretical analysis to evaluate the magnitude of the wave friction factor, f_w. From these experimental values of f_w, two empirical relationships for f_w as a function of the relative slope roughness were obtained. One of these relationships (eq. 124) leads to a simple expression for the slope friction angle (eq. 126) which shows the value of ϕ to be independent of the incident wave amplitude. Therefore, equation (126) is particularly convenient for use when the incident wave is given in terms of its amplitude spectrum. The other empirical relationship for f_w (eq. 125) leads to a more elaborate and accurate relationship for ϕ(eq. 127). With this relationship the reflection coefficient of rough slopes decreases slightly with increasing incident wave amplitude, thus reflecting the nonlinear nature of the energy dissipation on the slope.

The resulting semiempirical procedure for the prediction of reflection coefficients of rough impermeable slopes was tested against a separate set of experiments and yielded excellent results for values of the slope angle $1/3.0 \leq \tan\beta_s \leq 1/2.0$. For slopes steeper than corresponding to $\tan\beta_s = 1/2.0$ the procedure overestimates the reflection coefficient and a correction factor varying from 1.0 for $\tan\beta_s = 1/2.0$

to approximately 0.9 for $\tan\beta_s = 1/1.5$ should be applied to the predicted results.

It is important to realize that the procedure is empirical and therefore is limited by the range of the independent variables used in the experiments establishing the procedure. These limitations of the procedure are discussed in Section III.4.a.

Numerical Example. To illustrate the application of the procedure for prediction of reflection coefficients for rough impermeable slopes consider the following example specified in Table 4.

Table 4. Information used in numerical sample calculations.

	Prototype	Froude Model length scale 1:25
Incident wave amplitude a_i in feet	1.75	0.069
Wave period T in seconds	12.5	2.5
Water depth h_o in feet	29.2	1.167
Incident wavelength[1] L in feet	366.0	14.56
Slope angle $\tan\beta_s$ (1 on 1.5)	0.667	0.667
Surface stone size $d = 1/2\ (d_{max} + d_{min})$ in feet	3.12	0.125

[1]L obtained from linear wave theory using h_o and T.

Since a Froude model scales the slope frictional effects correctly for fully rough turbulent flow conditions, either the prototype or the model may be taken as the basis for the following numerical calculations. Choosing the model it is seen from the information presented in Table 4 that

$$\frac{\ell_s}{L} = \frac{h_o}{L \tan\beta_s} = \frac{1.167}{14.56(0.667)} = 0.12 \quad . \tag{132}$$

Taking first the simple expression for the slope friction angle (eq. 126)

$$\tan 2\phi = 0.25 \left(\frac{d}{h_o}\right)^{0.26} F_s \quad , \tag{133}$$

in which F_s is obtained directly from Figure 17

$$F_s = 0.83 \quad , \tag{134}$$

since F_s is not a function of ϕ for this low value of ℓ_s/L. For higher values of ℓ_s/L a value of F_s corresponding to an assumed value of ϕ is obtained from Figure 17 and substituted into the right-hand side of equation (133) to obtain a new value of ϕ. With this new value of ϕ a better estimate of F_s is obtained from Figure 17 and the procedure is continued until convergence is achieved.

In the present case equation (133) may be evaluated directly to give

$$\tan 2\phi = 0.25 \left(\frac{0.125}{1.167}\right)^{0.26} 0.83 = 0.25(0.56)(0.83) = 0.116 \quad , \tag{135}$$

and the value of ϕ is obtained

$$\phi = \frac{6.6^{\circ}}{2} = 3.3^{\circ} \quad . \tag{136}$$

With ℓ_s/L given by equation (132) and $\phi = 3.3^{\circ}$, Figure 15 gives the predicted value of the reflection coefficient

$$R_{ps} = 0.94 \quad . \tag{137}$$

The present calculation corresponds to a steep slope, $\tan\beta_s = 1/1.5$, and as discussed in Section III.4 the estimate given by equation (137) should be corrected by the factor $\langle R_m/R_p \rangle$ given in Table 2 corresponding to ϕ obtained from equation (126) and $\tan\beta_s = 1/1.5$. The estimate of the reflection coefficient therefore becomes

$$R_{ps} = \langle R_m/R_p \rangle \; 0.94 = 0.92(0.94) = 0.86 \quad . \tag{138}$$

If choosing the more elaborate expression for ϕ given by equation (127) the implicit relationship for ϕ becomes

$$\tan 2\phi = 0.29 \left(\frac{d}{h_o}\right)^{0.2} \left(\frac{|A|}{h_o \tan\beta_s}\right)^{0.3} F_s \quad . \tag{139}$$

The preceding calculation based on the simple formula for ϕ, may be used as a first guess for the value of ϕ. Therefore, with $\phi = 3.3^o$ and $\ell_s/L = 0.12$, Figure 16 gives:

$$R_u = \frac{|A|}{2a_i} = 1.3 \tag{140}$$

or

$$|A| = 2.6a_i = 2.6(0.069) = 0.138 \text{ foot} \quad , \tag{141}$$

and Figure 17 gives $F_s = 0.83$ as before. Equation (139) therefore becomes

$$\tan 2\phi = 0.29 \left(\frac{0.125}{1.167}\right)^{0.2} \left(\frac{0.138}{1.167 \text{ X } 0.667}\right)^{0.3} 0.83 =$$

$$0.29 \ (0.64)(0.64)(0.83) = 0.099 \tag{142}$$

or

$$\phi = \frac{5.64^o}{2} = 2.8^o \quad . \tag{143}$$

One should now return to Figures 16 and 17 with this new value of ϕ to reevaluate the values of R_u and F_s. In the present example the values corresponding to this new estimate of ϕ (eq. 139) are practically identical to those obtained for $\phi = 3.3^o$ so convergence is, in this example, rapidly achieved.

With $\phi = 2.8^o$ and $\ell_s/L = 0.12$, Figure 15 yields a reflection coefficient of

$$R_p = 0.95 \quad . \tag{144}$$

Due to the steep 1 on 1.5 slope this estimate should be corrected by the factor $\langle R_m/R_p \rangle$ in Table 2, corresponding to ϕ obtained from equation (127), i.e., the best estimate of the reflection coefficient becomes

$$R_p = \langle R_m/R_p \rangle \quad 0.95 = 0.89\ (0.95) = 0.84 \quad . \tag{145}$$

The two estimates for the reflection coefficient (eqs. 138 and 145) are in close agreement and they may be considered quite accurate since they correspond to values of $|A|/(d \tan\beta_s) = 1.6$ and $d/h_o = 0.107$ which are within the range of the data presented in Figure 22. The value of the Reynolds number defined by equation (131) is 1.1×10^4. This demonstrates that the flow in the model and therefore also in the prototype is fully rough turbulent and indicates that a Froude model will reproduce the energy dissipation on the rough impermeable slope correctly.

As discussed in conjunction with the numerical example presented in Section II, the numerical example in this section accounts for the external energy dissipation whereas the numerical example in Section II accounts for the partition of the remaining energy among reflected, transmitted and internally dissipated energy. Subtracting the energy dissipated on the rough slope (the external energy dissipation) from that of the incident wave assumed in Table 4 shows that the remaining energy may be regarded as the energy associated with an equivalent incident wave of amplitude $a_I = Ra_i$. With $a_i = 0.069$ foot, as specified in Table 4, and $R = 0.84$, from equation (145), the amplitude of the equivalent incident wave is $a_I = 0.84\ (0.069) = 0.058$ foot. This is seen to be the incident wave amplitude assumed in the numerical example in Section II, Table 1. The two numerical examples are therefore closely related and illustrate the details of the calculations involved in the procedure for the prediction of reflection and transmission coefficients of trapezoidal breakwaters, which is discussed in Section IV.

IV. AN APPROXIMATE METHOD FOR THE PREDICTION OF REFLECTION AND TRANSMISSION COEFFICIENTS OF TRAPEZOIDAL, MULTILAYERED BREAKWATERS

1. Description of the Approximate Approach.

In Section II an explicit solution for the transmission and reflection coefficients of homogeneous rectangular crib-style breakwaters was developed. In Section III a semiempirical procedure for the prediction of reflection coefficients of rough impermeable plane sloped structures was developed. When viewing the interaction of incident waves with a trapezoidal, multilayered breakwater as a problem of energy dissipation the problem treated in Section II may be regarded as an idealized analysis accounting for the internal dissipation of energy within the structure, $E_{D,int}$, whereas Section III may be regarded as an idealized analysis of the energy dissipation on the seaward face of the breakwater, i.e., the external energy dissipation, $E_{D,ext}$. This section presents a synthesis of the results obtained in Sections II and III into an approximate procedure for the prediction of wave reflection from and transmission through trapezoidal, multilayered breakwaters.

The basic assumptions of this approximate procedure are those inherent in the analyses and procedures developed in Sections II and III:

(a) Relatively long normally incident waves which may be considered adequately described by linear long wave theory.

(b) Incident waves do not break on the seaward slope of the breakwater, so that the external energy dissipation may be considered mainly due to bottom frictional effects.

(c) The cover layer on the seaward slope of the breakwater consists of natural stones, so that the empirical relationships for the wave friction factor developed in Section III.3.c may be considered valid.

With these assumptions stated, the following procedure is suggested as being physically realistic although approximate in nature.

For most trapezoidal, multilayered breakwaters, the stone size in the layer under the cover layer of the seaward slope is small relative to the stone size of the cover layer. As a first approximation the structure may therefore be regarded as resembling an impermeable rough slope. Thus, with the incident wave characteristics and the stone size, d_{II}, of the cover layer as well as the seaward slope of the trapezoidal breakwater, $\tan\beta_s$, specified, the procedure developed in Section III may be used to approximately account for the energy dissipation on the seaward slope, i.e., the external energy dissipation may be estimated. This energy dissipation approximately accounts for the dissipation of energy associated with the top layer of stones in the cover layer. The reamining wave energy may be expressed as the energy associated with a progressive wave of amplitude,

$$a_I = R_{II}\, a_i \quad , \tag{146}$$

in which a_i is the amplitude of the actual incident wave, and R_{II} is the reflection coefficient determined by the procedure developed in Section III.

With the energy dissipated on the seaward slope accounted for, the remaining energy is partitioned betweeen reflected, transmitted, and internally dissipated energy. This partition of energy is the problem dealt with in Section II of this report, and it is evaluated by regarding the remaining energy as an equivalent wave of amplitude, a_I, normally incident on an equivalent homogeneous rectangular breakwater. The role of this homogeneous rectangular breakwater is to reproduce the internal energy dissipation associated with the trapezoidal, multilayered breakwater, i.e., the two breakwaters should be hydraulically equivalent. A rational method for obtaining a homogeneous rectangular breakwater which is hydraulically equivalent to a trapezoidal, multilayered breakwater is developed in Section IV.2, based on steady flow considerations. By using the procedure developed in Section II, the partition of the remaining wave energy among reflected, transmitted, and internally dissipated energy is therefore approximately evaluated by determining the reflection coefficient, R_I, and the transmission coefficient, T_I, of the hydraulically equivalent homogeneous rectangular breakwater subject to an equivalent incident wave of amplitude, a_I.

Having now accounted for the external as well as the internal energy dissipation the amplitude of the reflected wave is found to be

$$|a_r| = R_I a_I = R_I R_{II} a_i \quad , \tag{147}$$

and the transmitted wave amplitude is

$$|a_t| = T_I a_I = T_I R_{II} a_i \quad . \tag{148}$$

The approximate values of the reflection and transmission coefficients, R and T, of a trapezoidal, multilayered breakwater are therefore

$$R = \frac{|a_r|}{a_i} = R_I R_{II} \tag{149}$$

and

$$T = \frac{|a_t|}{a_i} = T_I R_{II} \quad . \tag{150}$$

The approximate procedure described above is used to predict the reflection and transmission coefficients corresponding to the laboratory experiments performed by Sollitt and Cross (1972). When considering that the predicted results are obtained without any attempt being made to fit the experimentally obtained reflection and transmission coefficients from Sollitt and Cross, the comparison between predictions and experiments is favorable.

2. Determination of the Equivalent Rectangular Breakwater.

From the description given of the approximate method for obtaining the reflection and transmission coefficients of a trapezoidal, multilayered breakwater, the missing link for carrying out this analysis is the determination of the hydraulically equivalent homogeneous rectangular breakwater.

In Section II.2.a it was shown that a simple analysis, which essentially neglected unsteady effects, gave transmission and reflection coefficients (eqs. 45 and 46) equal to those obtained from the more complete analysis for structures of small width relative to the incident wavelength (eqs. 35 and 36). This observation suggests that a rational and reasonably simple determination of the hydraulically equivalent breakwater may be based on steady flow considerations. Therefore, a hydraulically equivalent breakwater is taken as the homogeneous rectangular breakwater which gives the same discharge, Q, as the discharge through the trapezoidal, multilayered breakwater. This definition will, according to the simple analysis presented in Section II.2.a, preserve the equality of transmission coefficients for the two structures and hence essentially give the same internal dissipation. This definition of the equivalent breakwater is illustrated schematically in Figure 23.

Figure 23 shows schematically a trapezoidal, multilayered breakwater consisting of several different porous materials. These porous materials are identified by their stone size, d_n, and their hydraulic characteristics, β_n, in the flow resistance formula (eq. 6). To keep the following determination of the equivalent breakwater reasonably simple, the flow resistance is assumed to be purely turbulent although in principle it is possible to perform the determination of the equivalent breakwater based on the more general form of the Dupuit-Forchheimer resistance formula. Since the energy dissipation associated with the top layer of stones on the seaward slope has been accounted for, the rectangular homogeneous breakwater which accounts approximately for the internal dissipation should be hydraulically equivalent to the trapezoidal, multilayered breakwater with the top layer of cover stones removed.

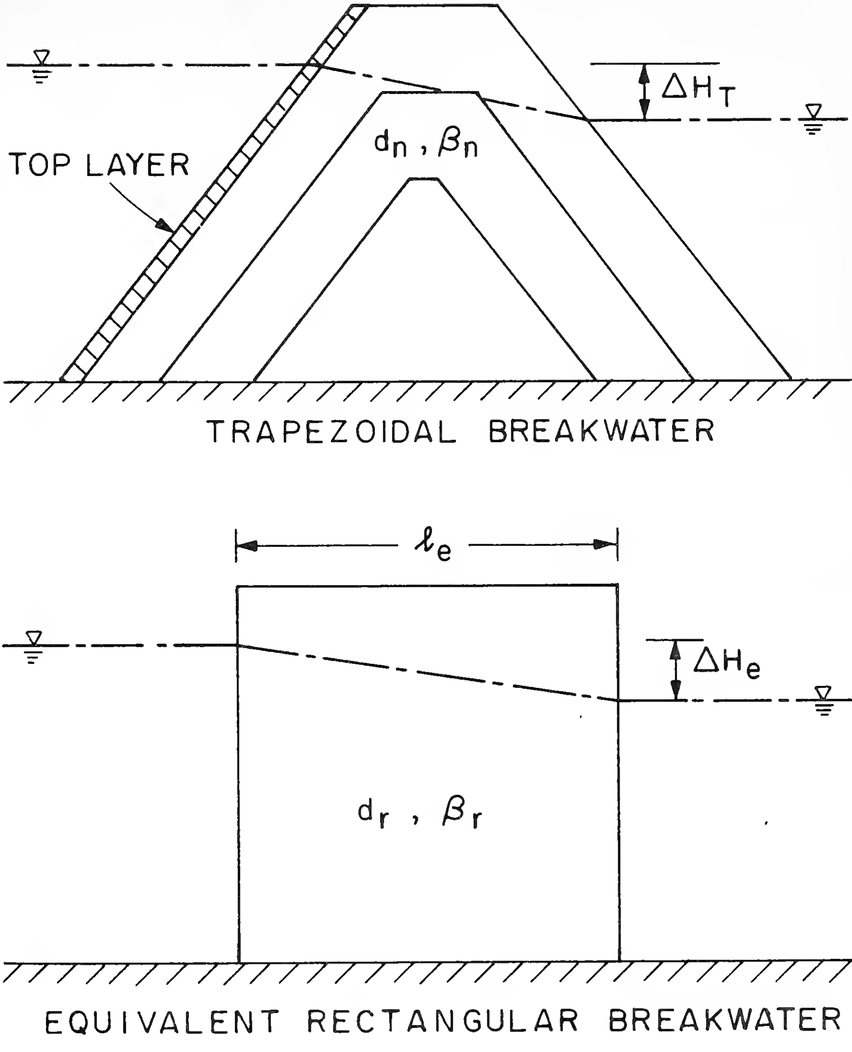

Figure 23. Definition sketch of trapezoidal, multilayered breakwater and its hydraulically equivalent rectangular breakwater.

The homogeneous rectangular breakwater consists of a reference material of stone size, d_r, and hydraulic characteristics, β_r. The reference material should be taken to be representative of the porous materials of the multilayered breakwater. To find the discharge per unit length of the rectangular breakwater, the flow is assumed to be essentially horizontal and one obtains

$$\rho g \frac{\Delta H_e}{\ell_e} = \rho \beta_r U^2 \quad , \tag{151}$$

in which ℓ_e is the width of the equivalent breakwater and ΔH_e is the head difference defined in Figure 23. The discharge per unit length is therefore obtained from equation (151) to be

$$Q = Uh_o = \{\frac{g\Delta H_e}{\beta_r}\}^{1/2} \frac{h_o}{\sqrt{\ell_e}} \tag{152}$$

To evaluate the discharge per unit length of the trapezoidal, multilayered breakwater a horizontal slice of height, Δh_j, is shown schematically in Figure 24.

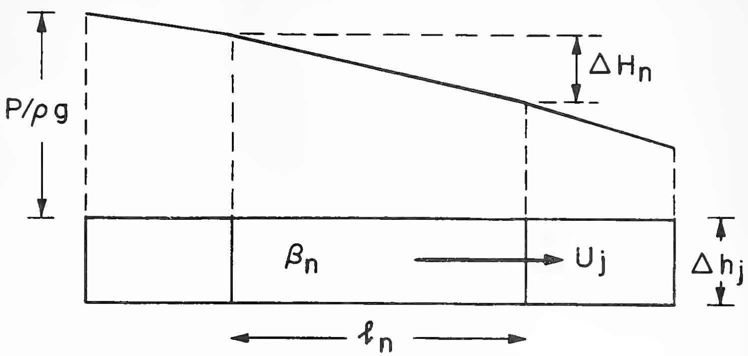

Figure 24. Horizontal slice of thickness, Δh_j, of multilayered breakwater.

This horizontal slice consists of segments of the different porous materials of lengths ℓ_n. From an assumption of purely horizontal flow it follows that the discharge velocity of the slice considered, U_j, must be the same in all segments and the total head loss across the breakwater must be equal to ΔH_T, the head difference shown in Figure 23. From this it is seen

$$\Delta H_T = \sum_n (\Delta H_n) \quad , \tag{153}$$

in which ΔH_n is the head loss associated with the segment of length, ℓ_n, and hydraulic characteristics, β_n. From equation (151) it is seen that

$$\Delta H_n = \beta_n \ell_n \frac{U_j^2}{g} = \beta_r \frac{U_j^2}{g} \left(\frac{\beta_n}{\beta_r} \ell_n\right) \quad , \tag{154}$$

in which β_r is the hydraulic characteristic of the reference material. Equation (153) may therefore be written:

$$\Delta H_T = \beta_r \frac{U_j^2}{g} \sum_n \left(\frac{\beta_n}{\beta_r} \ell_n\right) \quad , \tag{155}$$

in which the summation is carried out over the n different porous materials of the horizontal slice of thickness, Δh_j.

From equation (155) the discharge associated with the slice of thickness Δh_j is found to be

$$\Delta Q_j = U_j \Delta h_j = \left\{\frac{g \Delta H_T}{\beta_r}\right\}^{1/2} \frac{\Delta h_j}{\left\{\sum_n \left(\frac{\beta_n}{\beta_r} \ell_n\right)\right\}^{1/2}} \quad , \tag{156}$$

and by adding the contributions from all horizontal slices of the trapezoidal breakwater one obtains

$$Q = \sum_j \Delta Q_j = \left\{\frac{g \Delta H_T}{\beta_r}\right\}^{1/2} h_o \sum_j \left(\frac{1}{\left\{\sum_n \left(\frac{\beta_n}{\beta_r} \ell_n\right)\right\}^{1/2}} \frac{\Delta h_j}{h_o}\right) \quad . \tag{157}$$

Thus, requiring that the discharges per unit length given by equations (152) and (157) be identical, the width, ℓ_e, of the equivalent rectangular breakwater is

$$\ell_e = \{ \sum_j (\frac{1}{\{\Sigma(\frac{\beta_n}{\beta_r} \ell_n)\}^{1/2}} \frac{\Delta h_j}{h_o}) \}^{-2} (\frac{\Delta H_e}{\Delta H_T}) \quad . \tag{158}$$

This equation shows that the width of the equivalent breakwater may be determined from knowledge of the configuration of the trapezoidal, multilayered breakwater and the corresponding head differences, ΔH_e and ΔH_T.

As described in Section IV.1 the equivalent breakwater is subject to an equivalent incident wave of amplitude a_I given by equation (146). A simplified analysis of the interaction of incident waves and a rectangular homogeneous breakwater of small width relative to the length of the incident waves was presented in Section II.2.a. This simplified analysis essentially neglected unsteady effects and any phase difference between the incident, reflected, and transmitted waves. The runup on the seaward slope is for this analysis given by equation (38) and this runup is taken as a representative value of the head difference, ΔH_e, across the equivalent breakwater. With this assumption, which neglects the influence of a transmitted wave of small amplitude, one obtains

$$\Delta H_e = (1 + R_I)\, a_I = (1 + R_I)\, R_{II}\, a_i \quad , \tag{159}$$

in which R_I is the reflection coefficient of the equivalent breakwater.

The value of the head difference across the trapezoidal breakwater, ΔH_T, is in accordance with the argument presented for the equivalent rectangular breakwater taken as the runup on the seaward slope of the trapezoidal breakwater. This runup may in principle be determined by the procedure developed in Section III of this report. However, there is reason to believe that such an estimate, which would correspond to an impermeable slope, would be somewhat on the high side. In general one may, however, take

$$\Delta H_T = 2R_u\, a_i \quad , \tag{160}$$

where R_u is the best estimate available for the ratio of the runup to the incident wave height $H_i = 2a_i$ for given slope characteristics. If R_u is taken as determined from Figure 16 the estimate of ΔH_T is expected to be conservative.

Equations (159) and (160) show that the ratio

$$\frac{\Delta H_e}{\Delta H_T} = \frac{(1 + R_I) R_{II}}{2R_u} \quad , \tag{161}$$

is a function of the reflection coefficient, R_I, of the equivalent breakwater. Since this reflection coefficient cannot be determined until the width of the equivalent breakwater, ℓ_e , is known one is faced with a tedious iterative procedure. However, in most cases a sufficiently accurate estimate of R_I may be obtained by assuming initially that $\Delta H_e/\Delta H_T$ is unity and use this estimate along with the best estimate of R_u to obtain a new value of $\Delta H_e/\Delta H_T$ from equation (161).

Numerical Example of the Determination of the Equivalent Rectangular Breakwater. To illustrate the procedure for the determination of the equivalent rectangular breakwater the trapezoidal, multilayered breakwater configuration tested experimentally by Sollitt and Cross (1972) and shown in Figure 25 is considered. The breakwater is divided into five horizontal slices, I-V (Fig. 25), and the reference material is chosen as the material with stone size d_2 = 0.75 inch (1.9 centimeters). Since the porosities of the three porous materials were reported to be essentially equal by Sollitt and Cross (1972), the porosity of all materials as well as the reference material is assumed to be 0.435. This in turn means that the ratio of the hydraulic characteristics of the various porous materials, β_n, according to equation (52) with $\beta_o = 2.7$ reduces to the inverse of the ratios of the stone sizes, i.e.,

$$\frac{\beta_1}{\beta_2} = \frac{d_2}{d_1} = 0.5 \quad ; \frac{\beta_3}{\beta_2} = \frac{d_2}{d_3} = 2.0 \quad . \tag{162}$$

From the geometry of the breakwater shown in Figure 25, with the top layer of cover stones removed, the equivalent breakwater width is readily calculated as shown in Table 5.

Introducing the numerical result obtained in Table 5 in equation (158), the equivalent breakwater width, ℓ_e, is obtained as

$$\ell_e = (0.1819)^{-2} \frac{\Delta H_e}{\Delta H_T} \text{ inches} = 2.52 \frac{\Delta H_e}{\Delta H_T} \text{ feet} \quad . \tag{163}$$

Thus, the homogeneous rectangular breakwater which is hydraulically equivalent to the trapezoidal, multilayered breakwater (Fig. 25) consists of material of stone size $d = d_2$ = 0.0625 foot (1.9 centimeters) and porosity n = 0.435. The equivalent width, ℓ_e, is given by equation (163) and a first approximation may be obtained by taking $\Delta H_e/\Delta H_T = 1$, i.e., ℓ_e = 2.52 feet (0.77 centimeter).

It should be noted that the homogeneous rectangular breakwater assumed in the numerical example presented in Section II, Table 1, has the characteristics of the hydraulically equivalent breakwater given

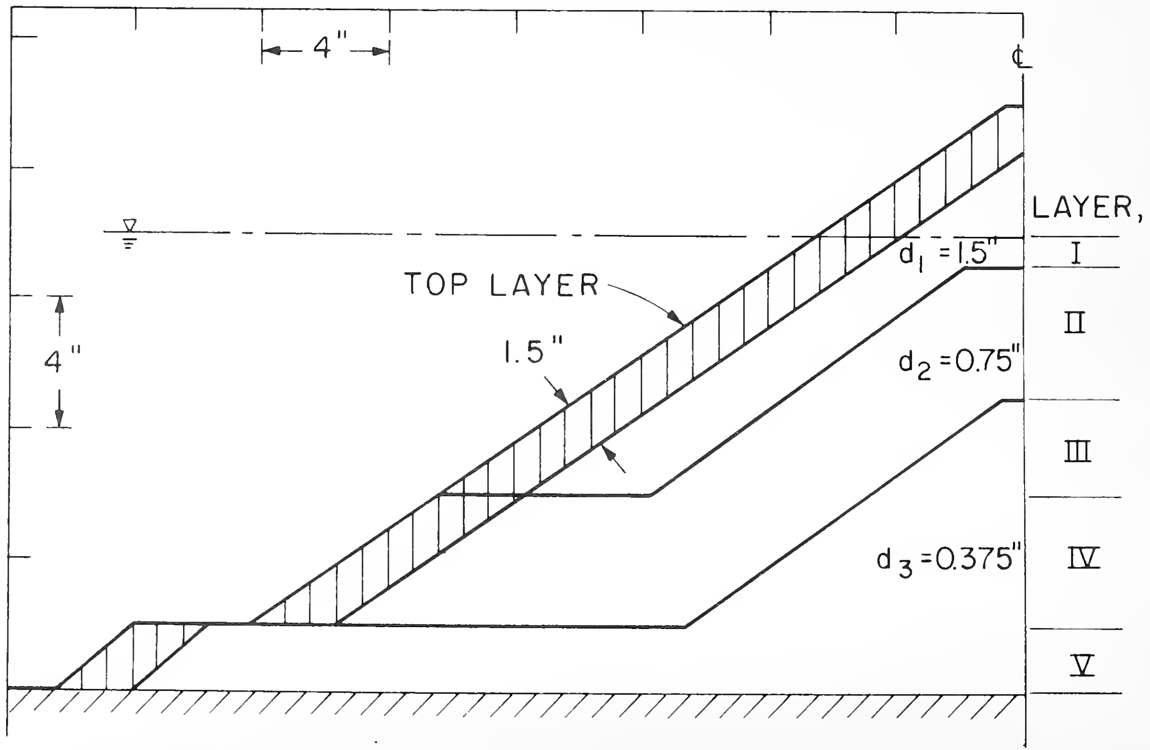

Figure 25. Breakwater configuration tested by Sollitt and Cross (1972).

Table 5. Evaluation of equivalent rectangular breakwater.

Layer, j	$\frac{\Delta h_j}{h_o}$	ℓ_1 inches	ℓ_2 inches	ℓ_3 inches	$\Sigma \frac{\beta_n}{\beta_r} \ell_n$ inches	$\frac{\Delta h_j}{h_o} \frac{1}{\{\Sigma_n (\frac{\beta_n}{\beta_r} \ell_n)\}^{1/2}}$ (inches)$^{-1/2}$
I	$\frac{1}{14}$	16.7	0	0	8.35	0.0247
II	$\frac{4}{14}$	15.0	9.2	0	16.7	0.0700
III	$\frac{3}{14}$	15.1	13.8	5.6	32.6	0.0376
IV	$\frac{4}{14}$	0	29.7	15.6	60.9	0.0366
V	$\frac{2}{14}$	0	0	60.7	121.4	0.0130
						Σ_j 0.1819

by equation (163) for the choice $\Delta H_e/\Delta H_T = 1$. Furthermore, the trapezoidal breakwater shown in Figure 25 has a seaward slope of 1 on 1.5 ($\tan\beta_s = 0.667$) which for the most part consists of stones of $d = d_{II} = 1.5$ inches (3.8 centimeters). These slope characteristics correspond to those assumed in the numerical example presented in Section III, Table 4.

The present numerical example of the determination of the hydraulically equivalent breakwater together with the numerical examples presented in Sections II and III therefore constitute an example of the computations involved in the procedure described in Section IV.1 for the determination of the reflection and transmission coefficients of the trapezoidal, multilayered breakwater shown in Figure 25.

3. Computation of Transmission and Reflection Coefficients for Trapezoidal, Multilayered Breakwaters.

Sollitt and Cross (1972, App. G) presented the results of a laboratory investigation of reflection and transmission characteristics of their model breakwater (Fig. 25). For the present purpose of comparison with predicted reflection and transmission coefficients only the tests performed by Sollitt and Cross (1972) with relatively long waves will be used.

Thus, the wave conditions to be used in the following for the purpose of demonstrating the computational aspects of the approximate method described in Section IV.1 are

$$h_o = 1.167 \text{ feet} \; ; \; T = 2.5 \text{ seconds} \; ; \; L = 14.56 \text{ feet} \quad , \tag{164}$$

and the breakwater configuration is that shown in Figure 25.

a. Determination of the External Energy Dissipation. As discussed in Section IV.1 the first step in the approximate procedure for evaluating the reflection and transmission coefficients of a trapezoidal, multilayered breakwater is to estimate the external energy dissipation on the seaward slope using the procedure developed in Section III.

From the breakwater characteristics shown in Figure 25 it is seen that the seaward slope consists of various stone sizes. Since the main part of the front face consists of stones of diameter $d_{II} = d_1 = 0.125$ foot (3.8 centimeters) it is reasonable to adopt this stone size as the roughness of the slope. This is further justified by the fact that this stone size is the size in the cover layer near the stillwater level, where one would expect the major part of the external energy dissipation to take place. Hence, for the purpose of estimating the external energy dissipation the slope characteristics are taken as:

$$\text{Roughness} = d_{II} = 0.125 \text{ foot} \quad ; \; \tan\beta_s = 1/1.5 = 0.667 \quad . \tag{165}$$

This information in addition to the incident wave characteristics specified by equation (164) is sufficient to use the procedure developed in Section III for the prediction of the reflection coefficient, R_{II}, of rough slopes when the incident wave amplitude, a_i, is specified.

Comparison of the incident wave characteristics (eq. 164) and the slope characteristics (eq. 165) with the corresponding values for the Froude model characteristics given in the numerical example presented in Table 4 show that the calculations presented there correspond to the conditions being considered here. The numerical example presented in

Section III may therefore be taken directly as an illustration of the computational aspects involved in the determination of the reflection coefficient of the seaward slope, R_{II}.

Thus, with the detailed computational aspects given in Section III the computations corresponding to the incident wave amplitudes reported by Sollitt and Cross (1972, App. G) are summarized in Table 6.

Table 6. Summary of calculations of external energy dissipation on seaward slope for experiments by Sollitt and Cross (1972, App. G).

Run No.	H_i feet	ϕ Degrees (eq. 127)	R_u (Fig. 16)	F_s (Fig. 17)	R_p (Fig. 15)	R_{II} = 0.89 R_p
428	0.0355	1.8	0.83	1.3	0.97	0.86
429	0.0365	1.85	0.83	1.3	0.97	0.86
472	0.0405	1.9	0.83	1.3	0.97	0.86
430	0.0474	2.0	0.83	1.3	0.97	0.86
427	0.056	2.2	0.83	1.3	0.96	0.85
471	0.075	2.3	0.83	1.3	0.96	0.85
470	0.115	2.6	0.83	1.3	0.96	0.85
469	0.162	2.9	0.83	1.3	0.95	0.84
465	0.202	3.1	0.83	1.3	0.95	0.84
466	0.260	3.3	0.83	1.3	0.94	0.84
467	0.310	3.5	0.83	1.3	0.94	0.84
468	0.374	3.7	0.83	1.3	0.94	0.84

As found in Section III the important parameters are:

$$\frac{\ell_s}{L} = \frac{h_o}{L \tan\beta_s} = 0.12 \; ; \; \frac{d_{II}}{h_o} = 0.107 \quad , \tag{166}$$

and the best estimate of the reflection coefficient, R_{II}, is obtained by multiplying the predicted value, R_p, by the correction factor 0.89 associated with the steep slope, $\tan\beta_s = 1/1.5$.

For comparison the numerical example carried out in Section III is seen to correspond to an incident wave amplitude between the incident wave amplitudes of Run Numbers 470 and 469 in Table 6.

b. Determination of the Internal Energy Dissipation. Having determined the energy dissipation on the seaward slope, the next step is to determine the internal energy dissipation. To perform this analysis one must first determine the characteristics of the rectangular breakwater which is hydraulically equivalent to the trapezoidal, multilayered breakwater shown in Figure 25. As an example of the computations involved, the homogeneous rectangular breakwater which is hydraulically equivalent to the breakwater configuration shown in Figure 25 was determined in Section IV.2. Thus, the equivalent rectangular breakwater has the characteristics obtained in Section IV.2, i.e.,

$$\text{Stone size} = d = 0.0625 \text{ foot} \quad ; \text{Porosity} = n = 0.435 \quad , \tag{167}$$

and a width ℓ_e given by equation (163)

$$\ell_e = 2.52 \frac{\Delta H_e}{\Delta H_T} \text{ feet} \quad , \tag{168}$$

in which ΔH_e and ΔH_T are the runup on the equivalent rectangular and on the trapezoidal breakwater, given by equations (159) and (160), respectively.

As discussed in Section IV.2, the determination of ℓ_e from equation (168) involves a tedious iterative procedure. A fairly good first guess for the value of the reflection coefficient, R_I, involved in determining the ratio $\Delta H_e/\Delta H_T$ from equation (161) may, however, be obtained by taking $\Delta H_e/\Delta H_T$ equal to unity. Hence, a preliminary solution is obtained by taking

$$\ell_e = 2.52 \text{ feet} \quad . \tag{169}$$

The equivalent rectangular breakwater characteristics are therefore given by equations (167) and (169). The incident wave characteristics are given by equation (164) with an equivalent incident wave amplitude, a_I, given by equation (146). The computations involved in determining the partition of the energy associated with the equivalent incident wave among reflected, transmitted, and internally dissipated energy is therefore carried out according to the procedure developed in Section II of this report. In Section II, the details of this computation were presented in the form of a numerical example. By inspection of the incident wave and breakwater characteristics used in the numerical example in Section II, these characteristics for the Froude model listed in Table 1 are identical to those given by equations (164), (167), and (169). The numerical example may therefore be consulted for the details of the computational aspects involved in the determination of the transmission and reflection coefficient of the equivalent breakwater, T_I and R_I, subject to incident waves of amplitude a_I.

The important parameters involved in the use of Figures 2 and 3 for this purpose were obtained in Section II

$$n\ k_o \ell_e = 0.435\ \left(\frac{2\pi}{14.56}\right)\ 2.52 = 0.47 \quad , \tag{170}$$

and the porosity correction factor (eq. 28),

$$S_* = \left(\frac{n}{0.45}\right)^2 = \left(\frac{0.435}{0.45}\right)^2 = 0.93 \quad . \tag{171}$$

The computations corresponding to the equivalent incident wave amplitudes, a_I, determined from the results obtained in Table 6 are summarized in Table 7.

Table 7. Summary of calculations of reflection and transmission coefficients of equivalent rectangular breakwater based on $\Delta H_e/\Delta H_T = 1$.

Run No.	H_i feet	R_{II} (Table 6)	$a_I = R_{II}H_i/2$ feet	f (eq. 57)	f/S_*	T_I (Fig. 2)	R_I (Fig. 3)
428	0.0355	0.86	0.015	1.92	2.1	0.30	0.66
429	0.0365	0.86	0.016	1.97	2.1	0.30	0.67
472	0.0405	0.86	0.0175	2.06	2.2	0.29	0.67
430	0.0474	0.86	0.020	2.16	2.3	0.28	0.68
427	0.056	0.85	0.024	2.34	2.5	0.27	0.68
471	0.075	0.85	0.032	2.62	2.8	0.24	0.70
470	0.115	0.85	0.049	3.17	3.4	0.20	0.72
469	0.162	0.84	0.069	3.70	4.0	0.17	0.74
465	0.202	0.84	0.085	4.10	4.4	0.15	0.75
466	0.260	0.84	0.109	4.63	5.0	0.13	0.76
467	0.310	0.84	0.130	5.02	5.4	0.12	0.77
468	0.374	0.84	0.157	5.50	5.9	0.11	0.77

For comparison the example calculation presented in Section II.4 corresponds to an equivalent incident wave amplitude between Run Numbers 470 and 469 and the transmission and reflection coefficients, (eq. 78), correspondingly fall between the results of Run Numbers 470 and 469 listed in Table 7.

The results obtained in Table 7 correspond, as previously stated, to the simplifying assumption that the magnitude of $\Delta H_e/\Delta H_T$ is unity. This simplifying assumption enabled a direct determination of the width of the equivalent breakwater, ℓ_e. With the ratios of runup on the equivalent rectangular breakwater to runup on the trapezoidal breakwater given by equation (161) the equivalent rectangular breakwater width may be obtained from equation (163),

$$\ell_e = 2.52 \frac{(1 + R_I)R_{II}}{2R_u} \text{ feet} \quad . \tag{172}$$

Adopting as a preliminary value of R_I the value obtained in Table 7 and the value of R_{II} given in Table 6 for a given experimental run, a better estimate of the equivalent breakwater width may be obtained from equation (172) provided a reasonable estimate of the runup to incident wave height ratio, R_u, is available. As previously mentioned the runup prediction afforded by the semiempirical procedure developed in Section III of this report and carried out in Section IV.3 may be expected to yield a conservative, i.e., too large, value of R_u. However, if this value of R_u (Table 6) is adopted the procedure developed here is entirely self-contained and although slightly conservative this choice of R_u is made here. Thus, with R_{II} and R_u obtained from Table 6 and R_I obtained from Table 7 the equivalent breakwater width may now be obtained from equation (172) for each experimental run performed by Sollitt and Cross (1972).

For each experimental run listed in Tables 6 and 7 the equivalent rectangular breakwater width, ℓ_e, is obtained from equation (172) and the corresponding value of the linearized friction factor, f, is obtained from equation (57) with $\ell = \ell_e$. This procedure is identical to the procedure illustrated in the numerical example, Section II.4, and with f obtained the values of T_I and R_I are obtained from Figures 2 and 3 using the appropriate value of $nk_o\ell_e$ and S_* given by equation (171).

The computations are summarized in Table 8. By comparison with the results listed in Table 7, the reflection coefficients are practically identical, thus justifying the use of R_I as obtained in Table 7 in equation (172) for the purpose of determining the width of the equivalent breakwater. Had the values of R_I obtained in Table 8 been drastically different from those given in Table 7 the computations should have been repeated using the updated values of R_I in equation (172).

Table 8. Summary of calculations of reflection and transmission coefficients of equivalent rectangular breakwater based on $\Delta H_e/\Delta H_T$ given by equation (161).

Run No.	a_I Table 7 feet	$\Delta H_e/\Delta H_T$ (eq. 161)	ℓ_e (eq. 172) feet	f (eq. 57)	f/S_*	T_I (Fig. 2)	R_I (Fig. 3)
428	0.015	0.55	1.39	2.34	2.5	0.39	0.62
429	0.016	0.55	1.39	2.39	2.6	0.38	0.62
472	0.0175	0.55	1.39	2.53	2.7	0.38	0.63
430	0.020	0.55	1.39	2.64	2.8	0.36	0.64
427	0.024	0.55	1.39	2.85	3.1	0.34	0.66
471	0.032	0.56	1.41	3.24	3.5	0.32	0.68
470	0.049	0.56	1.41	3.87	4.2	0.28	0.72
469	0.069	0.57	1.44	4.55	4.9	0.24	0.74
465	0.085	0.57	1.44	5.08	5.5	0.22	0.76
466	0.109	0.57	1.44	5.73	6.2	0.20	0.78
467	0.130	0.57	1.44	6.27	6.7	0.18	0.79
468	0.157	0.57	1.44	6.87	7.4	0.17	0.80

Whereas the reflection coefficient is essentially insensitive to the value of ℓ_e it is seen from Tables 7 and 8 that the transmission coefficient shows a significant change with the value of the equivalent breakwater width. The transmission coefficients obtained in Table 8 are considerably larger than the transmission coefficients obtained in Table 7, thus reflecting the smaller equivalent breakwater width. Since the equivalent breakwater width was obtained from equation (172) using the slightly conservative value of R_u obtained in Table 6, it may be anticipated that the equivalent breakwater width listed in Table 8 is on the lower side. Consequently, one may anticipate that the estimates of the transmission coefficients obtained in Table 8 are slightly on the high side.

The preceding discussion essentially shows that the reflection coefficient, R_I, may be regarded as relatively accurately determined whereas the transmission coefficient, T_I, is bracketed by the results listed in Tables 7 and 8.

c. Determination of the Transmission and Reflection Coefficient of Trapezoidal, Multilayered Breakwaters. From the results obtained in Sections IV.3.a and IV.3.b it is now possible to estimate the transmission and reflection coefficient of the trapezoidal, multilayered breakwater (Fig. 25) since the external as well as the internal energy dissipation has been accounted for. From the description of the procedure given in Section IV.1 it follows that the transmitted and reflected wave amplitudes, $|a_t|$ and $|a_r|$, are given by

$$|a_t| = T_I a_I = T_I R_{II} a_i \tag{173}$$

and

$$|a_r| = R_I a_I = R_I R_{II} a_i \quad . \tag{174}$$

The transmission coefficient, T, and reflection coefficient, R, are therefore obtained from the results listed in Tables 6, 7, and 8 since

$$T = \frac{|a_t|}{a_i} = T_I R_{II} \tag{175}$$

and

$$R = \frac{|a_r|}{a_i} = R_I R_{II} \quad . \tag{176}$$

The resulting estimates are shown in Table 9.

4. Comparison Between Predicted and Observed Transmission and Reflection Coefficients of a Trapezoidal, Multilayered Breakwater.

The preceding section has illustrated the use of the approximate method for the determination of transmission and reflection coefficients of trapezoidal, multilayered breakwaters described in Section IV.1. The breakwater characteristics as well as the characteristics of the incident waves used in Section IV.3 were chosen to correspond to the experiments performed by Sollitt and Cross (1972), and the predictions given in Table 9 may therefore be compared directly with the experimentally observed values of the transmission and reflection coefficients given by Sollitt and Cross (1972, App. G). This comparison between predicted and observed transmission and reflection coefficients is shown in Figure 26, where the values of T and R are plotted against the incident wave steepness, H_i/L.

From the comparison presented in Figure 26 the predicted reflection coefficients are in excellent agreement with the observed reflection coefficients for lower values of the incident wave steepness. For larger values of the incident wave steepness the predicted reflection

Table 9. Predicted reflection and transmission coefficients of trapezoidal, multilayered breakwater tested by Sollitt and Cross (1972, Appendix G).

Run No.	H_i/L x 10^3	R_{II} (Table 6)	$\Delta H_e/\Delta H_T = 1$				$\Delta H_e/\Delta H_T$ from (eq. 161)			
			T_I (Table 6)	R_I (Table 6)	T $=R_{II}T_I$	R $=R_{II}R_I$	T_I (Table 7)	R_I (Table 7)	T $=R_{II}T_I$	R $=R_{II}R_I$
428	2.4	0.86	0.30	0.66	0.26	0.57	0.39	0.62	0.33	0.53
429	2.5	0.86	0.30	0.67	0.26	0.58	0.38	0.62	0.33	0.53
472	2.8	0.86	0.29	0.67	0.25	0.58	0.38	0.63	0.32	0.54
430	3.2	0.86	0.28	0.68	0.24	0.58	0.36	0.64	0.31	0.54
427	3.8	0.85	0.27	0.68	0.23	0.58	0.34	0.66	0.29	0.56
471	5.1	0.85	0.24	0.70	0.20	0.60	0.32	0.68	0.27	0.58
470	7.9	0.85	0.20	0.72	0.17	0.61	0.28	0.72	0.23	0.61
469	11.0	0.84	0.17	0.74	0.15	0.63	0.24	0.74	0.20	0.63
465	13.8	0.84	0.15	0.75	0.13	0.63	0.22	0.76	0.19	0.64
466	17.8	0.84	0.13	0.76	0.11	0.64	0.20	0.78	0.17	0.65
467	21.2	0.84	0.12	0.77	0.10	0.65	0.18	0.79	0.15	0.66
468	25.5	0.84	0.11	0.77	0.09	0.65	0.17	0.80	0.14	0.67

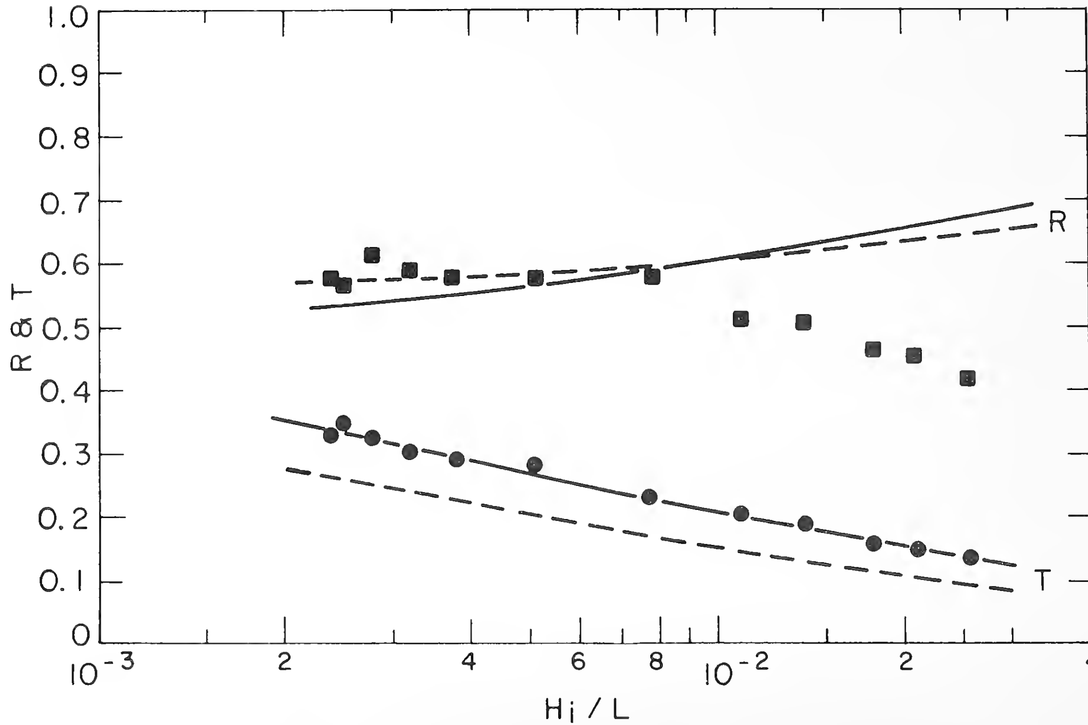

Figure 26. Comparison of predicted and observed reflection and transmission coefficient of trapezoidal, multilayered breakwater tested by Sollitt and Cross (1972, App. G, kh = 0.5). ■ Experimental reflection coefficient, ● experimental transmission coefficient, — — prediction based on $\Delta H_e/\Delta H_T = 1$, ——— prediction based on $\Delta H_e/\Delta H_T$ given by equation (161).

coefficient is seen to increase slightly whereas the observed reflection coefficients exhibit a decreasing trend with increasing wave steepness. As discussed previously this trend of the experimental reflection coefficients is generally observed and may be partly due to experimental errors in the determination of the reflection coefficient. This was discussed briefly in Section II.3.b and in detail in Section III.3.b.

The transmission coefficients predicted based on the assumption $\Delta H_e/\Delta H_T = 1$ are seen to be lower than the experimentally obtained values. This, of course, is the expected type of discrepancy since the runup on the seaward slope of the trapezoidal breakwater is almost certain to exceed the runup on the equivalent rectangular breakwater. Adopting the theoretical value of the runup, R_u, on the trapezoidal breakwater predicted by the procedure developed in Section III of this report is expected to give transmission coefficients slightly on the high side as discussed in Section IV.3.c. This anticipated behavior is not exhibited by the predicted transmission coefficients plotted in Figure 26. In fact, the agreement between observed and predicted transmission coefficients is excellent.

A slightly different estimate of the runup on the seaward slope of a trapezoidal breakwater may be obtained by adopting, for example, the results obtained by Jackson (1968), who reported values of R_u approximately equal to unity for test conditions similar to those of Sollitt and Cross (1972). In the present case this value of R_u would result in a slightly lower prediction of the transmission coefficient than the prediction indicated by the full line in Figure 26.

The procedure developed here for the prediction of transmission and reflection coefficients of a trapezoidal, multilayered breakwater did not rely on the experimental data shown in Figure 26 to obtain a "good fit". The overall comparison between predicted and observed transmission and reflection coefficients, which is analogous to the comparison given by Sollitt and Cross (1972, Fig. 4-14), must therefore be considered very good.

V. SUMMARY AND CONCLUSIONS

This report presents the results of an analytical study of the reflection and transmission characteristics of porous rubble-mound breakwaters. An attempt was made at making the procedures entirely self-contained by introducing empirical relationships for the hydraulic characteristics of the porous material and by establishing experimentally an empirical relationship for the friction factor that expresses energy dissipation on the seaward slope of a breakwater.

The results are presented in graphical form and require no use of computers, although the entire approach could be programmed. The procedures were developed in such a manner that the information required to carry out the computations can be expected to be available. Thus, for a trapezoidal, multilayered breakwater subject to normally incident, relatively long waves the information required is:

(a) Breakwater configuration: breakwater geometry and stone size and porosity of the breakwater materials

(b) Incident wave characteristics: wave amplitude, period, and water depth.

Only the porosity of the breakwater materials may be hard to come by. It is recommended that the sensitivity of the results to the estimate of the porosity, n, be investigated.

The hydraulic flow resistance in the porous medium is expressed by a Dupuit-Forchheimer relationship and empirical formulas are adopted. The investigation shows that reasonably accurate results are obtained by taking

$$\beta_o \simeq 2.7 \qquad\qquad (177)$$

$$\alpha_o \simeq 1150$$

in equations (51) and (52). To estimate reflection and transmission characteristics of a prototype structure only the value of β_o needs to be known. For laboratory experiments the value of the ratio, α_o/β_o is important in assessing the influence of scale effects. In a laboratory setup it is possible to determine the best values of α_o and β_o from the simple experimental procedure used by Keulegan (1973). Thus, it was found that the porous materials tested by Sollitt and Cross (1972) showed a value of α_o = 2,700, a better value than that given by equation (177). However, the important thing to note is that the analysis carried out in Section II of this report presents a method for assessing the severity of scale effects in hydraulic models of porous structures. The empirical relationships for the flow resistance of porous materials have been demonstrated to be fairly good for porous materials consisting of gravel-size stones, diameter less than 2 inches (5 centimeters).

The energy dissipation on a rough, impermeable slope was investigated in Section III. The experimental investigation revealed the need for an accurate method for the determination of reflection coefficients from experimental data. The simple procedure of seeking out the locations where the wave amplitudes are maximum and minimum, respectively, may lead to reflection coefficients which are much too low, unless the recorded surface elevation is analyzed and only the amplitude of the first harmonic motion is used to determine the reflection coefficient. Accurately determined reflection coefficients for slopes with roughness elements consisting of gravel led to an empirical determination of the friction factor (eqs. 124 and 125), expressing the energy dissipation on a rough slope due to bottom friction. Adopting this empirical relationship a procedure for estimating the reflection coefficient of rough impermeable slopes was developed. This procedure was quite accurate in reproducing the experimentally obtained reflection coefficients in a separate set of experiments. The procedure for the determination of the reflection coefficient of rough impermeable slopes is limited to slopes having roughness elements consisting of natural stones. To make the procedure generally applicable, empirical relationships for the friction factor should be determined for slopes whose roughness elements consist of models of concrete armor units.

The synthesis of the investigation is the development of an approximate procedure for the prediction of the reflection and transmission characteristics of trapezoidal, multilayered breakwaters. This procedure is entirely self-contained and yields excellent results when compared with the model scale experimental results obtained by Sollitt and Cross (1972).

It is emphasized that the analytical model for the reflection and transmission characteristics of trapezoidal, multilayered breakwaters developed here needs further verification before it can be used with complete confidence. However, the good agreement between predictions and observations exhibited in Figure 26 is encouraging and does indicate that a simple analytical model which may be used for preliminary design of rubble-mound breakwaters has been developed.

LITERATURE CITED

BEAR, J., et al., *Physical Principles of Water Percolation and Seepage*, United Nations Educational, Scientific and Cultural Organization, 1968.

EAGLESON, P.S. and DEAN, R.G., "Small Amplitude Wave Theory," *Estuary and Coastline Hydrodynamics*, McGraw-Hill, New York, 1966, pp. 1-92.

ENGELUND, F., "On the Laminar and Turbulent Flows of Ground Water through Homogeneous Sand," *Transactions of the Danish Academy of Technical Sciences*, Vol. 3, No. 4, 1953.

HILDEBRAND, F.B., *Advanced Calculus for Applications*, Prentice-Hall, Englewood Cliffs, N.J., 1965.

IPPEN, A.T., *Estuary and Coastline Hydrodynamics*, McGraw-Hill, New York, 1966.

JACKSON, R.A., "Design of Cover Layers for Rubble-Mound Breakwaters Subjected to Nonbreaking Waves," Research Report No. 2-11, U.S. Army Engineer Waterways Experiment Station, Vicksburg, Miss., 1968.

JONSSON, I.G., "Wave Boundary Layers and Friction Factors," *Proceedings 10th Conference on Coastal Engineering*, American Society of Civil Engineers, 1966, pp. 127-148.

KAJIURA, K., "On the Bottom Friction in an Oscillatory Current," *Bulletin of the Earthquake Research Institute*, Vol. 42, 1964, pp. 147-174.

KEULEGAN, G.H., "Wave Transmission through Rock Structures," Research Report No. H-73-1, U.S. Army Engineer Waterways Experiment Station, Vicksburg, Miss., 1973.

KONDO, H., "Wave Transmission through Porous Structures," *Journal of the Waterways, Harbors and Coastal Engineering*, Vol. 101, WW3, 1975. pp. 300-302.

MADSEN, O.S., "Wave Transmission through Porous Structures," *Journal of the Waterways, Harbors and Coastal Engineering*, Vol. 100, WW3, 1974, pp. 169-188.

MEYER, R.E. and TAYLOR, A.D., "Run-up on Beaches," *Waves on Beaches*, Academic Press, New York, 1972, pp. 357-412.

MICHE, M., "Pouvoir Reflechissant des Ouvrage Maritimes Exposes a L'action de Houle," *Annales des Ponts et Chaussees*, 1951, pp. 295-319.

PEREGRINE, D.H., "Equations for Water Waves and the Approximations Behind Them," *Waves on Beaches*, Academic Press, New York, 1972, pp. 95-123.

POLUBARINOVA-KOCHINA, P.Y., *Theory of Ground Water Movement*, Princeton University Press, Princeton, N.J., 1962.

SCHLICHTING, H., *Boundary Layer Theory*, 4th ed., McGraw-Hill, New York, 1960.

SOLLITT, C.K. and CROSS, R.H., "Wave Reflection and Transmission at Permeable Breakwaters," Technical Report No. 147, R. M. Parsons Laboratory, Department of Civil Engineering, Massachusetts Institute of Technology (MIT), Cambridge, Mass., 1972.

URSELL, F. et al., "Forced Small-Amplitude Water Waves," *Journal of Fluid Mechanics*, Vol. 7, Pt. 3, 1960, pp. 33-52.

WILSON, K.W., "Scale Effect in Rubble-Mound Breakwaters," unpublished Masters Thesis, Department of Civil Engineering, MIT, Cambridge, Mass., June 1971.

APPENDIX A

GOVERNING EQUATIONS AND THEIR SOLUTION

1. Long Waves over a Rough Bottom.

To derive the approximate equations governing the propagation of long waves over a rough bottom we take the basic equations expressing conservation of mass and momentum for an incompressible fluid. In two dimensions these equations read (Schlichting, 1960)

$$\frac{\partial U}{\partial x} + \frac{\partial W}{\partial z} = 0 \tag{A-1}$$

$$\rho \frac{DU}{Dt} = - \frac{\partial p}{\partial x} + \frac{\partial \tau}{\partial z} \tag{A-2}$$

$$\rho \frac{DW}{Dt} = - \frac{\partial p}{\partial z} - \rho g \tag{A-3}$$

in which U and W are the horizontal and vertical velocity components, respectively; ρ is the fluid density, p is the pressure, and g is the acceleration due to gravity. The coordinate system is defined in Figure A-1 and only the horizontal shear stress, τ, is retained in the horizontal momentum equation.

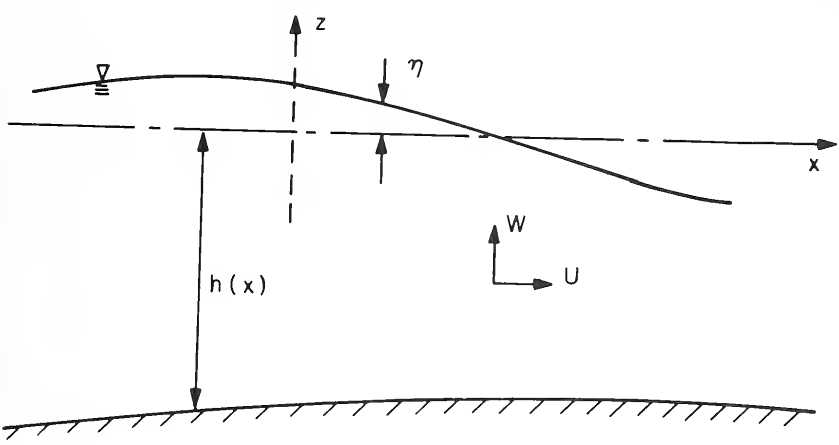

Figure A-1. Definition sketch.

The boundary conditions to be satisfied by these equations are that the pressure be zero at the free surface, $z = \eta(x,t)$,

$$p = p_\eta = 0 \quad \text{at } z = \eta, \tag{A-4}$$

and the kinematic boundary conditions

$$\frac{\partial \eta}{\partial t} + U_\eta \frac{\partial \eta}{\partial x} - W_\eta = 0 \quad \text{at } z = \eta \tag{A-5}$$

and

$$W_b + U_b \frac{\partial h}{\partial x} = 0 \quad \text{at } z = -h \quad , \tag{A-6}$$

where subscripts η and b refer to the conditions at the free surface and at the bottom, respectively.

To derive the continuity equation in the form normally encountered in work involving long waves, equation (A-1) is integrated over the depth of water

$$\int_{-h}^{\eta} \frac{\partial U}{\partial x}\, dz + \int_{-h}^{\eta} \frac{\partial W}{\partial z}\, dz = \int_{-h}^{\eta} \frac{\partial U}{\partial x}\, dz + W_\eta - W_b = 0 \quad , \tag{A-7}$$

and the remaining integral is evaluated using Leibnitz' rule (Hildebrand, 1965)

$$\int_{A(\sigma)}^{B(\sigma)} \frac{\partial f}{\partial \sigma}\, dz = \frac{\partial}{\partial \sigma} \int_{A}^{B} f\, dz - f(B) \frac{\partial B}{\partial \sigma} + f(A) \frac{\partial A}{\partial \sigma} \quad , \tag{A-8}$$

in order to obtain

$$\frac{\partial}{\partial x} \int_{-h}^{\eta} U\, dz + W_\eta - U_\eta \frac{\partial \eta}{\partial x} - W_b - U_b \frac{\partial h}{\partial x} = 0 \quad . \tag{A-9}$$

Introducing the concept of a mean velocity, $\overline{U}$, defined by

$$\overline{U} = \frac{1}{h+\eta} \int_{-h}^{\eta} U\, dz \quad , \tag{A-10}$$

and realizing that the boundary conditions (eqs. A-5 and A-6) may be used to simplify equation (A-9), the continuity equation becomes

$$\frac{\partial \eta}{\partial t} + \frac{\partial}{\partial x} \{\bar{U}(h+\eta)\} = 0 \quad . \tag{A-11}$$

From the continuity equation in its basic form (eq. A-1), introduction of the typical length scales, the wavelength, L, in the horizontal direction and the water depth, h, in the vertical direction, shows that the order of magnitude of the vertical velocity component is given by

$$W = 0 \left(\frac{h}{L} U\right) \quad . \tag{A-12}$$

Thus, for long waves, $h/L \ll 1$, we have that $W \ll U$. This observation suggests that the vertical fluid accelerations, DW/Dt, in equation (A-3) may be neglected. For long waves equation (A-3) therefore simplifies to a statement of hydrostatic pressure distribution,

$$p = \rho g(\eta - z) \quad , \tag{A-13}$$

where the boundary condition (eq. A-4) has been invoked.

Introducing p as given by equation (A-13) and making use of equation (A-1) the horizontal momentum equation may be written:

$$\frac{DU}{Dt} = \left(\frac{\partial U}{\partial t} + \frac{\partial U^2}{\partial x} + \frac{\partial UW}{\partial z}\right) = -g \frac{\partial \eta}{\partial x} + \frac{\partial \tau/\rho}{\partial z} \quad . \tag{A-14}$$

This equation may be integrated over the depth to yield:

$$\frac{\partial}{\partial t} \int_{-h}^{\eta} U \, dz + \frac{\partial}{\partial x} \int_{-h}^{\eta} U^2 \, dz - U_\eta \left\{\frac{\partial \eta}{\partial t} + U_\eta \frac{\partial \eta}{\partial x} - W_\eta\right\}$$

$$-U_b\left\{W_b + U_b \frac{\partial h}{\partial x}\right\} = -(h+\eta) \, g \frac{\partial \eta}{\partial x} + \frac{\tau_\eta}{\rho} - \frac{\tau_b}{\rho} \quad . \tag{A-15}$$

By virtue of the boundary conditions (eqs. A-5 and A-6), the bracketed terms vanish, and by introducing the concept of the momentum coefficient,

$$K_m = \frac{\int_{-h}^{\eta} u^2 \, dz}{(h+\eta)\ \overline{U}^2} \quad , \tag{A-16}$$

the integrated momentum equation may be written:

$$\frac{\partial}{\partial t}\{(h+\eta)\ \overline{U}\} + \frac{\partial}{\partial x}\{(h+\eta)\ K_m \overline{U}^2\} = -(h+\eta)\ g\ \frac{\partial \eta}{\partial x} - \frac{\tau_b}{\rho} \quad , \tag{A-17}$$

in which the shear stress on the free surface has been set equal to zero.

Using the results from linear wave theory (Eagleson and Dean, 1966), it may be shown that the value of K_m as given by equation (A-16) is 1.01 corresponding to a wave having h/L = 0.1. Thus, it is a good approximation to take K_m in equation (A-17) equal to unity as is normally done in open channel flow calculations. With K_m equal to unity and incorporating the continuity equation, equation (A-11), the momentum equation becomes:

$$\frac{\partial \overline{U}}{\partial t} + \overline{U}\ \frac{\partial \overline{U}}{\partial x} = -g\ \frac{\partial \eta}{\partial x} - \frac{\tau_b}{\rho\,(h+\eta)} \quad . \tag{A-18}$$

The appropriate equations governing the propagation of long waves over a rough bottom are therefore equations (A-11) and (A-18). However, these equations cannot be solved until the shear stress in equation (A-18) has been related to the kinematics of the problem. To this end we may introduce the concept of the wave friction factor, f_w, as defined by Jonsson (1966),

$$\tau_b = \frac{1}{2}\ \rho\ f_w |\overline{U}| \overline{U} \quad , \tag{A-19}$$

where $|\overline{U}|$ is the absolute value of the velocity. When this expression is introduced in equation (A-18) the governing equations become:

$$\frac{\partial \eta}{\partial t} + \frac{\partial}{\partial x}\ (h+\eta)\ U\} = 0 \tag{A-20}$$

and

$$\frac{\partial U}{\partial t} + U\ \frac{\partial U}{\partial x} = -g\ \frac{\partial \eta}{\partial x} - \frac{\frac{1}{2}\ f_w |U| U}{(h+\eta)} \quad , \tag{A-21}$$

where the overbar notation has been dropped.

a. Linearization and Solution Technique. To obtain closed form analytical solutions to the equations derived in the previous section it is necessary to linearize these equations. To justify a linearization of equations (A-20) and (A-21) we must impose the condition that

$$|\eta| << h \quad , \tag{A-22}$$

in which case $h+\eta$ may be replaced by h. This condition implies that the term $U\partial U/\partial x$ also may be omitted. Hence, the final task is to linearize the bottom friction term. Since we will be looking for periodic solutions to the linearized equations this is conveniently done by taking

$$f_b\omega = \frac{\frac{1}{2}\, f_w|U|}{h+\eta} = \frac{\frac{1}{2}\, f_w|U|}{h} \quad , \tag{A-23}$$

in which f_b is treated formally as a constant and ω is the radian frequency of the periodic motion.

Performing the above linearizations of the governing equations, we obtain

$$\frac{\partial \eta}{\partial t} + \frac{\partial}{\partial x}(hU) = 0 \tag{A-24}$$

and

$$\frac{\partial U}{\partial t} + g\,\frac{\partial \eta}{\partial x} + f_b\omega U = 0 \quad . \tag{A-25}$$

To illustrate the solution of this set of equations we consider the simple case of periodic waves of radian frequency, ω, propagating over a horizontal bottom, i.e., $h = h_o$ = constant. To facilitate the solution complex variables are introduced by defining

$$U = \text{Real}\,\{u\, e^{i\omega t}\}$$

$$\eta = \text{Real}\,\{\zeta\, e^{i\omega t}\} \quad , \tag{A-26}$$

where $i = \sqrt{-1}$ and the amplitude functions, u and ζ, are complex functions of x. The physical solution is given by the real part of the solution as indicated by the notation Real { }. Introducing equation (A-26) in equations (A-24) and (A-25), these may be written in terms of the amplitude functions:

$$i\omega\zeta + h_o\,\frac{\partial u}{\partial x} = 0 \tag{A-27}$$

and

$$i\omega(1-if_b)\ u + g\frac{\partial\zeta}{\partial x} = 0 \quad . \tag{A-28}$$

From equation (A-28) we obtain

$$u = -\frac{g}{i\omega(1-if_b)}\ \frac{\partial\zeta}{\partial x} \quad , \tag{A-29}$$

which may be substituted into equation (A-27) to yield the governing equation:

$$\frac{\partial^2\zeta}{\partial x^2} + \frac{\omega^2}{gh_o}\ (1-if_b)\zeta = 0 \quad , \tag{A-30}$$

which simplifies to the usual wave equation for f_b equal to zero.

The general solution of equation (A-30) is given by

$$\zeta = a_+ e^{-ikx} + a_- e^{+ikx} \quad , \tag{A-31}$$

in which a_+ and a_- are complex amplitudes, whose magnitudes give the physical wave amplitude, and k is the complex wave number defined by

$$k^2 = \frac{\omega^2}{gh_o}\ (1-if_b) \quad , \tag{A-32}$$

which may be written in terms of the usual wave number,

$$k_o = \frac{\omega}{\sqrt{gh_o}} \tag{A-33}$$

and

$$k = k_o\ \sqrt{1-if_b} = k_o\ \sqrt[4]{1+f_b^2}\ \ e^{-i\phi_b} \quad , \tag{A-34}$$

where

$$\tan 2\phi_b = f_b \quad . \tag{A-35}$$

Taking, for example, the wave solution of amplitude a_+ in equation (A-31), this reads:

$$\zeta_+ = a_+ e^{-ik_o \sqrt[4]{1+f_b^2}\,(\cos\phi_b - \sin\phi_b)\,x}$$

$$= a_+ e^{-k_o \sqrt[4]{1+f_b^2}\,\sin\phi_b\,x}\; e^{-ik_o \sqrt[4]{1+f_b^2}\,\cos\phi_b\,x} \quad , \qquad \text{(A-36)}$$

where a_+ may be considered a real number. When this is introduced in equation (A.26) and only the real part is retained we obtain

$$\eta_+ = a_+ e^{-k_o \sqrt[4]{1+f_b^2}\,\sin\phi_b\,x} \cos\,(\omega t - k_o \sqrt[4]{1+f_b^2}\,\cos\phi_b\,x), \qquad \text{(A-37)}$$

which shows the solution to be that of a sinusoidal wave propagating in the positive x-direction with an exponentially decreasing amplitude. In the same manner the wave solution of amplitude a_- in equation (A-31) may be shown to represent a wave propagating in the negative x-direction with an exponentially decreasing amplitude in the direction of propagation. Thus, we have obtained a formal solution to the problem of a long wave propagating over a rough bed. However, the solution must be considered formal since it depends on the value of the linearization factor f_b introduced through equation (A-23). To obtain the appropriate value of the constant f_b, it must be related to the true friction factor, f_w, and the wave characteristics.

b. Application of Lorentz' Principle. To obtain an explicit solution for the linearized friction factor, f_b, we use Lorentz' principle of equivalent work. This principle is a useful tool for obtaining approximate results from a set of linearized governing equations in which the nonlinear term expressing the flow resistance has been linearized. The principle (Ippen, 1966) states that the average rate of energy dissipation calculated from the "true" nonlinear friction term and that calculated from its linearized equivalent should be the same. As shown by Kajiura (1964), the instantaneous rate of energy dissipation per unit bottom area may be approximated by

$$E_D \simeq U\tau_b \quad . \qquad \text{(A-38)}$$

For a given area, A, and assuming a periodic motion of period, T, the average rate of energy dissipation becomes:

$$\overline{\overline{E}}_D = \frac{1}{A}\int_A dA\,\{\frac{1}{T}\int_0^T U\tau_b\,dt\} \quad , \qquad \text{(A-39)}$$

in which the double overbar signifies that spatial as well as temporal average is to be taken.

In the present context use of equations (A-19) and (A-23) in conjunction with Lorentz' principle yields:

$$\frac{1}{A}\int_A dA \left\{\frac{1}{T}\int_0^T \frac{1}{2}\rho\, f_w\, |U|U^2\, dt\right\} =$$

$$=$$

$$\frac{1}{A}\int_A dA \left\{\frac{1}{T}\int_0^T \rho\, f_b\, \omega h\, U^2\, dt\right\} \quad , \tag{A-40}$$

which leads to a determination of f_b in terms of known quantities.

As an illustration we take a progressive wave in a constant depth of water, $h = h_o$, and equation (A-40) may be written:

$$f_b = \frac{\frac{1}{2} f_w}{\omega h_o} \; \frac{\overline{\overline{|U_+|U_+^2}}}{\overline{\overline{U_+^{\,2}}}} \quad , \tag{A-41}$$

in which U_+ is given by equations (A-26) and (A-29) corresponding to the surface profile given by equation (A-36), i.e.,

$$U_+ = \mathrm{Re}\left\{\frac{g k_o a_+}{\omega\sqrt{1-if_b}}\; e^{-i(kx - \omega t)}\right\} =$$

$$U_o\, e^{-k_i x} \cos(\omega t - k_r x + \phi_b) \quad , \tag{A-42}$$

in which ϕ_b is given by equation (A-35) and

$$U_o = \frac{g k_o a_+}{\omega\sqrt[4]{1+f_b^{\,2}}} \tag{A-43}$$

and

$$k_r - ik_i = k = k_o \sqrt[4]{1+f_b^{\,2}} \; (\cos\phi_b - i \sin\phi_b) \quad . \qquad \text{(A-44)}$$

Introducing these expressions in equation (A-41) and performing the spatial average over an area of unit width and extending from $x = 0$ to $x = \ell$, the following equation is obtained:

$$f_b \sqrt[4]{1+f_b^{\,2}} = \frac{4}{3\pi} f_w \frac{k_o a_+}{(k_o h_o)^2} \left\{ \frac{2}{3} \; \frac{1-e^{-3k_i \ell}}{1-e^{-2k_i \ell}} \right\} \quad . \qquad \text{(A-45)}$$

Although not leading to an explicit equation for the friction factor, f_b, this expression may be solved iteratively from knowledge of f_w and the wave characteristics. The bracketed term in equation (A-45) arises from the spatial averaging process and becomes unity if $k_i \ell << 1$. Thus, in the immediate vicinity of $x = 0$ we have

$$f_b \sqrt[4]{1+f_b^{\,2}} = \frac{4}{3\pi} f_w \frac{k_o a_+}{(k_o h_o)^2} \quad , \qquad \text{(A-46)}$$

which may be shown to lead to the same rate of amplitude attenuation as the formula suggested by Putnam and Johnson (1949).

c. Limitation of the Solution. To discuss the limitations of the solutions obtained from the governing equations derived in the preceding sections we consider the solution obtained for a progressive wave in constant water depth, h_o, without bottom friction, i.e., $f_w = f_b = \phi_b = 0$. For this simple case we have from equations (A-37) and (A-42),

$$\eta_+ = a_+ \cos(k_o x - \omega t)$$

$$U_+ = \frac{a_+}{h_o} \sqrt{gh_o} \; \cos(k_o x - \omega t) \quad . \qquad \text{(A-47)}$$

The basic assumption made in the derivation of the equations leading to this solution was that the vertical accelerations were negligible. We may now reexamine this assumption by obtaining the expression for the vertical velocity, W_+, from equation (A-1),

$$W_+ = a_+ \omega \; (1 + \frac{z}{h_o}) \; \sin(k_o x - \omega t) \quad , \qquad \text{(A-48)}$$

and the leading term arising from the vertical fluid acceleration in equation (A-3) is

$$\rho \frac{\partial W_+}{\partial t} = -\rho a_+ \omega^2 \left(1 + \frac{z}{h_o}\right) \cos(k_o x - \omega t) \quad , \tag{A-49}$$

which integrated over depth gives:

$$\int_{-h_o}^{z} \rho \frac{\partial W_+}{\partial t} \, dz = - \frac{1}{2} \rho \, a_+ \omega^2 h_o \left(1 + \frac{z}{h_o}\right)^2 \cos(k_o x - \omega t) \quad . \tag{A-50}$$

From the derivation of the pressure distribution (eq. A-13), the term expressing the presence of the wave is

$$p_+ = \rho \, g a_+ \cos(k_o x - \omega t) \quad , \tag{A-51}$$

and to justify the neglect of the term given by equation (A-50) we must have that

$$\frac{1}{2} \rho \, a_+ \omega^2 h_o << \rho \, g a_+ \quad , \tag{A-52}$$

which with the aid of equation (A-33) may be stated as

$$\frac{1}{2} (k_o h_o)^2 << 1 \quad , \tag{A-53}$$

i.e., a requirement of long waves as previously stated.

Now, in the process of linearizing the governing equations it was mentioned that this linearization was justified if

$$\frac{|\eta_+|}{h_o} = \frac{a_+}{h_o} << 1 \quad , \tag{A-54}$$

because the terms then omitted would be smaller than the terms retained by the factor a_+/h. This in turn would be a consistent procedure only if the pressure term given by equation (A-50) is greater than (a_+/h) times the leading term given by equation (A-51), i.e., linearization of the governing equations and taking the pressure distribution to be hydrostatic is consistent only if

$$\frac{1}{2} \rho \, a_+ \omega^2 h_o >> \rho \, g a_+ \frac{a_+}{h_o} \quad , \tag{A-55}$$

which may be written as the requirement that the Stokes' parameter

$$\frac{a_+ L^2}{h_o^3} << 2\pi^2 \quad . \tag{A-56}$$

Thus, the limitations on the solutions obtained from the linearized set of governing equations are expressed as the inequalities given by equations (A-53), (A-54), and (A-56). For a derivation of the appropriate governing equations when equation (A-56) is violated the reader is referred to Peregrine (1972).

For a wave propagating over an uneven bottom a vertical velocity may be imposed by the bottom boundary condition (eq. A-6). So long as the velocity obtained from this boundary condition is smaller than that given by equation (A-48) the preceding limitations are applicable. This in turn may be stated as a requirement that the bottom slope,

$$\tan\beta_s = \left|\frac{\partial h}{\partial x}\right| \quad , \tag{A-57}$$

satisfy the inequality,

$$\frac{\tan\beta_s}{kh} < 1 \quad . \tag{A-58}$$

2. Long Waves in a Porous Medium.

To derive the equations governing the propagation of waves in a porous medium we consider an element as sketched in Figure A-2.

In a porous medium of porosity, n, the discharge per unit area in say the x-direction is given $U = nU_s$ where U_s is the seepage velocity, i.e., the actual mean velocity of the pore fluid, and U is termed the discharge velocity. With this definition it is seen that the discharge velocity, (U,W), for an incompressible fluid and medium must satisfy the continuity equation:

$$\frac{\partial U}{\partial x} + \frac{\partial W}{\partial z} = 0 \quad , \tag{A-59}$$

or for a homogeneous medium,

$$\frac{\partial U_s}{\partial x} + \frac{\partial W_s}{\partial z} = 0 \quad . \tag{A-60}$$

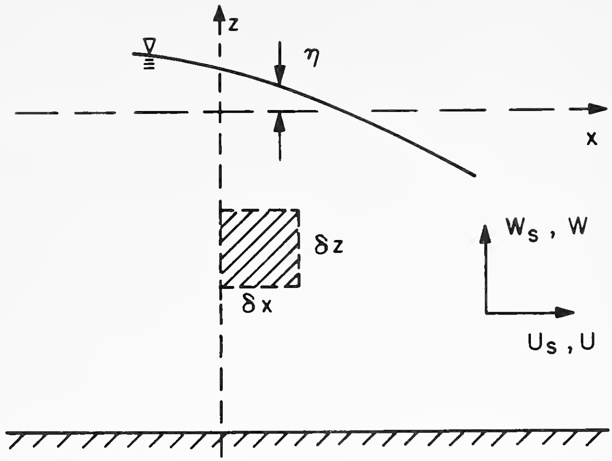

Figure A-2. Definition sketch.

To derive the horizontal momentum equation we consider the elementary control volume indicated in Figure A-2. The momentum equation states that the sum of the forces acting on the fluid within this element must equal the rate of increase in momentum plus the net momentum flux out of this control volume. Of forces acting on the fluid within the element we have the pressure force,

$$\delta F_p = - \frac{\partial p}{\partial x} \delta x \delta z \quad , \tag{A-61}$$

and a force resisting the fluid motion within the porous medium. In an unsteady motion this force will consist of a drag force, δF_d, and an inertia force, δF_I. For steady flow the drag force component is expressed as a volume force which may be taken as

$$\delta F_d = -\rho(\alpha + \beta\sqrt{U^2 + W^2})U \quad \delta x \delta z \quad , \tag{A-62}$$

where the hydraulic properties of the porous medium are given by the coefficients α and β. The coefficient α expresses the laminar flow resistance and β is associated with the turbulent flow resistance.

The inertial force, δF_I, is associated with the fluid acceleration. The fluid velocity, as seen by a solid particle in the porous medium, is the seepage velocity and by analogy with inertia forces acting on a single particle we may take

$$\delta F_I = -\rho(1+\kappa)\frac{DU_s}{Dt}\,\delta\forall_m = -\rho(1+\kappa)\frac{DU_s}{Dt}(1-n)\,\delta x\delta z \quad , \qquad \text{(A-63)}$$

where $\delta\forall_m$ is the volume of solids within the control volume and κ is the added mass coefficient. Little information is available on the magnitude of κ for a closely packed ensemble of irregular grains. For isolated spheres $\kappa = 0.5$ may serve as an indication of the order of magnitude.

The rate of change of momentum within the fixed control volume is given by

$$\frac{\partial M}{\partial t} = \rho\frac{\partial}{\partial t}(\partial\forall_f U_s) = \rho\, n\frac{\partial U_s}{\partial t}\,\delta x\delta z \quad , \qquad \text{(A-64)}$$

and the momentum flux out of the control volume is given by

$$M_F = \rho\left(\frac{\partial}{\partial x}\{U_s n U_s\} + \frac{\partial}{\partial z}\{U_s n W_s\}\right)\delta x\delta z =$$

$$\rho n\left(U_s\frac{\partial U_s}{\partial x} + W_s\frac{\partial U_s}{\partial z}\right)\delta x\delta z \quad , \qquad \text{(A-65)}$$

where the continuity equation has been invoked.

Now formulating the momentum equation,

$$\delta F_p + \delta F_d + \delta F_I = \frac{\partial M}{\partial t} + M_F \quad , \qquad \text{(A-66)}$$

and introducing equations (A-61 through A-65) the horizontal momentum equation is obtained as

$$\rho(1 + \kappa\,(1-n))\frac{DU_s}{Dt} = -\frac{\partial p}{\partial x} - \rho(\alpha + \beta\sqrt{U^2 + W^2})\,U \quad , \qquad \text{(A-67)}$$

which corresponds to the equation given by Polubarinova-Kochina (1962) for unsteady flow in a porous medium with the resistance term expressed by a Dupuit-Forchheimer type of formula. The coefficient attached to the acceleration term is somewhat different from the expression given by Sollitt and Cross (1972), but is believed to be correct in the present derivation.

A similar expression may be derived by considering the vertical momentum thus leading to the momentum equations for a homogeneous, imcompressible medium,

$$\rho S \frac{DU_s}{Dt} = - \frac{\partial p}{\partial x} - \rho\{n(\alpha + \beta\sqrt{U^2 + W^2})\} U_s \tag{A-68}$$

and

$$\rho S \frac{DW_s}{Dt} = - \frac{\partial p}{\partial z} - \rho g - \rho\{n(\alpha + \beta\sqrt{U^2 + W^2})\} \; W_s \quad , \tag{A-69}$$

where

$$S = 1 + \kappa(1 - n) \quad , \tag{A-70}$$

is expected to take on values within the range $1 \leq S \leq 1.5$.

The similarity of these governing equations and those given for waves over a rough bottom (eqs. A-1 through A-3) should be noted. Further development follows that given in Appendix A.1 and the boundary conditions to be satisfied are those previously given but now expressed in terms of the seepage velocity. Hence, integration of the continuity equation over depth gives:

$$n \frac{\partial \eta}{\partial t} + \frac{\partial}{\partial x} \{U(h + \eta)\} = 0 \quad , \tag{A-71}$$

and with the assumption of long waves, equation (A-69) yields a hydrostatic pressure distribution,

$$p = \rho g(\eta + z) \quad . \tag{A-72}$$

The horizontal momentum equation then becomes

$$S \frac{1}{n} \frac{DU}{Dt} = - g \frac{\partial \eta}{\partial x} - (\alpha + \beta|U|)U \quad , \tag{A-73}$$

where U should be interpreted as the depth averaged discharge velocity.

a. <u>Linearization and Solution Technique</u>. The linearized version of the governing equations may be taken as

$$n \frac{\partial \eta}{\partial t} + \frac{\partial}{\partial x} (hU) = 0 \tag{A-74}$$

and

$$\frac{S}{n}\frac{\partial U}{\partial t} + g\frac{\partial \eta}{\partial x} + f\frac{\omega}{n}U = 0 \qquad \text{(A-75)}$$

where the flow resistance term has been linearized by introducing the dimensionless factor, f, defined by

$$f\frac{\omega}{n} = \alpha + \beta|U| \quad , \qquad \text{(A-76)}$$

in which ω is the radian frequency of the wave motion, which is assumed periodic.

The solution technique is that used in the solution of the linearized equations governing the propagation of long waves over a rough bottom, i.e., we take

$$\eta = \text{Real}\,\{\zeta\, e^{i\omega t}\}$$

$$U = \text{Real}\,\{u\, e^{i\omega t}\} \quad . \qquad \text{(A-77)}$$

For the case of constant depth $h = h_o$ introducing equation (A-77) in the governing equations leads to

$$u = -\frac{g\,n}{i\omega(S-if)}\frac{\partial \zeta}{\partial x} \quad , \qquad \text{(A-78)}$$

and the equation governing the amplitude function

$$\frac{\partial^2 \zeta}{\partial x^2} + \frac{\omega^2}{gh_o}(S-if)\zeta = 0 \qquad \text{(A-79)}$$

Both of these equations are seen to be similar to those discussed in Appendix A.1.a and the results obtained there are readily generalized to give the solution for a progressive wave in a porous medium. The general solution consisting of waves propagating in the positive and negative x-direction is found to be given by

$$\zeta = a_+\, e^{-ikx} + a_-\, e^{ikx} \quad , \qquad \text{(A-80)}$$

where

$$k = k_o \sqrt{S-if} = k_o \sqrt[4]{S^2 + f^2} \; e^{-i\phi_p} \qquad \text{(A-81)}$$

and

$$\tan 2\phi_p = \frac{f}{S} \quad . \qquad \text{(A-82)}$$

As was the case in the solution for long waves over a rough bottom, the above solution is formal only, since the appropriate value to be assigned to the linearized resistance coefficient f has not been determined.

To obtain the appropriate value for f, Lorentz' principle is used with the rate of dissipation per unit volume given by

$$E_D = U \; \delta F_d \quad . \qquad \text{(A-83)}$$

Thus, we obtain:

$$f \frac{\omega}{n} \overline{\overline{U^2}} = \alpha\overline{\overline{U^2}} + \beta\overline{\overline{|U|U^2}} \quad , \qquad \text{(A-84)}$$

where the spatial average is to be taken over the volume occupied by the fluid.

As a simple example we consider the velocity given by

$$U = U_o \cos \omega t \quad , \qquad \text{(A-85)}$$

for which equation (A-84) yields:

$$f = \frac{n}{\omega}(\alpha + \frac{8}{3\pi} \beta \, U_o) \quad . \qquad \text{(A-86)}$$

In the discussion of long waves propagating over a rough bottom the result corresponding to equation (A-86) was given by equation (A-46). However, although the friction factor, f_w, in equation (A-46) may be considered known by applying Jonsson's (1966) empirical results, we have not established a similar empirical relationship for the hydraulic properties, α and β, of a porous medium.

Engelund (1953) reviewed a number of empirical formulas for the hydraulic properties of porous media consisting of sand. He recommended the following empirical relationships:

$$\alpha = \alpha_o \frac{(1-n)^3}{n^2} \frac{\nu}{d^2} \tag{A-87}$$

and

$$\beta = \beta_o \frac{1-n}{n^3} \frac{1}{d} \quad , \tag{A-88}$$

in which d is the grain size of the porous material, ν is the kinematic viscosity of the pore fluid, and α_o and β_o are constants whose values have been found to vary within the range,

$$780 < \alpha_o < 1{,}500 \text{ or greater}$$

$$1.8 < \beta_o < 3.6 \quad \text{or greater} \quad . \tag{A-89}$$

The coefficient α, which depends on the fluid viscosity, is expressing the Darcy-type resistance associated with laminar flow of the pore fluid. The flow resistance associated with the coefficient β is the velocity square-type normally associated with turbulent flow. From equation (A-86) it is seen that we may take

$$f = \frac{8}{3\pi} \frac{n}{\omega} \beta U_o (1 + \frac{3\pi}{8} \frac{\alpha}{\beta U_o}) \quad , \tag{A-90}$$

in anticipation of the domination of turbulent resistance in prototype flow of water through breakwaters. Written in this form the degree to which laminar resistance affects the results is given by

$$\frac{3\pi}{8} \frac{\alpha}{\beta U_o} = \frac{3\pi}{8} (1-n)^2 n \frac{\alpha_o}{\beta_o} (\frac{\nu}{dU_o}) \quad , \tag{A-91}$$

where equations (A-87) and (A-88) have been introduced. This expression may be written as:

$$\frac{3\pi}{8} \frac{\alpha}{\beta U_o} = \frac{R_c}{R_d} \quad , \tag{A-92}$$

in which R_d is a particle Reynolds number,

$$R_d = \frac{dU_o}{\nu} \quad , \tag{A-93}$$

and

$$R_c = \frac{3\pi}{8} (1-n)^2 n \frac{\alpha_o}{\beta_o} \simeq 0.17 \frac{\alpha_o}{\beta_o} \tag{A-94}$$

is a critical Reynolds number whose value is of the order 70 if the mean values of the ranges indicated by equation (A-89) are taken. The fact that the term $(1-n)^2n$ varies only slightly for $0.4 < n < 0.5$ has been used in establishing equation (A-94).

Thus, for values of $R_d >> R_c$ the flow resistance is purely turbulent and with β related to the physical characteristics of the porous material through equation (A-88) with β_o taken as 2.7, the problem of determining f may be considered resolved.

b. Limitation of the Solution. The basic assumption made in the derivation of the equations for the propagation of long waves in a porous medium was that the waves be long relative to the depth. Whereas this assumption in the context of long waves over a rough bottom was equivalent to the negligible effect of vertical fluid accelerations, the important term to consider in the context of waves propagating in a porous medium is the term expressing the resistance to vertical flow in equation (A-69).

For the simple case of a progressive wave in a porous medium the solution for the horizontal velocity component given by equation (A-78) is

$$u_+ = + \frac{g\ n\ k_o\ a_+}{\omega \sqrt{S-if}} e^{-ikx} \quad , \tag{A-95}$$

and from the continuity equation one may therefore obtain:

$$w_+ = -i \frac{g\ n\ k_o^2\ a_+ h_o}{\omega} (1 + \frac{z}{h_o}) e^{-ikx} \quad , \tag{A-96}$$

and the vertical resistance will contribute to the pressure distribution by an amount

$$\int_0^z \rho f \frac{\omega}{n} W_+ \, dz = -i \, \frac{1}{2}\left(1 + \frac{z}{h_o}\right)^2 \rho f \, g (k_o h_o)^2 \, a_+ \, e^{-ikx} \quad , \tag{A-97}$$

which is to be compared with the term retained, i.e., $\rho g \, a_+$.

Thus, for the term given by equation (A-97) to be negligible we must require that

$$\frac{1}{2} \, f(k_o h_o)^2 << 1 \quad , \tag{A-98}$$

which for values of f greater than unity is a more severe requirement than that given by equation (A-53). Thus, for values of $k_o h_o \underset{\sim}{\sim} 0.5$ and $f \underset{\sim}{\sim} 4$, which are reasonable values, the inequality (eq. A-98) is only approximately satisfied.

APPENDIX B

EXPERIMENTAL DATA

This Appendix presents the experimental data obtained under the present research program.

Tables B-1 and B-2 present the experimental data used in establishing the empirical relationship for the wave friction factor, Figure 22, and equations (124) and (125). Column 1 identifies the experimental run. Columns 2 and 3 give the slope roughness, d, and the period of the wavemaker, T, respectively. From the experimental data, when analyzed as described in Section III.3.a and Appendix C, the incident wave height, H_i, and the reflection coefficient, R_m, are obtained as listed in columns 4 and 7, respectively. The observed runup on the rough slope is listed in column 6, and the value of the horizontal extent of the slope relative to the incident wavelength obtained from linear wave theory, ℓ_s/L, is given in column 5. Thus, the first seven columns constitute experimental data.

With the values of ℓ_s/L and R_m from columns 5 and 7 the corresponding value of ϕ, the slope friction angle, is obtained from Figure 15. The value of ϕ, listed in column 8, along with the value of ℓ_s/L then enables Figures 16 and 17 to be used to evaluate R_u and F_s as listed in columns 9 and 10, respectively. Finally, $f_s = \tan 2\phi$ is evaluated and the value of f_w for a given experimental condition is computed from equation (116), using R_u as listed in column 9 from which column 13 is also obtained. The values listed in columns 12 and 13 are those plotted in Figure 22 from which the empirical relationships, equations (124) and (125) were obtained.

Columns 14 and 15 list the predicted values of the reflection coefficient when the procedure is used in reverse, i.e., when the empirical formulas (eqs. 124 and 125) are adopted for the value of f_w. Column 14 gives the predicted reflection coefficient, R_p, using the more elaborate empirical expression for f_w, equations (125) or (127). Column 15 gives the result, R_{ps}, obtained when the simple expressions, (eqs. 124 or 126) are used.

Tables B-3 and B-4 list the experimental results obtained from the separate set of experiments which were not involved in establishing equations (124) and (125). From the experimental conditions the reflection coefficients are predicted from equation (124), R_p, and from equation (126), R_{ps}, following the procedure described in Section III.4. The comparison between predicted and measured reflection coefficients, R_m, listed in Tables B-1 through B-4 is performed in Table 2.

Table B-1. Experimental results for 1:2.0 slope, h_o = 1 foot.

1 Run No.	2 d (in)	3 T (sec)	4 H_i (ft)	5 ℓ_s/L	6 $R_u = \frac{\lvert A \rvert}{H_i}$	7 R_m	8 ϕ (deg)	9 R_u	10 F_s	11 $\tan 2\phi$	12 f_w	13 $\frac{\lvert A \rvert}{\tan\beta_s d}$	14 R_p	15 R_{ps}
1	0.0	2.0	0.06	0.19	1.39	0.84	2.4	1.70	0.88	0.085	0.48			
2	0.0	2.0	0.05	0.19	1.53	0.82	2.9	1.67	0.88	0.103	0.69			
3	0.0	2.0	0.07	0.19	1.69	0.84	2.3	1.71	0.88	0.079	0.39			
4	0.0	2.0	0.08	0.19	2.02	0.89	1.6	1.76	0.88	0.054	0.22			
5	0.0	1.8	0.06	0.21	1.33	0.86	1.5	1.96	0.92	0.052	0.26			
6	0.0	1.8	0.06	0.21	1.38	0.85	1.5	1.96	0.92	0.053	0.23			
7	0.0	1.8	0.07	0.21	1.66	0.82	1.9	1.92	0.92	0.065	0.27			
8	0.0	1.8	0.08	0.21	1.85	0.85	1.5	1.96	0.92	0.064	0.19			
9	0.0	1.6	0.05	0.24	1.35	0.82	1.7	2.10	1.03	0.060	0.26			
10	0.0	1.6	0.06	0.24	1.37	0.85	1.2	2.16	1.03	0.043	0.16			
11	0.0	1.6	0.07	0.24	1.44	0.86	1.1	2.18	1.03	0.039	0.13			
12	0.0	1.6	0.09	0.24	1.51	0.87	1.0	2.19	1.03	0.035	0.09			
13	0.5	2.0	0.08	0.19	1.50	0.76	3.8	1.62	0.88	0.133	0.59	6.22	0.83	0.83
14	0.5	2.0	0.09	0.19	1.61	0.77	3.7	1.63	0.88	0.129	0.47	7.59	0.82	0.83
15	0.5	2.0	0.10	0.19	1.62	0.76	3.8	1.62	0.88	0.134	0.53	7.00	0.83	0.83
16	0.5	2.0	0.11	0.19	1.69	0.76	3.8	1.62	0.88	0.132	0.45	8.17	0.82	0.83
17	0.5	1.8	0.05	0.21	1.63	0.73	2.9	1.83	0.92	0.101	0.59	4.48	0.77	0.74
18	0.5	1.8	0.06	0.21	1.66	0.72	3.0	1.82	0.92	0.105	0.44	6.29	0.75	0.74
19	0.5	1.8	0.07	0.21	1.78	0.73	2.8	1.83	0.92	0.098	0.35	7.20	0.74	0.74
20	0.5	1.8	0.08	0.21	1.82	0.72	3.0	1.82	0.92	0.103	0.49	5.50	0.76	0.74
21	0.5	1.6	0.04	0.24	1.62	0.72	2.4	2.02	1.03	0.082	0.44	4.36	0.70	0.64
22	0.5	1.6	0.05	0.24	1.63	0.69	2.6	1.98	1.03	0.093	0.44	4.85	0.69	0.64
23	0.5	1.6	0.06	0.24	1.71	0.69	2.6	1.99	1.03	0.091	0.40	5.25	0.68	0.64
24	0.5	1.6	0.06	0.24	1.71	0.68	2.8	1.96	1.03	0.098	0.39	5.74	0.68	0.64
25	1.0	2.0	0.06	0.19	1.79	0.78	3.5	1.64	0.88	0.123	0.67	2.52	0.82	0.79
26	1.0	2.0	0.07	0.19	1.87	0.77	3.6	1.63	0.88	0.128	0.67	2.62	0.82	0.79
27	1.0	2.0	0.05	0.19	1.93	0.78	3.4	1.64	0.88	0.119	0.77	2.13	0.83	0.79
28	1.0	2.0	0.04	0.19	1.97	0.80	3.1	1.65	0.88	0.109	0.83	1.78	0.83	0.79
29	1.0	1.8	0.06	0.21	1.74	0.73	2.9	1.83	0.92	0.102	0.48	2.77	0.73	0.69
30	1.0	1.8	0.07	0.21	1.74	0.75	2.7	1.85	0.92	0.095	0.41	3.06	0.72	0.69
31	1.0	1.8	0.07	0.21	1.81	0.72	3.0	1.82	0.92	0.104	0.43	3.15	0.72	0.69
32	1.0	1.8	0.05	0.21	2.00	0.75	2.7	1.85	0.92	0.094	0.59	2.09	0.75	0.69
33	1.0	1.6	0.12	0.24	0.93	0.61	3.4	1.89	1.03	0.121	0.26	5.35	0.58	0.59
34	1.0	1.6	0.11	0.24	1.62	0.62	3.4	1.89	1.03	0.119	0.28	4.81	0.59	0.59
35	1.0	1.6	0.08	0.24	1.80	0.61	3.5	1.89	1.03	0.121	0.38	3.67	0.61	0.59
36	1.0	1.6	0.05	0.24	1.95	0.64	3.2	1.92	1.03	0.133	0.59	2.21	0.66	0.59
37	1.5	2.0	0.08	0.19	1.74	0.73	4.2	1.66	0.88	0.149	0.62	2.29	0.79	0.77
38	1.5	2.0	0.18	0.19	1.81	0.79	3.4	1.70	0.88	0.118	0.22	5.01	0.75	0.77
39	1.5	2.0	0.16	0.19	1.86	0.73	4.3	1.66	0.88	0.150	0.34	4.17	0.76	0.77
40	1.5	2.0	0.11	0.19	2.21	0.79	3.2	1.71	0.88	0.114	0.35	3.10	0.78	0.77
41	1.5	1.8	0.05	0.21	1.68	0.69	3.2	1.80	0.92	0.113	0.56	1.77	0.71	0.67
42	1.5	1.8	0.10	0.21	1.70	0.71	3.1	1.81	0.92	0.109	0.63	1.51	0.68	0.67
43	1.5	1.8	0.06	0.21	1.77	0.67	3.6	1.76	0.92	0.127	0.39	2.82	0.71	0.67
44	1.5	1.8	0.09	0.21	1.81	0.67	3.7	1.76	0.92	0.129	0.43	2.59	0.68	0.67
45	1.5	1.6	0.05	0.24	1.46	0.62	3.4	1.90	1.03	0.118	0.53	1.73	0.62	0.55
46	1.5	1.6	0.08	0.24	1.61	0.56	4.1	1.82	1.03	0.143	0.47	2.34	0.59	0.55
47	1.5	1.6	0.14	0.24	1.69	0.59	3.7	1.86	1.03	0.129	0.24	4.05	0.52	0.55
48	1.5	1.6	0.12	0.24	1.72	0.59	3.7	1.86	1.03	0.129	0.28	3.60	0.55	0.55
49	2.0	2.0	0.17	0.19	1.76	0.73	4.0	1.82	0.88	0.141	0.34	3.39	0.74	0.76
50	2.0	2.0	0.12	0.19	1.76	0.76	3.9	1.83	0.88	0.137	0.41	2.50	0.76	0.76
51	2.0	2.0	0.08	0.19	2.07	0.73	3.8	1.85	0.88	0.133	0.61	1.53	0.78	0.76
52	2.0	2.0	0.17	0.19	2.15	0.71	3.9	1.83	0.88	0.137	0.28	3.23	0.75	0.76
53	2.0	1.8	0.13	0.21	1.74	0.58	4.8	1.66	0.92	0.171	0.44	2.51	0.64	0.65
54	2.0	1.8	0.10	0.21	1.79	0.61	4.5	1.68	0.92	0.160	0.51	2.05	0.66	0.65
55	2.0	1.8	0.04	0.21	1.97	0.66	3.8	1.74	0.92	0.134	0.83	1.05	0.72	0.65
56	2.0	1.8	0.05	0.21	2.03	0.66	3.8	1.74	0.92	0.134	1.01	0.86	0.72	0.65
57	2.0	1.6	0.11	0.24	1.61	0.57	4.0	1.82	1.03	0.141	0.34	2.39	0.54	0.53
58	2.0	1.6	0.12	0.24	1.70	0.57	3.9	1.83	1.03	0.137	0.28	2.82	0.52	0.53
59	2.0	1.6	0.09	0.24	1.89	0.57	3.9	1.83	1.03	0.137	0.41	1.93	0.56	0.53
60	2.0	1.6	0.05	0.24	2.01	0.58	3.8	1.85	1.03	0.133	0.61	1.27	0.60	0.53

Table B-2. Experimental results for 1:3.0 slope, h_o = 1 foot.

1	2	3	4	5	6	7	8	9	10	11	12	13	14	15
Run No.	d (in)	T (sec)	H_i (ft)	ℓ_s/L	$R_u = \frac{\lvert A\rvert}{H_i}$	R_m	ϕ (deg)	R_u	F_s	$\tan 2\phi$	f_w	$\frac{\lvert A\rvert}{\tan\phi_s d}$	R_p	R_{ps}
61	0.0	2.0	0.05	0.28	1.70	0.84	1.3	2.28	1.30	0.044	0.10			
62	0.0	2.0	0.06	0.28	1.85	0.81	1.9	2.19	1.29	0.067	0.14			
63	0.0	2.0	0.06	0.28	2.08	0.80	2.0	2.15	1.30	0.070	0.14			
64	0.0	1.8	0.09	0.31	2.06	0.75	2.3	2.14	1.62	0.081	0.09			
65	0.0	1.8	0.06	0.31	2.21	0.77	2.0	2.18	1.62	0.070	0.11			
66	0.0	1.8	0.07	0.31	2.32	0.81	7.7	2.22	1.63	0.060	0.08			
67	0.0	1.8	0.05	0.31	2.50	0.80	1.8	2.20	1.62	0.063	0.12			
68	0.0	1.6	0.09	0.36	1.13	0.80	1.8	2.46	1.88	0.062	0.05			
69	0.0	1.6	0.09	0.36	1.99	0.79	2.0	2.35	1.94	0.069	0.06			
70	0.0	1.6	0.07	0.36	2.08	0.78	2.1	2.22	2.03	0.073	0.08			
71	0.0	1.6	0.09	0.36	2.42	0.79	1.9	2.40	1.91	0.068	0.09			
72	0.5	2.0	0.08	0.28	1.72	0.59	3.7	1.93	1.28	0.129	0.23	10.51	0.55	0.57
73	0.5	2.0	0.07	0.28	1.77	0.57	3.9	1.90	1.28	0.135	0.29	8.89	0.56	0.57
74	0.5	2.0	0.08	0.28	1.83	0.54	4.1	1.87	1.24	0.145	0.26	10.69	0.54	0.57
75	0.5	2.0	0.11	0.28	1.93	0.51	4.5	1.83	1.25	0.158	0.21	14.22	0.51	0.57
76	0.5	1.8	0.07	0.31	1.51	0.56	4.6	1.83	1.59	0.162	0.27	9.09	0.54	0.54
77	0.5	1.8	0.09	0.31	1.68	0.56	4.6	1.84	1.59	0.161	0.21	11.44	0.52	0.54
78	0.5	1.8	0.05	0.31	1.72	0.59	4.2	1.89	1.58	0.147	0.34	5.60	0.57	0.54
79	0.5	1.8	0.10	0.31	1.72	0.55	4.7	1.82	1.59	0.164	0.18	13.49	0.50	0.54
80	0.5	1.6	0.06	0.36	1.13	0.52	5.3	1.77	1.86	0.186	0.29	8.21	0.44	0.58
81	0.5	1.6	0.06	0.36	1.29	0.52	5.5	1.76	1.86	0.193	0.35	7.15	0.54	0.58
82	0.5	1.6	0.08	0.36	1.32	0.47	6.4	1.63	1.57	0.228	0.38	9.25	0.52	0.58
83	0.5	1.6	0.10	0.36	1.34	0.47	6.6	1.62	1.57	0.233	0.30	11.74	0.48	0.58
84	1.0	2.0	0.13	0.28	1.31	0.50	4.8	1.80	1.26	0.168	0.19	8.23	0.45	0.50
85	1.0	2.0	0.06	0.28	1.46	0.56	4.0	1.88	1.28	0.141	0.34	3.86	0.53	0.50
86	1.0	2.0	0.09	0.28	1.47	0.51	4.7	1.81	1.27	0.166	0.28	5.54	0.50	0.50
87	1.0	2.0	0.06	0.28	1.71	0.53	4.4	1.84	1.28	0.154	0.36	4.04	0.52	0.50
88	1.0	1.8	0.07	0.31	1.14	0.48	5.9	1.69	1.52	0.211	0.37	4.49	0.50	0.49
89	1.0	1.8	0.12	0.31	1.23	0.44	6.8	1.59	1.53	0.241	0.29	6.75	0.46	0.49
90	1.0	1.8	0.10	0.31	1.25	0.49	5.7	1.72	1.55	0.200	0.25	6.19	0.47	0.49
91	1.0	1.8	0.11	0.31	1.33	0.49	5.8	1.71	1.55	0.204	0.23	6.75	0.47	0.49
92	1.0	1.6	0.06	0.36	0.72	0.49	6.1	1.70	1.79	0.215	0.41	3.54	0.48	0.47
93	1.0	1.6	0.10	0.36	0.90	0.46	6.8	1.58	1.81	0.243	0.27	5.92	0.45	0.47
94	1.0	1.6	0.13	0.36	0.99	0.46	6.7	1.59	1.79	0.239	0.22	7.21	0.44	0.47
95	1.0	1.6	0.14	0.36	0.06	0.41	7.9	1.47	1.73	0.282	0.27	7.30	0.43	0.47
96	1.5	2.0	0.06	0.28	1.03	0.52	4.6	1.82	1.28	0.165	0.39	2.67	0.50	0.47
97	1.5	2.0	0.12	0.28	1.34	0.43	5.7	1.69	1.27	0.200	0.25	5.03	0.43	0.47
98	1.5	2.0	0.14	0.28	1.39	0.46	5.1	1.76	1.29	0.179	0.19	5.74	0.43	0.47
99	1.5	2.0	0.10	0.28	1.54	0.47	5.0	1.77	1.27	0.176	0.31	3.61	0.46	0.47
100	1.5	1.8	0.07	0.31	0.95	0.53	5.1	1.78	1.57	0.178	0.32	2.82	0.49	0.47
101	1.5	1.8	0.07	0.31	1.17	0.52	5.2	1.77	1.57	0.182	0.31	3.03	0.48	0.47
102	1.5	1.8	0.11	0.31	1.22	0.42	7.3	1.54	1.52	0.259	0.33	4.05	0.44	0.47
103	1.5	1.8	0.08	0.31	1.34	0.46	6.2	1.68	1.50	0.219	0.37	3.15	0.47	0.47
104	1.5	1.6	0.09	0.36	0.98	0.46	6.7	1.60	1.78	0.239	0.33	3.30	0.45	0.44
105	1.5	1.6	0.07	0.36	1.06	0.53	5.4	1.75	1.89	0.189	0.27	3.02	0.46	0.44
106	1.5	1.6	0.05	0.36	1.09	0.50	6.0	1.69	1.83	0.218	0.48	1.94	0.49	0.44
107	1.5	1.6	0.05	0.36	1.18	0.49	6.2	1.66	1.83	0.219	0.45	2.15	0.48	0.44
108	2.0	2.0	0.11	0.28	1.34	0.45	5.5	1.72	1.28	0.194	0.27	3.41	0.43	0.45
109	2.0	2.0	0.14	0.28	1.52	0.94	5.6	1.71	1.27	0.196	0.22	4.75	0.41	0.45
110	2.0	2.0	0.08	0.28	1.75	0.48	5.0	1.79	1.27	0.175	0.24	2.45	0.46	0.45
111	2.0	2.0	0.06	0.28	2.12	0.52	4.5	1.82	1.28	0.160	0.34	1.93	0.48	0.45
112	2.0	1.8	0.11	0.31	1.10	0.41	7.5	1.52	1.50	0.267	0.34	3.11	0.43	0.45
113	2.0	1.8	0.08	0.31	1.37	0.45	6.5	1.63	1.50	0.231	0.41	2.22	0.46	0.45
114	2.0	1.8	0.10	0.31	1.60	0.43	7.0	1.57	1.51	0.249	0.34	2.93	0.44	0.45
115	2.0	1.8	0.06	0.31	1.83	0.49	5.9	1.69	1.54	0.209	0.46	1.76	0.48	0.45
116	2.0	1.6	0.10	0.36	1.24	0.40	8.3	1.42	1.67	0.297	0.41	2.61	0.42	0.43
117	2.0	1.6	0.13	0.36	1.25	0.38	8.9	1.36	1.65	0.320	0.35	3.28	0.41	0.43
118	2.0	1.6	0.17	0.36	1.37	0.34	10.4	1.22	1.48	0.512	0.56	3.69	0.40	0.43
119	2.0	1.6	0.08	0.36	1.60	0.43	7.6	1.50	1.73	0.271	0.45	2.11	0.44	0.43

Table B-3. Experimental results for 1:2.5 slope, h_o = 1 foot.

1	2	3	4	5	6	7	8
	d	T	H_i	$R_u = \frac{\lvert A \rvert}{H_i}$	R_m	R_p	R_{ps}
Run Number	(in)	(sec)	(ft)				
175	0.0	2.0	0.07	1.64	0.84		
176	0.0	2.0	0.06	1.39	0.83		
177	0.0	2.0	0.05	1.56	0.82		
178	0.0	2.0	0.08	2.02	0.89		
179	0.0	1.8	0.08	1.82	0.85		
180	0.0	1.8	0.07	1.64	0.82		
181	0.0	1.8	0.06	1.48	0.85		
182	0.0	1.8	0.05	1.46	0.86		
183	0.0	1.6	0.09	1.51	0.87		
184	0.0	1.6	0.06	1.39	0.85		
185	0.0	1.6	0.07	1.34	0.86		
186	o.5	2.0	0.09	1.86	0.65	0.65	0.66
187	0.5	2.0	0.07	2.03	0.67	0.67	0.66
188	0.5	2.0	0.06	1.73	0.70	0.68	0.66
189	0.5	2.0	0.04	1.58	0.71	0.71	0.66
190	1.0	2.0	0.04	1.70	0.65	0.68	0.61
191	1.0	2.0	0.06	1.73	0.64	0.64	0.61
192	1.0	2.0	0.08	1.83	0.64	0.63	0.61
193	1.0	2.0	0.07	1.79	0.64	0.64	0.61
194	1.5	2.0	0.05	1.66	0.63	0.64	0.57
195	1.5	2.0	0.04	1.43	1.65	0.66	0.57
196	2.0	2.0	0.06	1.73	0.59	0.60	0.54
197	2.0	2.0	0.04	1.70	0.61	0.64	0.54
198	0.5	1.8	0.03	1.40	0.68	0.67	0.59
199	0.5	1.8	0.06	1.73	0.64	0.62	0.59
200	0.5	1.8	0.07	1.79	0.63	0.61	0.59
201	0.5	1.8	0.08	1.96	0.63	0.59	0.59
202	1.0	1.8	0.08	1.95	0.58	0.54	0.52
203	1.0	1.8	0.07	1.79	0.59	0.56	0.52
204	1.0	1.8	0.05	1.88	0.60	0.59	0.52
205	1.0	1.8	0.03	2.1	0.64	0.62	0.52
206	1.5	1.8	0.11	1.71	0.56	0.48	0.47
207	1.5	1.8	0.08	1.56	0.57	0.52	0.47
208	1.5	1.8	0.06	1.73	0.59	0.55	0.47
209	1.5	1.8	0.10	1.77	0.58	0.48	0.47
210	2.0	1.8	0.11	1.52	0.52	0.45	0.44
211	2.0	1.8	0.09	1.39	0.53	0.48	0.44
212	2.0	1.8	0.07	2.53	0.54	0.50	0.44
213	2.0	1.8	0.03	1.39	0.57	0.58	0.44
214	0.5	1.6	0.17	1.59	0.50	0.48	0.54
215	0.5	1.6	0.15	1.67	0.52	0.49	0.54
216	0.5	1.6	0.10	1.67	0.57	0.52	0.54
217	0.5	1.6	0.06	1.57	0.60	0.56	0.54
218	1.0	1.6	0.17	1.84	0.47	0.44	0.49
219	1.0	1.6	0.12	1.57	0.53	0.47	0.49
220	1.0	1.6	0.09	1.62	0.56	0.49	0.49
221	1.0	1.6	0.06	1.73	0.57	0.52	0.49
222	1.5	1.6	0.15	1.46	0.48	0.43	0.45
223	1.5	1.6	0.12	1.65	0.50	0.44	0.45
224	1.5	1.6	0.09	1.73	0.52	0.47	0.45
225	1.5	1.6	0.05	1.67	0.54	0.53	0.45
226	2.0	1.6	0.10	1.46	0.48	0.45	0.43
227	2.0	1.6	0.08	1.3	0.49	0.47	0.43
228	2.0	1.6	0.06	1.65	0.51	0.49	0.43
229	2.0	1.6	0.04	1.58	0.52	0.52	0.43

Table B-4. Experimental results for 1:1.5 slope, h_o = 1 foot.

1	2	3	4	5	6	7	8
	d	T	H_i	$R_u = \frac{A}{H_i}$	R_m	R_p	R_{ps}
Run Number	(in)	(sec)	(ft)				
120	0.0	2.0	0.13	1.85	0.82		
121	0.0	2.0	0.09	1.29	0.91		
122	0.0	2.0	0.12	1.35	0.87		
123	0.0	1.8	0.05	1.74	0.87		
124	0.0	1.8	0.06	1.74	0.85		
125	0.0	1.8	0.06	2.01	0.85		
126	0.0	1.8	0.06	2.30	0.86		
127	0.0	1.6	0.03	2.3	0.87		
128	0.0	1.6	0.05	2.08	0.81		
129	0.0	1.6	0.06	2.31	0.89		
130	0.5	2.0	0.04	1.56	0.87	0.95	0.93
131	0.5	2.0	1.06	1.39	0.86	0.95	0.93
132	0.5	2.0	0.06	1.39	0.86	0.95	0.93
133	0.5	2.0	0.07	1.34	0.86	0.95	0.93
134	1.0	2.0	0.11	1.43	0.81	0.93	0.92
135	1.0	2.0	0.14	1.33	0.86	0.92	0.92
136	1.0	2.0	0.10	2.46	0.81	0.93	0.92
137	1.5	2.0	0.05	1.16	0.84	0.94	0.87
138	1.5	2.0	0.07	1.32	0.79	0.93	0.87
139	1.5	2.0	0.07	1.49	0.81	0.93	0.87
140	1.5	2.0	0.09	1.29	0.81	0.93	0.87
141	2.0	2.0	0.11	2.65	0.83	0.92	0.82
142	2.0	2.0	0.09	1.29	0.84	0.92	0.82
143	2.0	2.0	0.07	1.49	0.85	0.93	0.82
144	2.0	2.0	0.05	0.43	0.85	0.93	0.82
145	0.5	1.8	0.04	1.56	0.81	0.92	0.89
146	0.5	1.8	0.02	1.56	0.84	0.93	0.89
147	0.5	1.8	0.04	1.56	0.80	0.92	0.89
148	0.5	1.8	0.05	1.46	0.81	0.92	0.89
149	1.0	1.8	0.08	1.30	0.80	0.89	0.91
150	1.0	1.8	0.07	1.24	0.78	0.89	0.91
151	1.0	1.8	0.07	1.11	0.79	0.89	0.91
152	1.5	1.8	0.05	1.03	0.87	0.89	0.86
153	1.5	1.8	0.08	0.97	0.78	0.89	0.86
154	1.5	1.8	0.10	0.87	0.77	0.88	0.86
155	1.5	1.8	0.10	1.04	0.78	0.88	0.86
156	2.0	1.8	0.11	0.95	0.72	0.87	0.79
157	2.0	1.8	0.08	1.08	0.74	0.88	0.79
158	2.0	1.8	0.07	1.74	0.74	0.89	0.79
159	2.0	1.8	0.06	1.74	0.74	0.89	0.79
160	0.5	1.6	0.07	1.49	0.79	0.86	0.84
161	0.5	1.6	0.06	1.39	0.77	0.87	0.84
162	0.5	1.6	0.04	1.56	0.79	0.88	0.84
163	0.5	1.6	0.03	1.74	0.80	0.88	0.84
164	0.0	1.6	0.11	0.95	0.83	0.83	0.90
165	1.0	1.6	0.09	1.93	0.73	0.84	0.90
166	1.0	1.6	0.10	1.13	0.73	0.83	0.90
167	1.0	1.6	0.12	1.15	0.85	0.83	0.90
168	1.5	1.6	0.04	3.12	0.73	0.86	0.85
169	1.5	1.6	0.05	2.90	0.74	0.85	0.85
170	1.5	1.6	0.07	2.68	0.78	0.84	0.85
171	2.0	1.6	0.15	2.30	0.69	0.79	0.78
172	2.0	1.6	0.12	2.08	0.71	0.80	0.78
173	2.0	1.6	0.08	2.08	0.71	0.80	0.78
174	2.0	1.6	0.06	2.08	0.68	0.83	0.78
230	1.0	2.0	0.12	1.91	0.88	0.92	0.90

APPENDIX C

DETERMINATION OF REFLECTION COEFFICIENTS

During the preliminary experimental runs performed to determine the reflection coefficients of steep, rough slopes it was observed that an appreciable effect of second or higher harmonic motions was present in the wave flume. It was also found that if one sought out the locations along the constant depth part of the flume where the wave height, i.e., distance between crest and trough, was maximum and minimum, respectively, the resulting estimate of the reflection coefficient could vary as much as from 0.45 to 0.75 depending on the choice of maximum and minimum wave height. With the intended use of the experiments such a variation of the experimentally determined reflection coefficient is clearly undesirable.

The theoretical foundation for using the formula for the experimental determination of the reflection coefficient,

$$R = \frac{H_{max} - H_{min}}{H_{max} + H_{min}} \quad , \tag{C-1}$$

is based on an analysis assuming linear waves, i.e., the motion consists of purely sinusoidal waves of one frequency. Hence, the appearance of higher harmonics is an indication of the inapplicability of equation (C-1) for the prediction of reflection coefficients. Furthermore, the physical concept of a reflection coefficient really makes sense only if superposition, i.e., linear waves, may be assumed.

If the motion in the wave flume was purely sinusoidal, the surface variation should at any point vary sinusoidally with a period, T, equal to that of the wavemaker. Since this was not the case it was decided to extract from the measured surface variation at each station the amplitude of the motion having a period equal to that of the wavemaker. This amplitude of the first harmonic is the one which, according to linear theory, should vary in such a manner that equation (C-1) provides a determination of the reflection coefficient, R.

The experimental procedure used was the following. For a particular experimental run the wave generator was started from rest. The wave motion in the flume was allowed to reach a quasi-steady state in which the motion at any point along the flume was periodic, i.e., the motion, although not purely sinusoidal, repeated itself with a period equal to that of the wavemaker. It generally took 2 to 3 minutes for this quasi-steady state to be reached in the present experimental setup. As mentioned in Section III of the report it was not possible to attain this quasi-steady state for large amplitude incident waves, which limited the test conditions for which reflection coefficients could be determined.

After reaching the quasi-steady state the wave gage was positioned at the first station. The motion was observed on the paper tape of the Sanborn recorder and was visually determined to be periodic. With the maximum paper speed, 100 millimeters per second, three to four wave periods were recorded. The gage was moved to the next location, 10 centimeters away, and the procedure was repeated. This was done over a distance of approximately one wavelength of the incident waves so that at least two maxima and minima were recorded.

Of the three to four wave periods recorded at a given station one was chosen for analysis. This variation of the free surface during one wave period was digitized manually at intervals of 1/20 the wave period. Since the motion is assumed periodic the two end points of the digitized data should be identical and the mean value of the two end points was chosen whenever they were not exactly the same. This way 20 equally spaced (in time) values of the surface elevation were obtained and these values were used as input to a simple computer program which performed a Fourier series analysis of the data and gave the amplitude of the first harmonic motion as output.

When realizing that each experimental run required the measurement of the wave motion at some 30 stations it is quite obvious that the manual procedure of digitizing the wave records means that it is an extremely time-consuming effort to obtain the reflection coefficient. However, the end result (Fig. 20) rewards the effort in producing reflection coefficients which vary only within $\pm$ 0.02 with choice of node and antinode. The experimental data listed in Appendix B (Tables B-2 and B-4) were all obtained and analyzed in this manner.

Modifications of the Hewlett-Packard Computer System at the Ralph M. Parsons Laboratory made it possible to interface this computer with the wave tank experiments. This enabled the tedious manual reduction of the data to be circumvented and to feed the experimental data directly into the computer. A multifunction meter triggered the computer to start taking data by imposing a high voltage. After being triggered the computer starts taking data at the rate of 14.5 readings per second, i.e., a reading per Δt seconds, where:

$$\Delta t = 0.069 \text{ seconds.} \tag{C-2}$$

The computer program was designed to take a total of 50 readings, i.e., cover a period of approximately 3.5 seconds, thus ensuring that an entire wave period is recorded. Of these 50 equally spaced values the first 15 are discarded to avoid transient effects and from the 16^{th} reading on, the next D1+1 values are adopted for computations where D1 is the integer most closely approximating

$$D1 = \frac{T}{\Delta t} \quad . \tag{C-3}$$

These D1+1 values are treated as previously described for the manually digitized data for which D1=20. All this is done internally in the computer and the output is the amplitude of the first harmonic motion at consecutive measurement stations. A search routine was also included in the computer program so that the maximum and minimum values of the wave amplitude were determined and the resulting estimates of the reflection coefficient were printed out for each experimental run. Although the computerized procedure was thoroughly checked against the manual procedure before the former was adopted for the experiments listed in Appendix B, Tables B-1 and B-3, the procedure of obtaining a paper tape wave record was continued to avoid possible loss of experimental data.

An example of the added accuracy involved when a more exact method is inacted is seen by examining the example described in Section III.3.b, Figure 20. From Figure 20, as previously noted, the raw data from the experiment (the open circles) do not reproduce a well-behaved wave amplitude variation. Through the use of the Fourier series computer program, the raw data were corrected, i.e., only the first-order wave amplitude was retained, and the corrected data are seen in Figure 20 as the solid circles. It is observed from studying the corrected data that the minimum amplitude locations are not precise and one must fit a theoretical curve to the corrected data to determine the minimum wave amplitude and the resulting reflection coefficient. The theoretical curve with R=0.88 appears to fit the data presented in Figure 20 well, but as it will be demonstrated, the wave amplitudes immediately surrounding a minimum have to be determined at a much closer spacing than used in the experiments presented in Figure 20 if the curve-fitting procedure is to be eliminated.

Figure C-1 is a graphical representation of equation (123) close to a node location for various reflection coefficients. It is clearly seen that, as the spacing between measurements becomes larger, one is able to have relatively large errors in obtaining the minimum location especially for high reflection coefficients. For example, a 4-inch (10 centimeters) spacing corresponds to a measurement interval, $\Delta x/L$, of 0.03 for the 2-second wave in the present experiment. The maximum deviation would occur when the measurement locations were equally spaced around the minimum, i.e., $\Delta x/L$ equal to 0.015 on either side of the minimum. If one had an actual reflection coefficient of R=0.88 one would obtain a value of a/a_{max} equal to 0.115 for a maximum displacement from the actual minimum. Therefore,if one assumed that the reading of a/a_{max} = 0.115 was the correct minimum value, then the reflection coefficient would be determined from Figure C-1 R=0.79 which is approximately a 10-percent error. Similarly, if one has an actual reflection coefficient of R=0.60 and collected data at the maximum deviation locations, the error incurred would only be of the order 3 percent. It is apparent that the errorsrors are most prevalent when one has high reflection coefficients. The computer program described previously allows one to collect a large number of data points and analyze them quickly so that the measurement interval can be reduced in the vicinity of nodes, thus resulting in smaller errors.

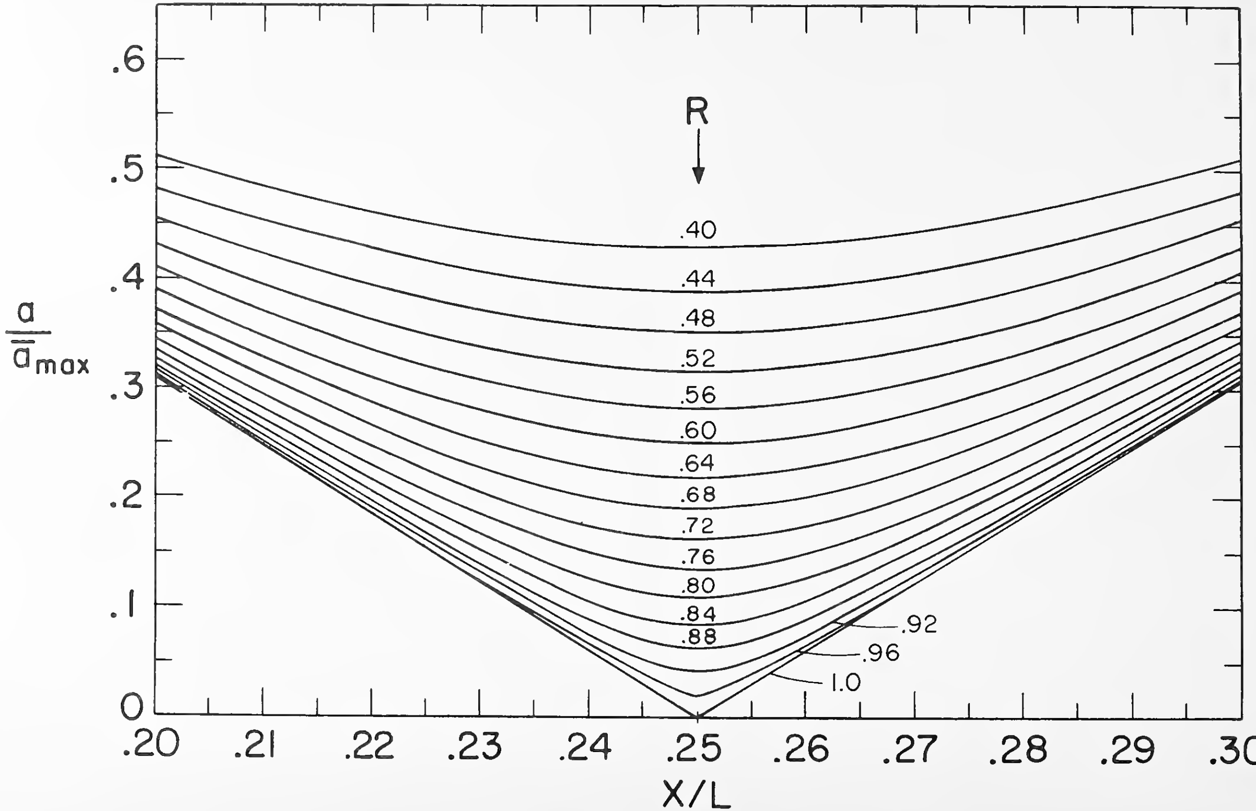

Figure C-1. Theoretical wave amplitude variation, from equation (123) in the immediate vicinity of a node for various reflection coefficients.

After observing how important it is to have the minimum amplitude defined as accurately as possible, the experiment used in Section III.3.b was repeated with the measurement interval surrounding the observed minimum reduced to $\Delta x/L$ equal to 0.39 inch (1 centimeter). Figure C-2 is a plot of the raw and corrected data for measurements taken in the immediate vicinity of two node locations, L/2 apart. Two observations can be made. First, the raw data show a slight discrepancy between the minimum locations and, secondly, one cannot assume that the actual minimum, i.e., the first harmonic amplitude, will fall where the raw data minimum occurs. In order to ensure that the actual minimum location is found, one must use the smaller measurement intervals for a sufficient distance around the observed minimum to ensure the location of the actual minimum to be occupied. By substituting the results obtained from Figure C-2 into the calculations made in Section III.3.b, one will calculate an average reflection coefficient of $R \simeq 0.90$ which is much larger than the reflection coefficient suggested by the raw data ($R \simeq 0.62$) and slightly higher than obtained from the corrected data ($R \simeq 0.88$) with a measurement interval of 4 inches (10 centimeters) when the best fit value of R is chosen. The accuracy, using the more refined acquisition system, does not produce, in this case, a far superior product. To avoid the somewhat subjective and tedious curve fitting procedure, the refined system of closely spaced measurements near nodes is recommended. Figure C-2 shows how the amplitude at the node as well as the location of the minimum amplitude itself is affected by higher order wave harmonics.

Through the use of a high-speed computer, the data can be quickly examined and the resolution required may easily be obtained. The computer program which was used for the computerized procedure for determining the reflection coefficient is listed on the following pages. With the preceding description of the program and the extensive use of comments in the program this should be self-explanatory.

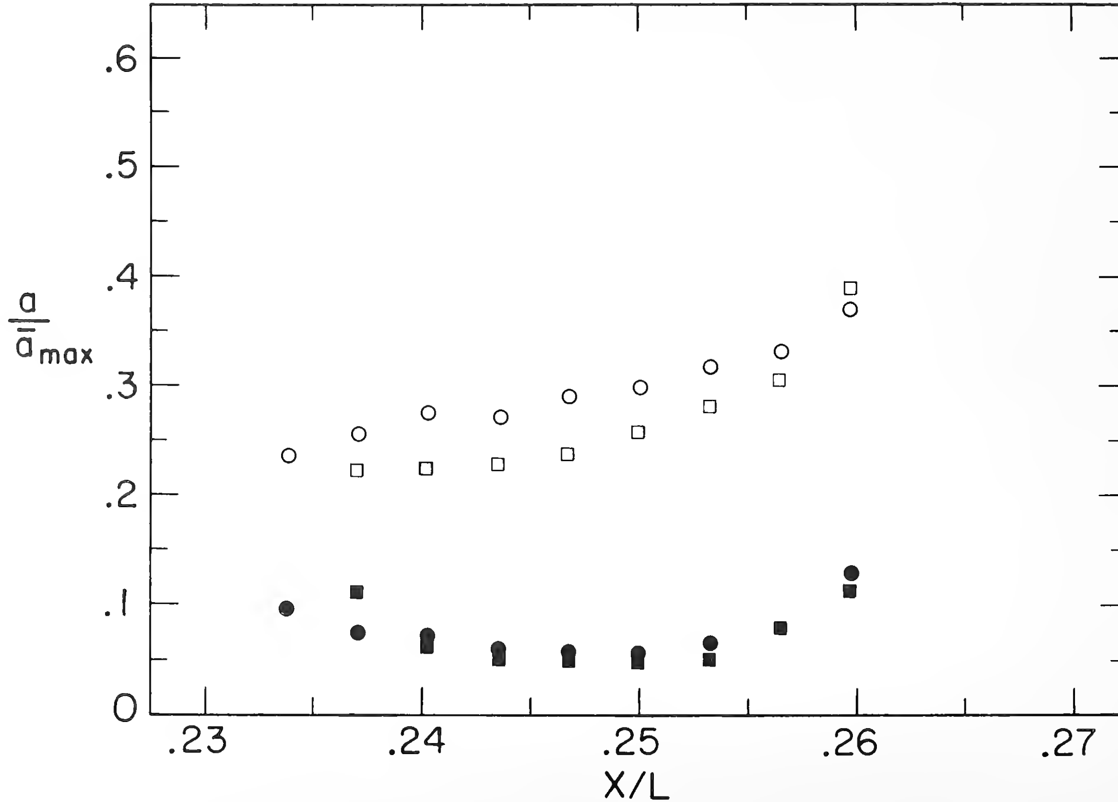

Figure C-2. Observed and corrected data of wave amplitude variation in the immediate vicinity of a node corresponding to the experiment presented in Figure 20.

```
1  REM *** ANALYSIS OF A WAVE PROFILE ***
2  REM *** BY FOURIER SERIES APPROXIMATION ***
3  REM THIS PROGRAM MUST BE RUN FROM A POSITION A STATION BEFORE
4   REM A MAXIMUM AMPLITUDE.  CALCULATE THE NUMBER OF STATIONS TO BE
5   REM MEASURED (S) AND THE NUMBER OF POINTS TO BE USED IN THE
6  REM PROGRAM DEPENDING UPON FREQUENCY (D1). S1>D1+15
7  REM T=PERIOD,D1=NO. OF PTS. USED,K1=ORDER SOUGHT
8  REM Q=MAX VOLTAGE TO TRIGGER,S=NO. OF STATIONS EXPECTED
9  REM S1=NO. OF DATA PTS.,T5=TEST NUMBER,C1=CONVERSION(FT.-V)
1Ø  DIM A[1Ø],B[1Ø],C[5Ø,1Ø],F[5Ø],E[3,5Ø],G[5Ø,5Ø],R[4],Z[3]
11  READ T,D1,K1,Q,S,S1,T5,C1
12  GOSUB 1ØØØ
13  PRINT
14  PRINT " ********** TEST NUNBER",T5,"**********"
15  PRINT
16  PRINT " CORRECTION FACTOR =",C1
17  PRINT
18  FOR N1=1 TO S
19  CALL (1,D,F)
2Ø  IF D >= Q THEN 22
21  GOTO 19
22  CALL (1,D,F)
23  IF D <= Q THEN 25
24  GOTO 22
25  FOR N2=1 TO S1
26  CALL (1,D,F)
27  LET G[N1,N2]=D
28  NEXT N2
31  FOR X=1 TO D1+1
33  LET F[X]=G[N1,X+15]
35  NEXT X
4Ø  GOSUB 75
45  NEXT N1
5Ø  GOSUB 38Ø
6Ø  GOSUB 7Ø5
7Ø  STOP
75  REM SUBPROGRAM TO CALCULATE MAXIMUM AMPLITUDE USING FOURIER
76  REM SERIES AT EACH STATION.
8Ø  FOR X=1 TO D1+1
85  LET F[X]=G[N1,X+15]
9Ø  NEXT X
91  LET E=D1+1
92  LET G=K1
1ØØ  LET F[1]=(F[1]+F[E])/2
1Ø2  LET F[E]=F[1]
111  LET A4=1/2*F[1]
112  LET H=T/D1
115  FOR J=2 TO D1
116  LET A4=A4+F[J]
118  NEXT J
12Ø  LET A=1/(2*3.1416)*H*(A4+1/2*F[D1+1])
```

```
124   FOR K=1 TO K1
130   LET T1=0
135   LET A0=(F[1]*COS(T1))*.5
140   LET B0=(F[1]*SIN(T1))*.5
150   FOR N=2 TO D1
160   LET X=((2*3.1416)*(N-1)*H/T)*K
165   LET A0=A0+F[N]*COS(X)
170   LET B0=B0+F[N]*SIN(X)
180   NEXT N
190   LET T9=(2*3.1416)*D1*H/T*K
195   LET A0=A0+(F[D1+1]*COS(T9))*.5
200   LET B0=B0+(F[D1+1]*SIN(T9))*.5
205   LET A[K]=2/D1*A0
210   LET B[K]=2/D1*B0
230   FOR M=1 TO E
240   LET T5=(3.1416*2)*((M-1)*H/T)*K
250   LET C[M,K]=A+A[K]*COS(T5)+B[K]*SIN(T5)
260   NEXT M
262   LET Z[K]=SQR(A[K]*A[K]+B[K]*B[K])
263   PRINT "STATION NUMBER:",N1
264   PRINT "H=    ",H,"SECONDS"
265   LET Z[K]=Z[K]/C1
266   PRINT " MAXIMUM AMPLITUDE =",Z[K],"FT.     FOR K =",K
267   LET E[K,N1]=Z[K]
270   NEXT K
280   PRINT
281   PRINT
290   RETURN
380   REM SUBPROGRAM TO SEEK MAXIMUM AND MINIMUM LOCATIONS
381   REM AND CALCULATES REFLECTION COEFFICIENTS AND INCIDENT
383   REM WAVE HEIGHTS.  CAN ONLY BE USED IF ATTENUATOR IS LEFT
384   REM AT ONE SETTING THROUGHOUT THE EXPERIMENT.
390   FOR K=1 TO K1
395   LET N1=1
400   LET A5=E[K,N1]
410   LET N1=N1+1
420   IF N1>S THEN 599
430   IF E[K,N1] >= A5 THEN 400
440   LET A6=A5
445   LET A5=E[K,N1]
450   LET N1=N1+1
455   IF N1>S THEN 600
460   IF E[K,N1] <= A5 THEN 445
465   LET R[1]=(A6-A5)/(A6+A5)
470   LET A7=A5
480   LET A5=E[K,N1]
490   LET N1=N1+1
495   IF N1>S THEN 614
500   IF E[K,N1] >= A5 THEN 480
505   LET R[2]=(A5-A7)/(A5+A7)
510   LET A8=A5
```

```
520  LET A5=E[K,N1]
530  LET N1=N1+1
535  IF N1>S THEN 620
540  IF E[K,N1] <= A5 THEN 520
545  LET R[3]=(A8-A5)/(A8+A5)
550  LET A9=A5
560  LET A5=E[K,N1]
570  LET N1=N1+1
580  IF N1>S THEN 595
590  IF E[K,N1] >= A5 THEN 560
595  LET R[4]=(A5-A9)/(A5+A9)
596  GOTO 640
599  LET A6=0
600  LET A7=0
602  LET R[1]=0
603  LET R[2]=0
605  LET A8=0
608  LET R[3]=0
610  LET A9=0
611  LET R[4]=0
612  GOTO 640
613  LET R[2]=0
614  LET A9=0
615  LET R[3]=0
616  LET A8=0
617  LET R[4]=0
618  GOTO 640
620  LET A9=0
621  LET R[3]=0
622  LET R[4]=0
630  LET R[4]=0
640  LET R=(R[1]+R[2]+R[3]+R[4])/4
650  LET H5=(A5+A6+A8)/3+(A7+A9)/2
660  PRINT " REFLECTION COEFFICIENT:"
661  PRINT A6
662  PRINT "                    ",R[1]
663  PRINT A7
664  PRINT "                    ",R[2]
665  PRINT A8
666  PRINT "                    ",R[3]
667  PRINT A9
668  PRINT "                    ",R[4]
669  PRINT A5
670  PRINT
675  PRINT "      R=",R
677  PRINT
680  PRINT " INCIDENT WAVE HEIGHT=",H5,"FT."
685  PRINT
690  PRINT
700  NEXT K
702  RETURN
```

```
705  REM SUBPROGRAM TO PRINT OUT DATA USED IN THE CALCULATION
706  REM OF THE MAXIMUM WAVE AMPLITUDES AT EACH STATION.
710  FOR Y=1 TO S
715  PRINT
720  PRINT " STATION NUMBER:",Y
730  FOR Y1=15 TO 15+D1
732  DEF FNR(X)=INT(X*10000+.5)/10000
740  PRINT FNR(G[Y,Y1]),
750  NEXT Y1
760  NEXT Y
770  RETURN
800  STOP
1000  REM SUBPROGRAM TO CALCULATE CONVERSION FACTOR FROM VOLTS
1001  REM TO FEET. START AT STILL WATER AND INCREASE THE DEPTH
1002  REM OF THE PROBES BY 0.05 FEET.
1010  LET Y4=0
1014  LET Y3=0
1016  FOR N1=1 TO 10
1018  CALL (1,D,F)
1020  IF D >= Q THEN 1040
1030  GOTO 1018
1040  CALL (1,D,F)
1050  IF D <= Q THEN 1070
1060  GOTO 1040
1070  FOR N2=1 TO 50
1080  CALL (1,D,F)
1090  LET G[N1,N2]=D
1100  NEXT N2
1105  LET Y=0
1110  FOR X=15 TO 50
1120  LET Y=Y+G[N1,X]
1130  NEXT X
1140  LET Y3=Y/36+Y3
1145  IF N1=1 THEN 1160
1150  LET Y4=ABS(Y3)+Y4
1160  NEXT N1
1170  LET C1=(Y4/10)*2
1180  RETURN
1400  REM DATA
9999  END
```

Madsen, Ole Secher
Reflection and transmission characteristics of porous rubble-mound breakwaters / by Ole Secher Madsen and Stanley M. White. – Fort Belvoir, Va. : U.S. Coastal Engineering Research Center, 1976.
138 p. : ill. (Miscellaneous report – Coastal Engineering Research Center ; no. 76-5)
Bibliography : p. 102.

This report presents the results of a study of the reflection and transmission characteristics of porous rubble-mound breakwaters, introducing empirical relationships for hydraulic characteristics of the porous material and the friction factor that expresses energy dissipation on the seaward slope of a breakwater.
1. Energy dissipation. 2. Rubble mound breakwaters. 3. Wave reflection. 4. Wave transmission. I. Title. II. White, Stanley M., joint author. III. Series : U.S. Coastal Engineering Research Center. Miscellaneous report no. 76-5.

Madsen, Ole Secher
Reflection and transmission characteristics of porous rubble-mound breakwaters / by Ole Secher Madsen and Stanley M. White. – Fort Belvoir, Va. : U.S. Coastal Engineering Research Center, 1976.
138 p. : ill. (Miscellaneous report – Coastal Engineering Research Center ; no. 76-5)
Bibliography : p. 102.

This report presents the results of a study of the reflection and transmission characteristics of porous rubble-mound breakwaters, introducing empirical relationships for hydraulic characteristics of the porous material and the friction factor that expresses energy dissipation on the seaward slope of a breakwater.
1. Energy dissipation. 2. Rubble mound breakwaters. 3. Wave reflection. 4. Wave transmission. I. Title. II. White, Stanley M., joint author. III. Series : U.S. Coastal Engineering Research Center. Miscellaneous report no. 76-5.

TC203 .U581mr no. 76-5 627 .U581mr

Madsen, Ole Secher
Reflection and transmission characteristics of porous rubble-mound breakwaters / by Ole Secher Madsen and Stanley M. White. – Fort Belvoir, Va. : U.S. Coastal Engineering Research Center, 1976.
138 p. : ill. (Miscellaneous report – Coastal Engineering Research Center ; no. 76-5)
Bibliography : p. 102.

This report presents the results of a study of the reflection and transmission characteristics of porous rubble-mound breakwaters, introducing empirical relationships for hydraulic characteristics of the porous material and the friction factor that expresses energy dissipation on the seaward slope of a breakwater.
1. Energy dissipation. 2. Rubble mound breakwaters. 3. Wave reflection. 4. Wave transmission. I. Title. II. White, Stanley M., joint author. III. Series : U.S. Coastal Engineering Research Center. Miscellaneous report no. 76-5.

TC203 .U581mr no. 76-5 627 .U581mr

Madsen, Ole Secher
Reflection and transmission characteristics of porous rubble-mound breakwaters / by Ole Secher Madsen and Stanley M. White. – Fort Belvoir, Va. : U.S. Coastal Engineering Research Center, 1976.
138 p. : ill. (Miscellaneous report – Coastal Engineering Research Center ; no. 76-5)
Bibliography : p. 102.

This report presents the results of a study of the reflection and transmission characteristics of porous rubble-mound breakwaters, introducing empirical relationships for hydraulic characteristics of the porous material and the friction factor that expresses energy dissipation on the seaward slope of a breakwater.
1. Energy dissipation. 2. Rubble mound breakwaters. 3. Wave reflection. 4. Wave transmission. I. Title. II. White, Stanley M., joint author. III. Series : U.S. Coastal Engineering Research Center. Miscellaneous report no. 76-5.

TC203 .U581mr no. 76-5 627 .U581mr

Madsen, Ole Secher
Reflection and transmission characteristics of porous rubble-mound breakwaters / by Ole Secher Madsen and Stanley M. White. – Fort Belvoir, Va. : U.S. Coastal Engineering Research Center, 1976.
138 p. : ill. (Miscellaneous report – Coastal Engineering Research Center ; no. 76-5)
Bibliography : p. 102.

This report presents the results of a study of the reflection and transmission characteristics of porous rubble-mound breakwaters, introducing empirical relationships for hydraulic characteristics of the porous material and the friction factor that expresses energy dissipation on the seaward slope of a breakwater.
1. Energy dissipation. 2. Rubble mound breakwaters. 3. Wave reflection. 4. Wave transmission. I. Title. II. White, Stanley M., joint author. III. Series : U.S. Coastal Engineering Research Center. Miscellaneous report no. 76-5.

TC203 .U581mr no. 76-5 627 .U581mr

Madsen, Ole Secher
Reflection and transmission characteristics of porous rubble-mound breakwaters / by Ole Secher Madsen and Stanley M. White. – Fort Belvoir, Va. : U.S. Coastal Engineering Research Center, 1976.
138 p. : ill. (Miscellaneous report – Coastal Engineering Research Center ; no. 76-5)
Bibliography : p. 102.

This report presents the results of a study of the reflection and transmission characteristics of porous rubble-mound breakwaters, introducing empirical relationships for hydraulic characteristics of the porous material and the friction factor that expresses energy dissipation on the seaward slope of a breakwater.
1. Energy dissipation. 2. Rubble mound breakwaters. 3. Wave reflection. 4. Wave transmission. I. Title. II. White, Stanley M., joint author. III. Series : U.S. Coastal Engineering Research Center. Miscellaneous report no. 76-5.

TC203 .U581mr no. 76-5 627 .U581mr

Madsen, Ole Secher
Reflection and transmission characteristics of porous rubble-mound breakwaters / by Ole Secher Madsen and Stanley M. White. – Fort Belvoir, Va. : U.S. Coastal Engineering Research Center, 1976.
138 p. : ill. (Miscellaneous report – Coastal Engineering Research Center ; no. 76-5)
Bibliography : p. 102.

This report presents the results of a study of the reflection and transmission characteristics of porous rubble-mound breakwaters, introducing empirical relationships for hydraulic characteristics of the porous material and the friction factor that expresses energy dissipation on the seaward slope of a breakwater.
1. Energy dissipation. 2. Rubble mound breakwaters. 3. Wave reflection. 4. Wave transmission. I. Title. II. White, Stanley M., joint author. III. Series : U.S. Coastal Engineering Research Center. Miscellaneous report no. 76-5.

TC203 .U581mr no. 76-5 627 .U581mr

Madsen, Ole Secher
Reflection and transmission characteristics of porous rubble-mound breakwaters / by Ole Secher Madsen and Stanley M. White. – Fort Belvoir, Va. : U.S. Coastal Engineering Research Center, 1976.
138 p. : ill. (Miscellaneous report – Coastal Engineering Research Center ; no. 76-5)
Bibliography : p. 102.

This report presents the results of a study of the reflection and transmission characteristics of porous rubble-mound breakwaters, introducing empirical relationships for hydraulic characteristics of the porous material and the friction factor that expresses energy dissipation on the seaward slope of a breakwater.
1. Energy dissipation. 2. Rubble mound breakwaters. 3. Wave reflection. 4. Wave transmission. I. Title. II. White, Stanley M., joint author. III. Series : U.S. Coastal Engineering Research Center. Miscellaneous report no. 76-5.

TC203 .U581mr no. 76-5 627 .U581mr